Institute for Geosciences
Christian-Albrechts-University
Kiel, Germany

Hydrography, Hydrothermalism, Paleoceanography in the Red Sea

FINAL REPORT

Sonne 121 - Red Sea
July 1997 – June 1999

Project Leader: Prof. Dr. P. Stoffers
Kiel University

Editors:
Prof. Dr. Peter Stoffers
Dr. Mark Schmidt

With contributions from:

Project leader/ Chief scientist:
Peter Stoffers, IFG Kiel
Co-Chief Scientist:
Mustafa Moammar, FMS Jeddah
Hydrography/Water chemistry:
Martin Hartmann, Dieter Garbe-Schönberg, Mark Schmidt, Jan Scholten, Tom Arpe, Sonja Klauke, IFG Kiel
P. Krause, B. Grote-Bartscher, CAS Sheffield
Organic and isotope geochemistry:
Reiner Botz, Mark Schmidt: IFG Kiel
Gisela Winckler, Reinhold Bayer, Steffen Schuler, IUP Heidelberg
Werner Aeschenbach-Hertig, Rolf Kipfer, EAWAG/ETH Zürich
Walter Michaelis, Sabine Beckmann, Stefan Boldt, Angela Jenisch-Anton, Richard Seifert: IFBM Hamburg
Manfred Schmitt: GCA Sehnde-Ilten
Jürgen Poggenburg: BGR Hannover
Hydrothermal mineralisation:
Jan Scholten, IFG Kiel
Dietmar Schöps: Jena, RTWH Aachen
Dietrich Ackermand: MPI Kiel
Erimias Yohannes , MEM Asmara
Palaeoclimatology-Palaeoceanography, Sedimentology:
Susanne Geiselhart, Thomas Mühlstrasser: GPI Tübingen
Jan Scholten, Anett Wismann: IFG Kiel
Dominik Fleitmann, Dieter Goedecke: GPI Göttingen
Mohammed Abu-Ouf, FMS Jeddah
Osma Mohammed Hassan Alassif, FMS Jeddah
M. H. El-Mamoney, NIOF Alexandria
Khaled Moussa, NIOF Alexandria
Abu el Gasim H. A. El-Garafi, Sudan
Microbiology:
Wolfgang Eder, Wolfgang Ludwig, Robert Huber, K.O. Stetter: Regensburg
Navy observer
Yahia Mohammed Al-Hazim, Saudi Arabia
Lieutenant Colonel M.M. M. Mohamed Shbalaby, Egypt
Institutes:
IFG Kiel: Institute for Geosciences, Olshausenstr. 40, D-24118 Kiel
FMS: Faculty of Marine Science, King Abdulaziz University, P.O. Box 1540, Jeddah 21441, Saudi Arabia
NIOF: National Inst. of Oceanography and Fisheries, Alexandria Branch, 21556 Alexandria, Egypt
MEM: Ministry of Energy and Mines, Asmara, Eritrea
MPI Kiel: Mineralogisch-Petrographisches Institut, Olshausenstr. 40, D-24118 Kiel
GPI Tübingen: Geologisch-Paläontologisches Institut, Sigwartstr. 10, D-72076 Tübingen
GPI Göttingen: Geologisch Paläontologisches Institut, Goldschmidtstr. 3, D-37077 Göttingen
IFBM: Institut für Biogeochemie und Meereschemie, Bundesstr. 55, D-20146 Hamburg
BGR: Bundesanstalt für Geowissenschaften und Rohstoffe, Stilleweg 2, D-30655 Hannover
GCA: Geochemische Analysen, Glückaufstr. 50, D-31319 Sehnde-Ilten
Institut für Geowissenschaften, Burgweg 11, D-07749 Jena
RTWH: Rheinisch-Westfälische Technische Hochschule, FB 5, Templergraben 55, D-52056 Aachen
Lehrstuhl für Mikrobiologie und Archaeenzentrum, Universitätsstr. 31, D-93043 Regensburg
CAS: Centre for Analytical Sciences, Dept. of Earth Sciences, Sheffield S3 7HF, UK
IUP: Institut für Umweltphysik, Universität Heidelberg Im Neuenheimer Feld 229, D-69120 Heidelberg, Germany
EAWAG/ETH: Environmental Physics, Swiss Federal Institute of Technology (ETH), Swiss Federal Institute for Environmental Science and Technology (EAWAG), CH-8600 Dübendorf, Switzerland

Table of Contents page

1. Abstract

The Red Sea is a very young ocean, and is one of the most interesting areas on Earth (ocean in statu nascendi). It is the only ocean where hydrothermal activity associated with ore formation occurs in a sterile environment (anoxic, hot, saline brines). In addition, its geographical position means that it is predestined to record the monsoonal history of the region in detailed sedimentary sequences.

The major aim of the present project was to investigate the dynamics of hydrothermal systems in selected Deeps (Atlantis-II-, Discovery-, Kebrit-, Chain-Deep) in the central and northern part of the Red Sea. Geochemical (hydrocarbons, gas and trace element cycles) and microbiological questions have been addressed. Furhermore, paleontological studies have been made and will be reported in a forthcoming report.

Specific aims were:

1. To study hydrographic changes in individual Deeps (hydrothermal region Atlantis-II, Discovery Deep) during the last few years (compared to Meteor-cruise 31/2 in 1995) and to investigate the brine compositions and brine-seawater interfaces.
2. Investigating hydrothermal mineral deposits to get more information about the hydrothermal history in the Red Sea rift area.
3. Claryfing the influence of hydrothermalism on the sedimentary organic matter in the Deeps and the hydrocarbon gasesin the brines. In particular, the production and degradation processes of hydrocarbons have been studied.
4. Documentating microbiological activity associated with hydrothermal activity in aan extreme (hypersaline and hot) environment. In detail, to separate microorganisms from the brines and to characterise them in terms of their metabolic physiology and ecology, and to describe their taxonomy.
5. To clarify the palaeoceanographic conditions, sea-level changes and the climatic history (relationship of the circulation system and nutrient supply to the monsoon) of the southern Red Sea (forthcoming report).

2. Acknowledgements

The project „SO 121“ was funded by the German Bundesministerium für Bildung, Wissenschaft, Forschung und Technologie (BMBF).

The foreign ministeries of Saudi Arabia, Egypt, Eritrea and Sudan are highly acknowledged for the the working permissons and their support during this project.

3. Summary of Results

Introduction

The Red Sea represents an ocean "in statu nascendi", evolving from continental rifting to seafloor spreading. During the late Oligocene the first phase of the Red Sea formation started with the break-up of the Arabian plate from Africa, accompanied by intense magmatic activity and continental rifting. Seafloor spreading started in the early Miocene (Girdler and Styles, 1974). Whereas it is generally accepted that in the last 5 million years seafloor spreading formed a mid-oceanic ridge in the southern Red Sea there is a lively debate about the nature of crust in the marginal regions of the Red Sea. Thick Miocene evaporates sedimented in the Red Sea depression which makes the identification of a clear ocean-continent boundary difficult. Based on the good match of the African and Arabian coastlines one hypothesis assumes seafloor spreading to have formed oceanic basement in the entire Red Sea in Miocene times (Girdler and Styles, 1974; Girdler, 1985; McKenzie et al. 1970). Accordingly, most of the Red Sea basement is supposed to be of basaltic composition. This model, however, cannot explain the existence of continental crust in the Southern Red sea and the Afar Triangle (Makris and Rihm, 1991). An alternative model postulates diffuse thinning and stretching of the continental crust and assumes the Red Sea basement to be composed of some kind of intermediate crust (Cochran, 1983; Wernicke, 1985; LePichon and Gaullier, 1988). These models may explain the outcrops of Precambrian basement off the coast such as at Zabarged Island and basaltic intrusions found in Miocene evaporates (Bonatti and Seyler, 1987; Lowell and Genik, 1972).

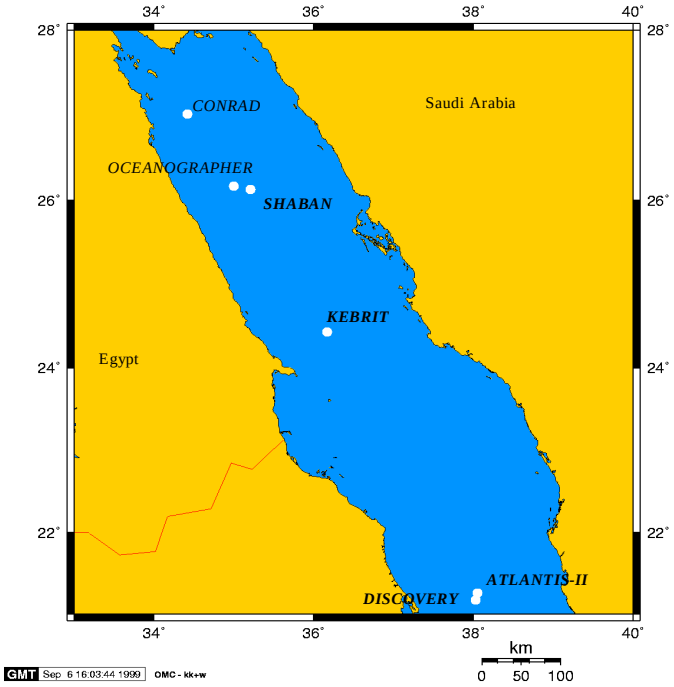

During the past 4 to 5 million years a spreading rate of about 1 cm/yr formed a continuous oceanic rift with a 1500m to 2000m deep axial graben in the Southern Red Sea (Bäcker et al., 1975). Towards the north-west the axial zone narrows and the age of the oceanic crust gets younger

(Izzeldin, 1987). North of about 21°N no continuous rift is present, and isolated deeps alternate with smooth intertrough zones. Oceanic basement, basaltic intrusions and magnetic anomalies suggest these deeps to be nucleation points for oceanic rifts. As rifting propagates the more or less regularly spaced deeps could join to form a continuous axial rift valley (Bonatti, 1985).

A characteristic feature of the central and northern Red Sea are isolated topographic depressions which are filled with geothermal brines, i.e. waters characterized by elevated salinities and temperatures (e.g. Bäcker and Schoell, 1972; Degens and Ross, 1969; Pautot et al., 1984). The high salinities are caused by leaching of the Miocene evaporites that underlie the entire Red Sea (e.g.Craig, 1969). The brines occur in one or more horizontally uniform layers, separated by thin interfaces with sharp gradients of temperature and salinity (e.g.Anschutz et al., 1998; Hartmann et al., 1998)

In 1997, three deeps, the Atlantis II Deep and the Discovery Deep in the central Red Sea and the Kebrit Deep in the northern Red Sea were revisited during SO121-cruise (Fig.1). The Atlantis II Deep is the largest and best studied brine pool within the unique geological environment (Miller et al. 1966). Isotope investigations demonstrated that the Atlantis II brine is part of an active hydrothermal system e.g. (Blanc et al., 1995; Lupton et al., 1977; Zierenberg and Shanks III, 1986) but, inspite of numerous studies, there is still considerable debate concerning the detailed origin e.g. (Anschutz et al., 1995) and the dynamics of the brine system (Anschutz et al., 1998; Faber et al., 1998). In case of the northern brine pools their origin and formation process is still poorly understood.

Hydrography and Trace element cycles in brine-filled deeps

The interconnected basins of the Atlantis-II, Chain, and Discovery Deep within the axial trough of the Red Sea are filled with one or more discrete brine layers and have been investigated in great detail with respect to sediment and brine bulk composition. Studies targeting on processes within the brine interfaces, however, and on redox-related particle-water interactions in particular, are void.

During cruise *Sonne 121* in July 1997 brine interfaces have been sampled with high vertical spatial resolution down to 0.3 m by means of hydrocast and deLange's Interface Sampler IS-1. All samples were filtrated and trace elements were analysed with AAS and HRICPMS.

Salinity gradients in the LCL/ UCL-1 and UCL-1/ UCL-2 interfaces are very steep extending over only 2-3 m. We report first results showing that dissolved Fe, Mn, Zn, Cu, Pb, Tl, W, Sb, Re, Ag, Cd, In; Li, B, Rb, Sr, Cs, Ba are highly enriched in the LCL while U (and sulfate) is depleted. Mo, U,

and Co are highly enriched in the turbid zones above each interface suggesting complex redox-cycles.

Gas chemistry of brine-filled deeps

Hydrocarbon gases

High resolution gas measurements of water samples from the Red Sea show significant increase of methane from Red Sea Deep Water to hypersaline brine in several brine-filled deeps. Methane concentrations vary from 10^1nl/l in surface waters to 10^3nl/l in the transition zones and up to 10^7nl/l in brine layers. Highest concentrations were measured in the lower brine layers (LCL) between 24µl/l (Discovery deep) and 150µl/l (Atlantis-II deep) and 14ml/l (Kebrit deep).

Small amounts of ethane and higher hydrocarbons were detected in brine samples and calculated ratios of methane to higher HC's (C_1/C_{2+}) indicate a thermogenic origin of the hydrocarbon gases. Furthermore, stable isotope measurements ($\delta^{13}C$) of methane gives evidence for microbial and/or abiogenic hydrocarbon oxidation processes in the brine seawater interfaces (maximum $\delta^{13}C_{CH4}$=+50‰ at Discovery brine seawater interface). Although, hydrocarbon loss from the brine reservoir to the Red Sea deep water by diffusion is a major process. However, the stable carbon isotope composition of hydrocarbons in the brine is probably influenced by the local geological situations of the depressions. This is indicated by more negative $\delta^{13}C_{CH4}$ values in the Kebrit brine (off axis, sediment filled depression) than in the Atlantis-II-deep brine (basalt-rich, hydrothermally influenced, axial depression).

Helium Isotopes

Hydrothermal brines from the Atlantis II Deep, Red Sea, have been sampled *in-situ* and analyzed for noble gases. The atmospheric noble gas concentrations (Ne, Ar_{atm}, Kr, Xe) in the deepest layer (LCL) are depleted by 20-30 % relative to the initial concentrations in ambient Red Sea Deep Water without a systematic mass fractionation between the different noble gases. Sub surface boiling during the hydrothermal circulation and subsequent phase separation is shown to be a consistent explanation for the observed depletion pattern. Using a conceptual model of phase separation under sub-critical conditions, in which gases are partitioned according to Henry's Law, we reconstruct the fluid history prior to injection into the Atlantis II Deep: after having circulated through evaporites and young oceanic crust, where it becomes enriched in He_{MORB} and Ar_{MORB}, the ascending fluid boils, and the residual liquid becomes depleted in noble gas concentrations. The depleted fluid rises to the sediment surface and feeds the Atlantis II basin. The relatively low boiling degree of about 3% (i.e., the

percentage of fluid removed as vapour) derived from the model indicates that the Atlantis II system represents an early stage of boiling with relatively small gas loss, in contrast to hydrothermal systems at sediment-free mid-ocean ridges.

Brines from three deeps along the axis of the Red Sea, the Atlantis II, the Discovery and the Kebrit Deep, were sampled and analyzed for helium and argon isotopes. We identified two principally different geochemical fingerprints that reflect the geological setting of the deeps.

The Atlantis II and the Discovery brine located in the central Red Sea show ^{4}He concentrations up to 1.2ccSTP$\cdot g^{-1}$ and a $^{3}He/^{4}He$ ratio of 1.2 ($9.2\cdot R_a$). The MORB-like $^{3}He/^{4}He$ ratio is typical of an active hydrothermal vent system and clearly indicates a mantle origin of the brines. $^{40}Ar/^{36}Ar$ ratios are up to 305 implying that mantle-derived radiogenic ^{40}Ar excesses of up to 3% of the total argon concentration are present in the brines and transported along with the primordial ^{3}He signal. The $^{4}He/^{40}Ar$ ratio is very close to the mantle production ratio MORB like helium isotope ratio and indicates that the mantle volatiles present in the brine are acquired from fresh unfractionated basalts.

In the Kebrit Deep located in the northern Red Sea Deeps we found a helium excess of $5.7*10^{-7}$cc STP$\cdot g^{-1}$. The low $^{3}He/^{4}He$ ratio of $1*10^{-6}$points to a radiogenically dominated source of the helium excess with only a minor mantle contribution of 8%. We propose a new scenario assuming that the Kebrit brine accumulates a diffusive He flux that migrates from deep sedimentary or crustal horizons. In contrast to the Atlantis-II and Discovery Deep, the Kebrit brine shows no sign of an active hydrothermal input.

Hydrothermal deposits

Hydrothermal activity in the Red Sea is linked to the divergent movement of the African and Nubian continental plates and the subsequent formation of new oceanic crust. The formation of hydrothermal deposits is facilitated in the Red Sea because of two reasons: i) The development of new oceanic crust is focused on relatively small areas, i. e. isolated deeps. ii) The occurrence of high saline brines in these deeps favours the preservation of the hydrothermal fluids and deposits. As a result, iron, manganese, sulfate and sulfide sediment facies types can be observed in the Red Sea deeps. The most concentrated deposits occur in the brine-filled Atlantis-II-Deep, an area which was extensively investigated during the past approximately 40 years. The Atlantis-II-Deep is thus one of the few locations in marine geoscience where the time variability of a hydrothermal system can be investigated. Between 1965 and 1997 a temperature increase of the lower brine in the Atlantis-II-Deep from 55.9°C to 67.2°C has been observed suggesting an increase of hydrothermal activity. In

the same time-period concentrations of dissolved Mn and Fe in the brine slightly increased whereas the concentrations of Cu decreased. Although active vents have never been observed, there are strong indications that hydrothermal fluids discharge in the SW-basin of the Atlantis-II-Deep. Based on paragenesis of authigenic minerals in the sediments, formation temperatures of hydrothermal precipitates in between 110°C and <450°C have been estimated.

Apart from the Atlantis-II-Deep hydrothermal deposits have been found in the Thetis, Nereus, Vema and Gypsum deeps, but in these deeps ore concentrations are lower. Massive sulfides from the brine-filled Kebrit-Deep are another type of hydrothermal mineralisations in the Red Sea. The porous and fragile sulfides, which are sometimes impregnated with tar, consist of two types of sulfides: The first type (type I) is characterised by a mineral assemblage of pyrite, marcasite, bravoite, sphalerite, digenite, chalcocite, jarosite, and minor amounts of galena. They have relatively high Zn and Pb concentrations. The second type (type II) of massive sulfides consists almost exclusively of pyrite with low trace metal contents. The lack of significant Cu enrichments in all the sulfides and the mineral structure suggests a low formation temperature. Lead isotope data of the sulfides indicate that the lead metals may have derived from mixing between a basaltic and a more radiogenic end member source. Age estimates of the sulfides suggest that the type I deposits formed between 20,000 and 28,000 years ago, whereas type I sulfides are much younger (<5,000 years). Periods of hydrothermal activity with obviously different chemical composition of the hydrothermal fluids have been observed also in the Thetis Deep. To what extent periods of hydrothermal activities in the Red Sea deeps are connected to each other by, e. g. tectonic activity is a matter of speculation and needs further investigation.

Microbiology

In this study, we report on first 16S rRNA gene sequences from highly saline brine sediments, taken in a depth of 1515 m in the Kebrit Deep, northern Red Sea. Microbial DNA, extracted directly from the sediments, was subjected to PCR amplification with primers specific for bacterial and archaeal 16S rRNA gene sequences. The PCR products were cloned and a total of 11 (6 bacterial and 5 archaeal) clone types were determined by restriction endonuclease digestion. Phylogenetic analysis revealed that most of the cloned sequences were unique, showing no close association with sequences of cultivated organisms or sequences derived from environmental samples. The bacterial clone sequences form a novel phylogenetic lineage (KB1 group), branching between the *Aquificales* and *Thermotogales*. The archaeal clone sequences group within the *Euryarchaeota*. Some of the

sequences cluster with the group II and group III uncultivated archaea sequence clones, while two clone groups form separate branches. Our results suggest that so far unknown archaea and bacteria may thrive in highly saline brines of the Red Sea under extreme environmental conditions.

Organic geochemistry

Considerable geochemical differences exist between the Kebrit Deep and the Atlantis II Deep.

-While carbonates contribute about 50% to the Kebrit Deep sediments, only traces are present in Atlantis II Deep sediments.

-The content of organic carbon in the sediments and in the pore waters of the upper 5 m of the sediment column is much higher in the Kebrit Deep. Below 5 mbsf, concentrations of sedimentary carbon and pore water DOC increase strongly in the Atlantis II Deep, but not in the Kebrit Deep.

-DOC concentrations in Kebrit Deep brine waters exceed those found in the Atlantis II Deep.

High concentrations of dissolved organic carbon appear close to pycnolclines at the upper brine – sea water boundary.

Sediments of enhanced organic carbon content reveal high Corg to N ratios. This might indicate impregnation with hydrothermally altered and mobilised organic matter. The appearance of those indications within distinct horizons in the upper part of the sediment column argues for lateral inputs, at least in case of the Kebrit Deep.

Extracts from samples of the Kebrit Deep contained normal, branched and cyclic alkanes typical for an autochthonous sedimentation of organic substances. An increase of maturation with depth is observed (increase of α,β-hopanes and of the unresolved complex mixture). The in situ thermal alteration of the sediments should be minimal because unusually high concentrations of immature polar compounds are present.

The sources of the sedimentary organic matter could be characterised by biomarkers. Identified are contributions from marine algae (diatoms, haptophytes), cyanobacteria, archaebacteria, and aerobic bacteria.

For Atlantis II Deep samples, the different thermal maturities give evidence for an impregnation of the Recent, immature autochthonous material by hydrothermally derived organic compounds from deeper sections. The migrating organic phase increasingly dominates the recent organic material with greater depth.

Palaeoceanography

Our present studies are concerned with a reconstruction of the climatic history of the Red Sea. From the available sample material, we have been able to reconstruct the climate - primarily in the central Red Sea - over the last 370 000 years (four stages of relatively high aridity, oxygen isotope stages 2, 6, 8, 10, and four relatively humid stages). During cruise Meteor 31/2, these studies were expanded through the collection of long cores in the central and northern Red Sea. Time constraints meant that it was not possible to collect all the required sediment cores from the southern region. This southern area is however a key region in the Red Sea, as it is influenced by influx and outflux through the straits of Bab el Mandeb in response to sea-level changes. Especially during periods of low sea-level, these straits are the major controlling influence on the palaeocirculation in the Red Sea. At the present-day, the straits have a water depth of 137m. During the last glacial maximum (LGM) sea levels sank by 120m, meaning that in the straits possibly only 17m water depths existed. Although 17m is probably enough to permit a minimal circulation in the Red Sea, it is at the lowermost end of permittable values. This reasoning is based on the assumption that the Straits of Bab el Mandeb have been tectonically quiet since the LGM. Results from cores in the central and northern Red Sea suggest that the water depths here at the time of the LGM were if anything deeper. The missing information from the southern Red Sea and the inner Gulf of Aden will be provided by a series of long cores (>20m) in this region. The results of these investigations will be presented in a future report to BEO.

References

Anschutz P., Blanc G., and Stille P. (1995) Origin of fluids and the evolution of the Atlantis II deep hydrothermal system,Red Sea Geochim. Et Cosmochim. Acta **59**, 4799

Anschutz P., Turner J. S., and Blanc G. (1998) The development of layering, fluxes through double - diffusive interfaces, and location of hydrothermal sources of brines in the Atlantis II Deep: Red Sea. *Journal of Geophysical Research - Oceans* **103**, 27809 - 27819.

Bäcker H. and Schoell M. (1972) New deeps with brines and metalliferous sediments in the Red Sea. *Nature (Phys. Sci.) **240**, 153 - 158*

Bäcker H., Lange K., and Richter H. (1975) Morphologie of the Red Sea Central Graben between Subair Islands and Abul Kizaan. *Geol. Jahrb.* **D 13**, 79.

Bonatti E. and Seyler M. (1987) Crustal underplating and evolution in the Red Sea rift: uplifted gabbro / gneiss crustal complexes on Zarbargad and Brothers Islands. *J. Geophys. Res.* **92**, 12803

Bonatti E. (1985) Punctiform initiation of seafloor spreading in the Red Sea during transition from a continental to an oceanic rift. *Nature* **316**, 33 - 37.

Cochran J. R. (1983) A model for the development of the Red Sea. *Bull. Amer. Assoc. Pet. Geol.* **67**, 41

Craig H. (1969) *Geochemistry and origin of the Red Sea brines.* Springer Verlag.

Degens E. T. and Ross D. A. (1969) *Hot Brines and Recent Heavy Metal Deposits in the Red Sea*. Springer Verlag..

Faber E., Botz R., Poggenburg J., Schmidt M., Stoffers P., and Hartmann M. (1998) Methane in Red Sea brine waters. *Org. Geochemistry* **29**(1-3), 363-379.

Girdler R. W. and Styles P. (1974) Two stage Red Sea floor spreading. *Nature* **247**, 7.

Girdler R. W. (1985) Problems concerning the evolution of organic lithosphere in the Northern Red Sea. *Tectonophysics* **116**, 109.

Hartmann M., Scholten J. C., Stoffers P., and Wehner F. (1998) Hydrographic structure of brine-filled deeps in the Red Sea - new results from the Shaban, Kebrit, Atlantis II, and Discovery Deep. *Mar. Geol.* **144**, 311-330.

Izzeldin Y. A. (1987) Seismic, gravity and magnetic surveys in the central part of the Red Sea ; their interpretation and implications for the structure and evolution of the Red Sea. *Tectonophysics* **143**, 269.

Le Pichon X. and Gaullier J. M. (1988) The rotation of the Arabia and Levant Fault System. *Tectonophysics* **153**, 271.

Lowell J. D. and Genik G. J. (1972) Sea - Floor Spreading and Structural Evolution of Southern Red Sea. *American Association of Petroleum Geologist Bulletin* **56 No.2**, 247 - 259.

Lupton J. E., Weiss R. F., and Craig H. (1977) Mantle helium in the Red Sea brines. *Nature* **266**, 244 - 246.

Makris J. and Rihm R. (1991) Shear - controlled evolution of the Red Sea: pull apart model. *Tectonophysics* **198**, 441.

McKenzie D. P., Davies D., and Molnar P. (1970) Plate tectonics of the Red Sea and East Africa. *Nature* **226**, 243.

Miller A. R., Densmore C. D., Degens E. T., Hathaway J. C., Manheim F. T., McFarlin P. F., Pocklington R., and Jokela A. (1966) Hot brines and recent iron deposits in deep of the Red Sea. *Geochimica et Cosmochimica Acta* **30**, 341 - 359.*ys. Sci.)* **240**, 153 - 158.

Pautot G., Guennoc P., Coutelle A., and Lyberis N. (1984) Discovery of a large brine deep in the northern Red Sea. *Nature* **310**, 133 - 136.

Wernicke B. (1985) Uniform sense normal simple shear of the continental lithosphere. *Can. J. Sci.* **22**, 108.

Zierenberg R. A. and Sharks III W. C. .(1986) Isotopic constraints on the origin of the Atlantis II, Suakin and Valdivia brines, Red Sea. *Geochimica et Cosmochimica Acta* **50**, 2205 - 2214.

4. Hydrographic structure of brine-filled deeps in the Red Aea: correction of Atlantis II Deep temperatures

M. Hartmann, J. C. Scholten, P. Stoffers

During the Meteor Expedition M31/2 in 1995 higher temperatures were measured compared to those determined earlier in the Atlantis II Deep LCL brine (up to 71.6°C) and the Discovery lower brine section (nearly 50°C) (Hartmann et al., 1997). This suggested an exceptionably strong increase in the temperature gradient during the previous two years, pointing to strongly enhanced hydrothermal / volcanic activity having taken place during this time. The CTD device used during this expedition had been adapted for the high temperatures and calibrated up to 60°C (+ 0.03°C) by the ADM Company, Kiel-Warnau. Repeated lowerings of the device seemed to confirm the temperatures in the respective basins, and normal Red Sea deep water temperatures (near 21.6°C) were found in the expected range. Therefore we saw no reason to distrust these results.

During a new expedition with RV Sonne (SO121, 14 July to 6 August 1997) we had two disposable CTD devices from the ME - Company, Trappenkamp, both adapted and calibrated for temperatures up to 80°C. The temperatures readings received with these CTDs were identical to within 0.1°C in the respective brine sections.

The profiles taken with these devices revealed that the temperatures are about 4 to 5°C lower compared to the values measured two years before in the Atlantis II Deep LCL brine and in the Discovery Deep lower brine section.

The highest temperature measured just below the Atlantis II Deep LCL upper interface was 67.7°C near the western boundary of the SW basin. Temperatures of 67.1 to 67.3°C were found in the deeper sections of the LCL brine of the SW basin during the SO121 expedition. Values of 56.4 and 52.0°C respectively, were measured for the UCL1 and UCL2 sections (compared to 61.1 and 55.3°C respectively measured in 1995 with an incorrectly calibrated CTD).

The temperature of 45.0°C measured this year in the upper section of the Discovery Deep homogeneous brine corresponds very near to 44.7°C measured between 1965 and 1977.This means that no significant changes occurred during this time. This is a clear indication that the temperature of 49.0°C measured in this section in 1995 must have been too high by about 4°C.

Fig. 1 gives the corrected temperature increase of the Atlantis II Deep LCL brine with time since 1965. This shows that the gradient of temperature increase was nearly constant since 1978, and it has slowed down slightly since 1992 when Anschutz and Blanc (1996) measured a value of 66.1°C. This means that in contrast to our conclusions based on the 1995 results (Hartmann et al., 1997) the hydrographic conditions of the Atlantis II Deep brine system and/or the hydrothermal activity remained narly constant or led to a slightly reduced temperature in the LCL section in the last few years.

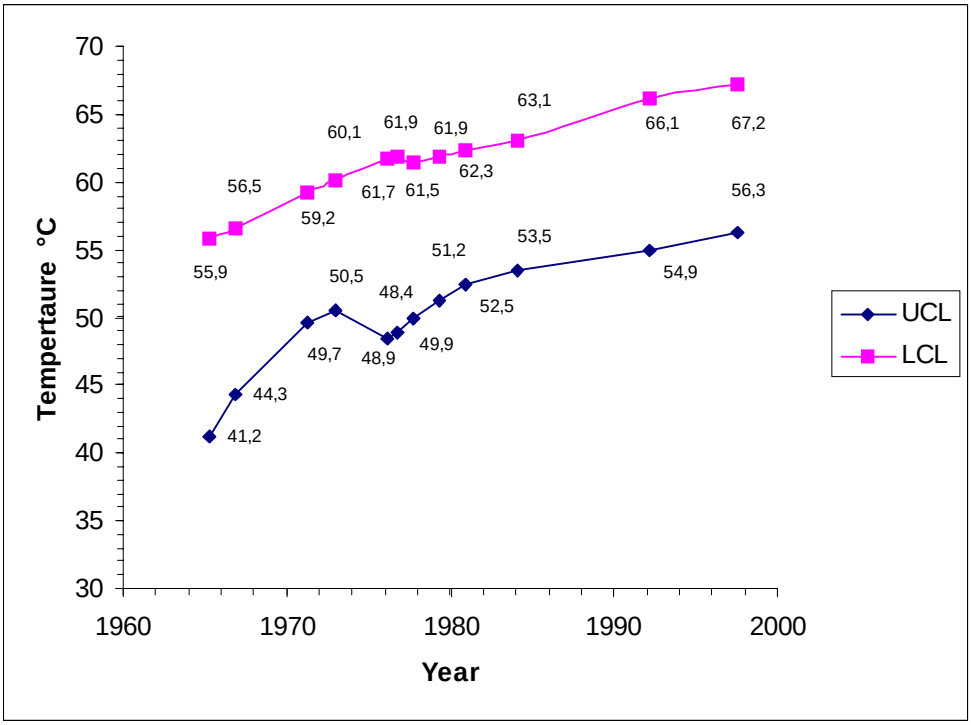

Fig. 1

References

Anschutz P. and Blanc G. (1996) Heat and salt fluxes in the Atlantis II Deep (Red Sea). *Earth Planet. Sci. Lett.* **142**, 147-159.

Hartmann M., Scholten J. C., Stoffers P., and Wehner F. (1998) Hydrographic structure of brine-filled deeps in the Red Sea - new results from the Shaban, Kebrit, Atlantis II, and Discovery Deep. *Mar. Geol.* **144**, 311-330.

5. Trace element chemistry of brines and brine-interfaces in the Atlantis-II, Chain, and Discovery Deep

C.-Dieter Garbe-Schönberg[§], Jan C. Scholten[§], Mustafa O. Moammar[&], and Peter Stoffers[§]

[§] Institute for Geosciences, Dept. of Geology, University of Kiel, 24098 Kiel, Germany

[&] Faculty of Marine Sciences, Marine Chemistry Dept., King Abdulaziz University, Jeddah 21444, Kingdom of Saudi Arabia

Introduction

The interconnected basins of the Atlantis-II, Chain, and Discovery Deep within the axial trough of the Red Sea (**Fig.1**) are filled with one or more discrete warm brine layers (LCL, UCL 1- 3) and have been investigated in great detail with respect to sediment and brine bulk composition (Hartmann et al., 1998; Anschutz and Blanc, 1996; Miller et al., 1966). Studies targeting on processes withinthe brine interfaces, however, and on redox-related particle-water inter-actions in particular, are void.

.

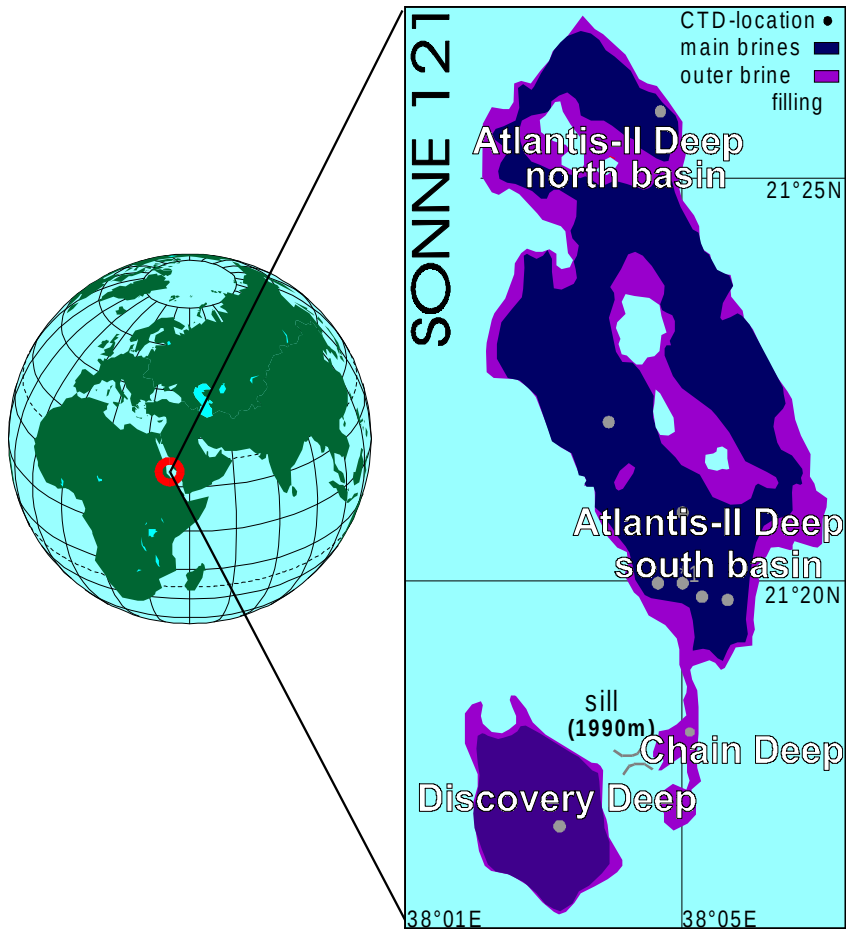

Fig. 1

Results and Discussion

During cruise *Sonne 121* in July 1997 brine interfaces have been sampled for the first time with high vertical spatial resolution down to 0.3 m by means of hydrocast and deLange's Interface Sampler IS-1 (**Fig. 2**). All samples were 0.4 µm membrane filtrated on-board and trace elements were analysed by AAS and HRICPMS for major and 47 trace elements.

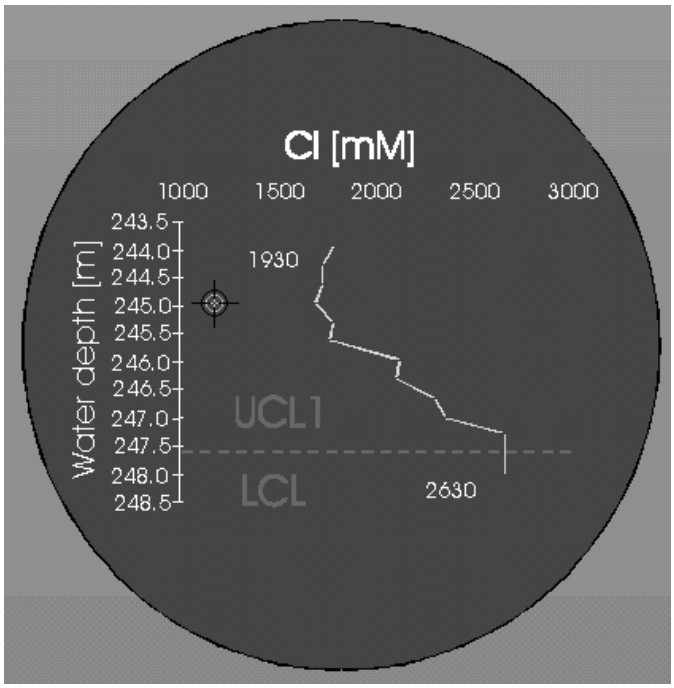

Fig. 2: The salinity gradient in the LCL/ UCL-1 (and in the UCL-1/ UCL-2) interface is very steep extending over only 1.5 ± 0.3 m.

In the Atlantis-II Deep up to 4 discrete brine layers were observed during the SONNE 121 cruise (**Fig.3**): Lower Convective Layer (LCL; 67 °C, 2630 mM Cl^-) and Upper Convective Layers 1 to 3 (UCL 1; 56 °C, 1930 mM Cl^-; UCL-2; 52 °C, 1340 mM Cl^-; UCL-3; 49-41 °C, 1170-1090 mM Cl^-) overlain by a Transition Zone (TZ) to normal Red Sea bottom water. All brine interfaces are characterized by sharply defined maxima in suspended particulate matter (SPM) with abundant Fe-oxyhydroxide (LCL/UCL-1 interface) and Mn-oxide (UCL-3/TZ) (**Fig. 4**).

Fig. 3: Bathymetry and hydrography of the brine-filled deeps with discrete layers: Lower Convective Layer (LCL), Upper Convective Layer (UCL) 1-3, Transition Zone (TZ)

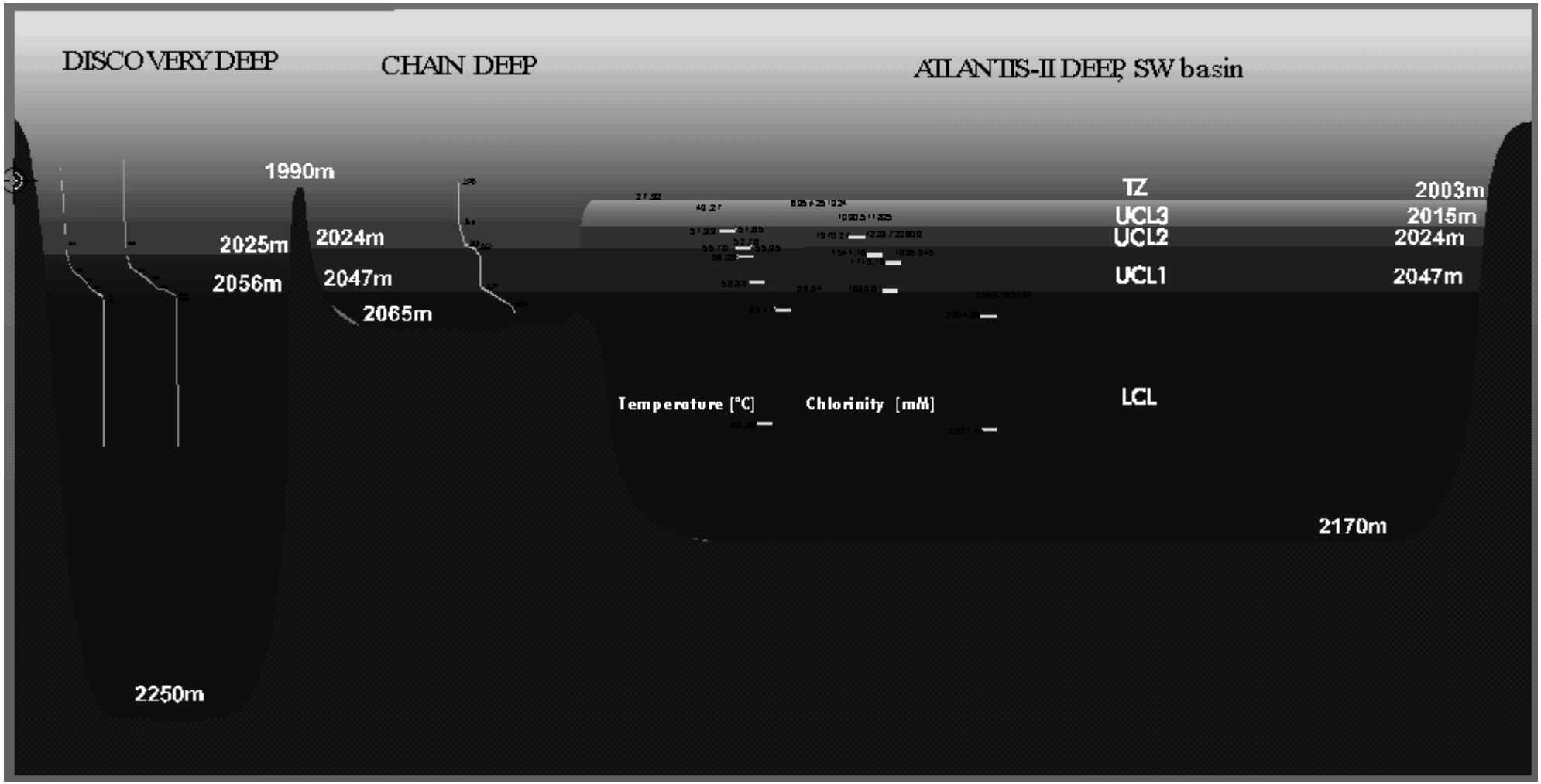

Dissolved elements

Concentrations of dissolved Fe, Mn, Zn, Cu, Pb, Tl, W, Sb, Re, Ag, Cd, In, Li, B, Rb, Sr, Cs, Ba are enriched in the **LCL** while U (and sulfate) is depleted (**Table 1**). Mo, U, and Co are highly enriched in the turbid zones above each interface suggesting complex redox-cycling of these elements (see Garbe-Schönberg et al., 1998).

Tab. 1

		Atlantis II Deep							Chain Deep		Discovery D.
		SW Basin				N Basin					
		LCL	UCL-1	UCL-2	UCL-3	LCL	UCL-1	UCL-2	LCL	UCL1	D-LCL
Mn	mg/l	99.8	105	67.1	43.0	90.9	92.1	69.2	108	43.1	63.2
Fe	mg/l	88.5	2.82	< 2	< 2	84.8	< 2	< 2	1.10	0.97	< 2
Sr	mg/l	50.4	29.1	18.9	15.9	48.8	24.0	19.0	49.2	23.4	52.1
Li	µg/l	8366	4771	2463	1689	7753	3611	2536	6029	2785	6291
Co	µg/l	15.2	35.0	12.4	6.0	13.0	30.4	13.5	12.3	6.3	13.3
Ni	µg/l	161	71	22	30	155	81	45	437	194	275
Zn	µg/l	3611	2493	407	398	3365	1795	441	7453	1009	461
Rb	µg/l	2698	1477	806	610	2640	1167	845	2556	1029	2593
Mo	µg/l	19.6	26.7	23.2	20.8	19.3	29.7	23.9	65.3	58.3	14.0
Cd	µg/l	3.2	1.8	0.7	0.6	3.2	1.6	0.8	11.4	1.2	2.1
Sb	µg/l	1.89	0.97	0.59	0.45	2.02	1.27	1.14	4.20	1.52	1.99
Cs	µg/l	64.4	32.4	16.0	11.3	63.4	24.4	17.3	55.8	18.0	51.8
Ba	µg/l	2547	1695	1064	654	2343	1484	1371	963	303	832
Tl	µg/l	3.69	3.10	1.94	1.28	3.63	2.72	1.85	3.60	1.25	1.77
Pb	µg/l	38.9	12.7	1.5	1.6	51.9	6.6	2.2	38.7	1.8	7.3
U	µg/l	1.32	2.98	2.08	2.59	1.26	3.21	1.91	1.29	1.64	0.87

Particulate elements

At the LCL/UCL-1 interface dissolved Fe-II is oxidized to particulate Fe-III-oxihy-droxides. These particles are effective scavengers of trace metals, e.g., Co,Cd, Ba. (**Fig. 4**). The TZ/UCL-3 interface region is characterized by oxidation of Mn-II to particulate MnO_2. Associated to this latter process is e.g., U.

References

Anschutz P. and Blanc G (1996) *Earth Planet Sci Lett*, **142**: 147-159

Bäcker H. and Richter H. (1973) *Geol Rdsch*, **62**: 697-741

Garbe-Schönberg C.-D., Scholten J.C., Moammar M.O., and Stoffers P. (1998) *EOS Transactions*, **AGU Vol. 79**: F947

Hartmann M., Scholten J., and Stoffers P. (1998) *Mar Geol*, **144**, 331-332

Miller A.R., Densmore C.D., Degens E.T., and co-authors (1966) *Geochim Cosmochim Acta*, **26**, 1029-1043.

Fig. 4: Profiles of Light Transmission and selected particulate trace elements (in ng/l) in the Atlantis-II Deep. Brine interfaces are characterized by high SPM concentrations as illustrated by photographs of SPM-loaded membrane filters. The LCL/UCL-1 interface is high in particulate Fe, The UCL-3/TZ interface is high in particulate Mn.

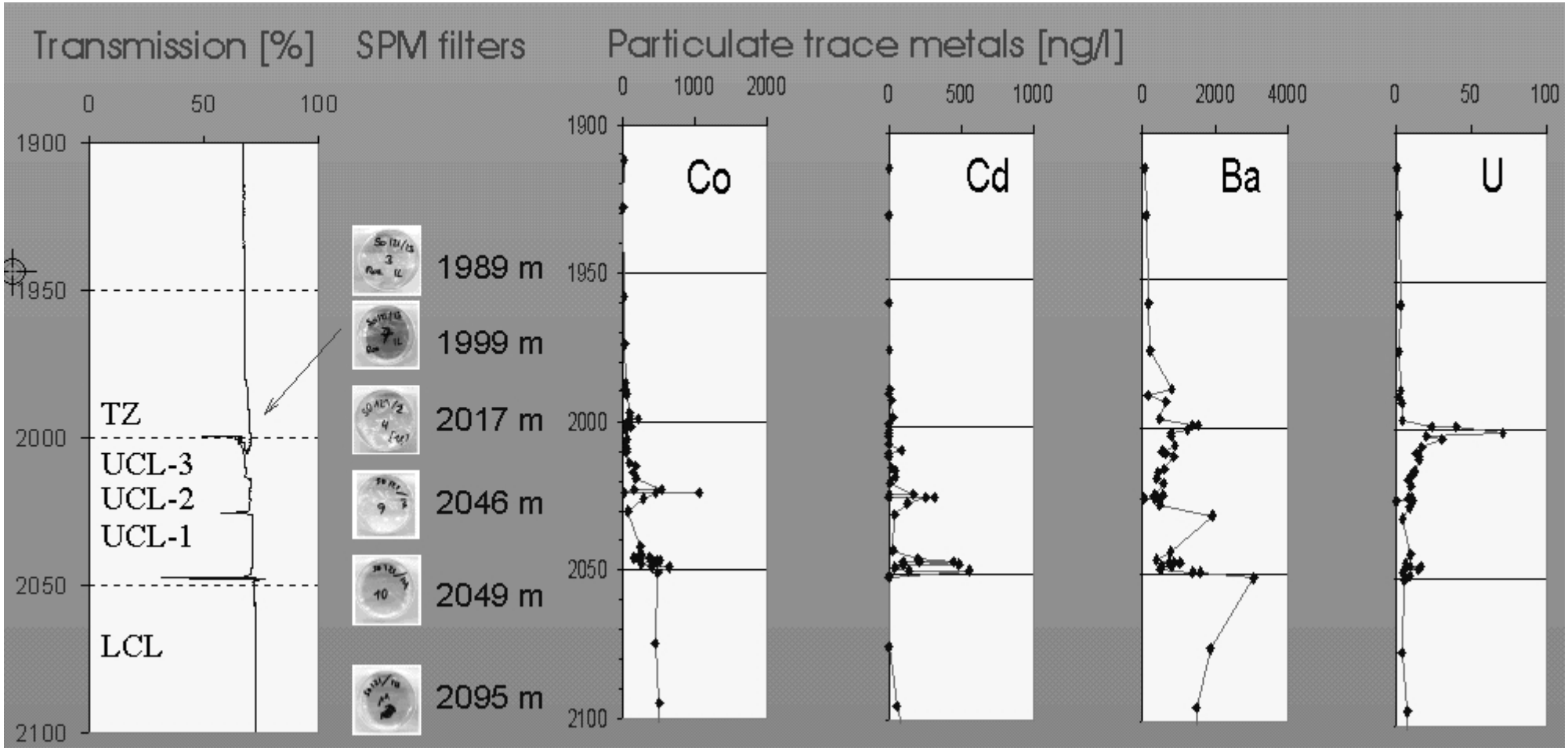

6. Direct determination of trace elements in seawater by sector-field HR-ICPMS using a micro-nebulizer and membrane desolvation.

C.-Dieter Garbe-Schönberg, Thomas Arpe, Petra Krause, Bettina Grote-Bartscher

Geologisches Institut, Universität Kiel, Olshausenstrasse 40, D-24098 Kiel, Germany
Centre for Analytical Sciences, University of Sheffield, Department of Earth Sciences, Sheffield S3 7HS, U.K.
FMS-CETAC GmbH, Hohenhainer Strasse 7, D-57258 Freudenberg

Trace metals in open ocean seawater can be analyzed by ICPMS after automated immobilized chelation ion exchange [1, 2, 3] or liquid-liquid [3] trace-matrix separation and pre-concentration procedures and/or flow-injection techniques. Only a few elements - e.g. Mo, U - can be directly determined by (ID-) ICPMS. However, matrix separation and pre-concentration procedures are relatively labour-intensive and time consuming and inherently bear the risk for contamination and poor recovery.

The direct determination of trace metals is hampered by the high matrix content of seawater leading to physical interferences like e.g. cone clogging, and to numerous severe polyatomic ion interferences originating from matrix components like Na, Mg, Cl, SO_4. Sample dilution or application of flow-injection techniques will overcome some of these problems but, consequently, many trace elements will then be found below actual detection limits, and this holds true if HR-ICPMS instruments are used. With HR-ICPMS most of the matrix interferences can be resolved but due to a loss of transmission with higher mass resolution detection limits are not sufficient for some elements .

Dry aerosols from desolvating sample introduction systems are characterized by higher transport and ionisation efficiencies leading to a significant signal enhancement for many elements with most ICPMS instruments. The improved detection limits may compensate for the loss of analyte concentration in diluted seawater. Moreover, solvent removal of the desolvated aerosol diminishes polyatomic interferences from solvent components. In addition, matrix species which can be transferred into the vapour and gas phase of the heated aerosol (e.g. Cl, F in their mineral acids and

in acidified samples) are significantly reduced. This effect may reduce the need of high mass resolution for the determination of elements like As in seawater.

This study focuses on the application of a micro-concentric nebulizer with membrane desolvation (Cetac MCN 6000) coupled to a double-focusing sector-field HR-ICPMS (Micromass PlasmaTrace2) for the direct determination of trace elements in 20fold diluted seawater and river water as well as 200fold diluted brines from the Red Sea. During careful parameter optimization (nebulizer gas flow, nitrogen admixture, argon sweep gas flow, ICP gas flows, ion otics) two optima for the argon sweep gas flow were found depending if nitrogen was added or not. Finally, no nitrogen was added avoiding the generation of new interferences from nitrogen polyatomics. Under optimized conditions oxide formation rate was reduced to $LaO^+/La^+<0.03\%$, and doubly charged ions (Ba^{2+}/Ba^+) were < 0.4 %. In acidified seawater Cl^+ abundances and Cl polyatomic ions ($ArCl^+$, Cl_2^+) were significantly reduced opening chances for a determination of e.g. Cr, V, As in low mass resolution.

The instrument signal enhancement under these conditions was factor 3 (Co) to 20 (U, Th) with >1 GHz count rate for 1 ppm Th. Instrumental detection limits (3sigma blank) for several elements were in the low pg l^{-1} range. The detection limit for the determination of As in high resolution mode (10,000 $\Delta M/M$) was 10 ng l^{-1}.

Compared to conventional spray chamber nebulization where large surface areas are in contact with the wet aerosol, memory effects and wash out times are reduced with dry aerosol sample introduction systems. Active sample uptake with a peristaltic pump and the microconcentric nebulizer was 60 to 100 µl. Passive sample uptake by the free aspirating nebulizer was found to be not stable over long periods. This must be ascribed to the high content of total dissolved solids of the diluted seawater (0.15%).

Quantitative results will be shown for As, Ba, Cd, Cr, Co, Cu, Fe, Mn, Mo, Ni, Pb, Sb, U, V, and Zn in international standard reference materials NASS-4 (Open ocean seawater) and SLRS-3 (River water) and in brines from the Red Sea.

[1] Beauchemin, D. and Berman, S.S., *Anal. Chem.*, 1989, **61**, 1857.

[2] Garbe-Schönberg, C.-D., Bruhn, R. and Michaelis, M., *ICP Information Newsl*, 1993, **18**, 769

[3] Hall, G. E., Vaive, J. E. and Pelchat, J.-C., J Anal Atom Spectrom, 1996, **11**, 779

[4] Kremling, K., In: Grasshoff, K., Ehrhardt, M., Kremling, K. (Eds.*) Methods of seawater analysis*. Verlag Chemie, 1983,189

7. Origin of hydrocarbon trace gases in brine-filled Red Sea deeps

M. Schmidt[1], E. Faber[2], R. Botz[1], J. Poggenburg[2], M. Schmitt[3], P. Stoffers[1]

[1] Geologisch-Paläontologisches Institut, Universität Kiel, Olshausenstr. 40-60, D-24118 Kiel
[2] Bundesanstalt für Geowissenschaften und Rohstoffe, Stilleweg 2, D-30655 Hannover
[3] Geochemische Analysen, Glückaufstr. 50, D-31319 Sehnde-Ilten

Introduction

Gas composition of marine seawater in hydrothermal active areas, especially hydrocarbon trace gases gives information about fluid input e.g. mantle emanation (Welhan and Craig, 1988), about their sources and further degradation (e.g. bacterial methanogenesis and oxidation, Whiticar, Schoell and Faber, 1986). During Meteor cruise 1995 high concentrations of methane were recognized in Red Sea brines which fill several local depressions in the Red Sea graben like Atlantis II and Discovery deep (The hydrographic situation is shown in the following sketch). First isotopic investigations gave evidence for bacterial methane oxidation in brine/seawater interfaces (Faber et al., 1998). High resolution sampling of brine interfaces during Sonne cruise 121 should provide a better understanding of brine gas reservoir, the exchange with overlying sea water and bacterial degradation processes.

Sketch of hydrographic situation in Red Sea deeps

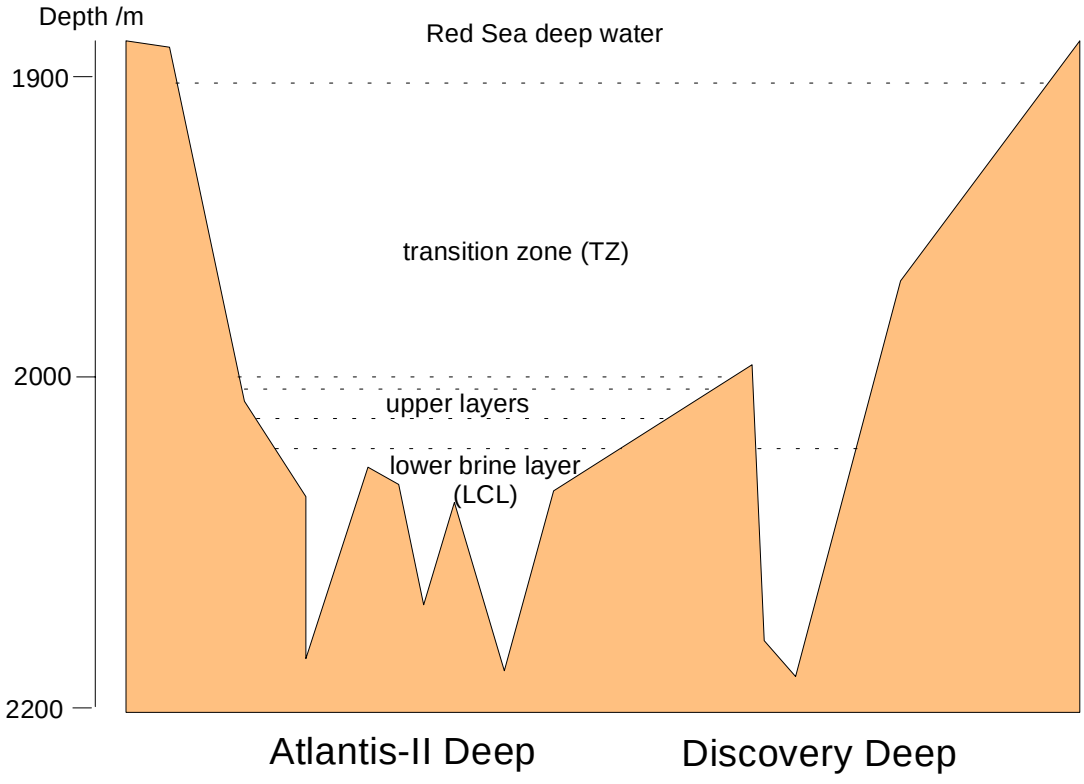

Sampling and Methods

Water columns of Red Sea Atlantis II-SW, Atlantis II-N, Discovery and Kebrit-Deep were sampled with Hydrobios-Water-Sampler. Insitu-sampling was performed using 5l Niskin (PE) bottles and the stainless steel gastight "Schmitt-Schöpfer". Temperature, sound velocity, transmission and pressure were measured by CTD (Fa. ME). Seawater-/brine samples were degassed onboard using ultrasonic-/vacuum extraction (Schmitt et al., 1991). Gas samples were stored in glass bottles for further stable isotope ratio ($^{13}C/^{12}C$, $^{18}O/^{16}O$, D/H) measurements (Finnigan MAT 252 IRMS). Gas compositions were determined by GC-analyses (DANI Gaschromatograph, Al_2O_3/KCl-column, FID-Detector, N_2/H_2-carrier gas) on board.

Results and Discussion

High resolution (depths intervals of 5m) gas measurements show significant increase of methane from Red Sea Water to hypersaline brine in the investigated deeps. Methane concentrations vary from 10^1nl/l in surface waters to 10^3nl/l in the transition zones and up to 10^7nl/l in brine layers. Highest concentrations were measured in the lower brine layers (LCL) between 24µl/l (Discovery deep) and 150µl/l (Atlantis-II deep) and 14ml/l (Kebrit deep).

Small amounts of ethane and higher hydrocarbons were detected in brine samples and calculated ratios of methane to higher HC's (C_1/C_{2+}) indicate a thermogenic origin of the hydrocarbon gases (Tab. 1).

Tab.1: LCL-brine samples of Red Sea deeps

deeps	max. depth	temperature	Salinity	PH	C1/C2	$\delta^{13}C$ (CH_4)	$\delta^{13}C$(C_2H_6)	δD (CH_4)
	(m)	(°C)	(NaCl g/l)			(‰ PDB)	(‰ PDB)	(‰ SMOW)
Atlantis-II (SW)	2065	67,1	260	5,03	48	-16,2	-18,9	
Atlantis-II (N)	2065	64,4	264	4,98	54	-16,1	-17,6	-84
Discovery	2085	45,0	260	6,92	105	-7,0		
Kebrit	1514	23,4	263	5,5	53	-22,4	-11,3	-141

Furthermore, methane concentrations vary slightly in brine bodies related to brine layer structures (Fig. 1a-c).

$^{13}C/^{12}C$ composition of CH_4 is in the range from -22,4 to -7,0‰ which is more positive than thermal methane isotope signature probably reflecting the extent of oxidation by metalliferous sediments (Kiyosu, 1989) or thermochemical sulfate reduction (Cross, 1998) rather than a major abiogenic gas

input. D/H-isotope values of methane LCL-samples of about -84‰ (SMOW) also indicate oxidation processes.

Methane concentrations decrease rapidly at brine-seawater interface (assigned by temperature curves in Fig. 1a-c) to about 100 nl/l in the transition zone (TZ). Decrease is controlled by diffusion (~50% in Atlantis-II deep by 1.Fick's law calculation) from stable convective layers to sea water and the diffusion loss of hydrocarbons is covered by further degradation process (~50%) mainly caused by bacterial oxidation (increase of $\delta^{13}C$ (CH4) to +10‰ and +49‰ and decrease of SO_4^{2-}concentration of about 5 mM/l in Atlantis-II deep and Discovery deep, resp).

No evidence for bacterial oxidation process was found abough H_2S-containing Kebrit brine by isotope enrichment.

Further investigation on rare gas contents of brine samples will characterize abiogenic mantle and crust contribution of fluid input to brine bodies. Hydrocarbon exchange of brines with overlying seawater will be described by diffusion-reaction modeling (Devol et al. 1984) considering methane and sulfate data.

Acknowledgments

This work was fundet by German Ministry for Education, Science, Research and Technology (BMBF) through grant no. 03G0121A to Kiel University.

References

Cross, M. M., Manning, D. A. C., Champness, P. E., Worden, R. H., Boltrell, S. H. (1998). Experimental and isotopic determination of the kinetics and mechanisms of Thermochemical Sulphate Reduction (TSR) reactions at reservoir conditions of pressure and temperature. *Mineralogical Magazine* **62A**: 358 - 359.

Devol, A. H., Anderson, J. J., Kuivila, K., Murray, J. W. (1984) A model for coupled sulfate reduction and methane oxidation in the sediments of Saanich Inlet. *Geochim. Cosmochim. Acta* **48**, 993-1004.

Faber, E., Botz, R. Poggenburg, J., Schmidt, M., Stoffers, P. and Hartmann, M.(1998). Methane in Red Sea brine waters. *Org. Geochem.* **29**, 363-379.

Kiyosu, Y., Krouse, H. R. (1989) Carbon isotope effect during abiogenic oxidation of methane. *EPSL* **95**, 302-306.

Schmidt, M., Faber, E., Botz, R., Poggenburg, J., Schmitt, M., Stoffers, P. (1998) Origin of hydrocarbon trace gases in brine-filled Red sea deeps. *Mineralogical Magazin* **62A**, 1347-1348.

Schmitt, M., Faber, E., Botz, R. and Stoffers, P. (1991) Extraction of methane from seawater using ultrasonic vaccum degassing. *Anal. Chem.* **63**, 529-532.

Welhan, J. A. and Craig, H. (1983) Methan, hydrogen and helium in hydrothermal fluids of 21°N on the East Pacific Rise. In: P. A. Rona, K. Boström, L. Laubier and K. L. Smith, Jr. (Editors), *Hydrothermal Processes at Seafloor Spreading Centers.* Plenum, New York, N.Y. 391-409.

Whiticar, M. J., Faber, E. and Schoell, M. (1986) Biogenic methane formation in marine and freshwater environments: CO_2 reduction vs. acetate fermentation - isotope evidence. *Geochim. Cosmochim. Acta* **50**, 693-709.

Fig. 1a-c: Methane profiles in Red Sea deeps

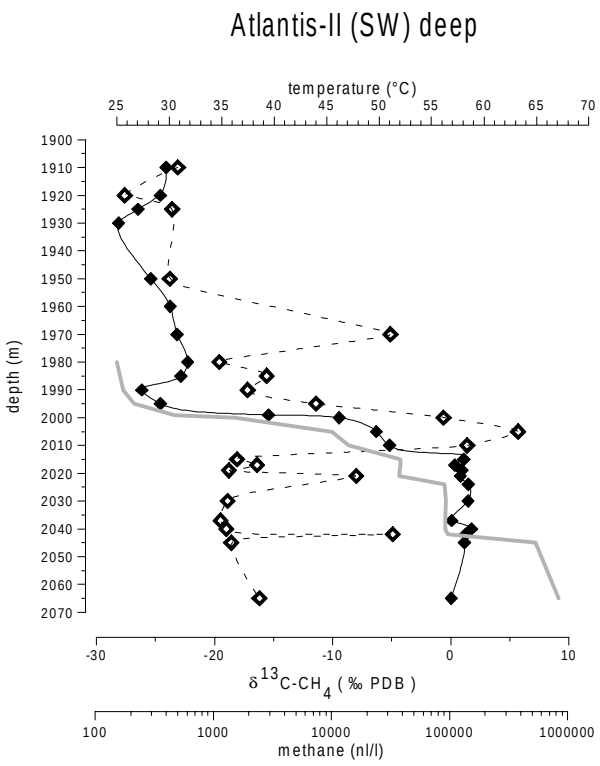

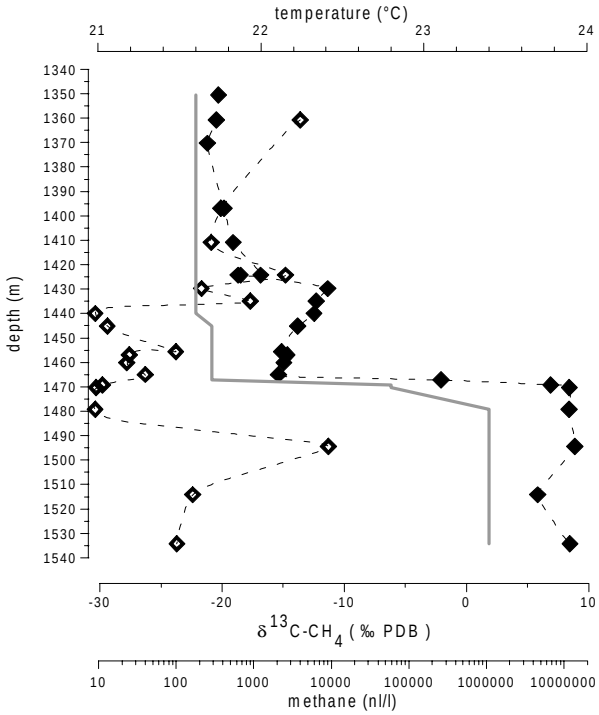

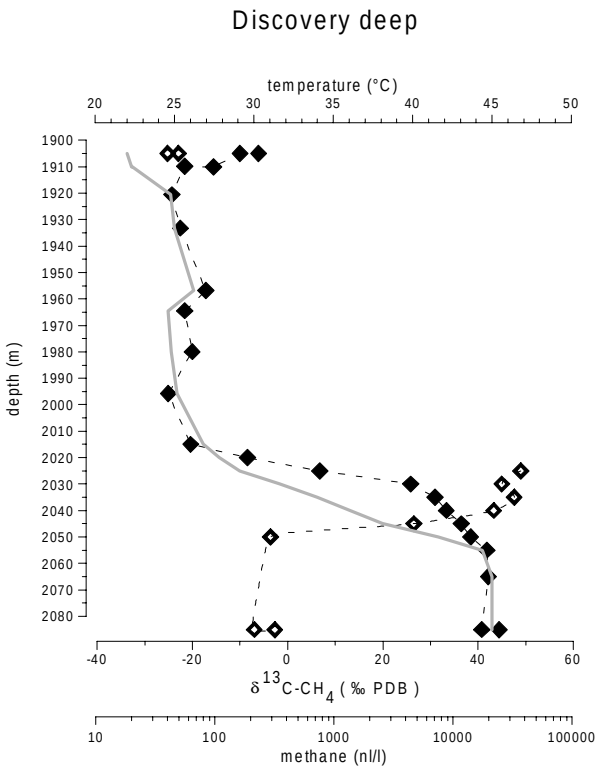

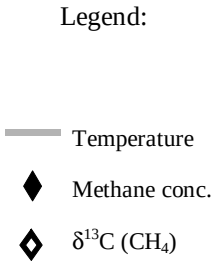

8. Sub sea floor boiling of Red Sea Brines - New indication from noble gas data

GISELA WINCKLER,[1,*] ROLF KIPFER,[2] WERNER AESCHBACH-HERTIG,[2] REINER BOTZ,[3] MARK SCHMIDT,[3] STEFFEN SCHULER,[1] REINHOLD BAYER[1]

[1] Institut für Umweltphysik, Universität Heidelberg, Im Neuenheimer Feld 229, D-69120 Heidelberg, Germany
[2] Environmental Physics, Swiss Federal Institute of Technology (ETH), Swiss Federal Institute for Environmental Science and Technology (EAWAG), CH-8600 Dübendorf, Switzerland
[3] Geologisch-Paläontologisches Institut, Universität Kiel, Olshausenstraße 40, D-24118 Kiel, Germany

1. Introduction

Since the discovery of oceanic hydrothermal activity and its impact on global cycling of chemical species, much attention has been focused on the processes that control the chemistry of hydrothermal vents. However, it is still one of the major challenges to create a model of the sub sea floor circulation and the physical processes occurring prior to injection of the hydrothermal fluid into the ocean.

The first hydrothermal field was discovered in the central rift zone of the Red Sea (Miller et al., 1966), which is presently known to contain more than 20 morphological depressions filled by highly saline brines (Hartmann et al., 1998a). The Atlantis II Deep, located on the axial zone at around 21°20'N (Fig. 1), is the most prominent depression within this unique geological environment of present submarine hydrothermal activity (Degens and Ross, 1969). Below 1900 m, it encloses a volume of about 17 km^3 and its maximum depth is 2200 m. Recently, Blanc and Anschutz (1995) have shown that the brine pool consists of four well-mixed layers, named, from bottom to top, the lower convective layer (LCL) and upper convective layers 1, 2 and 3 (UCL1, UCL2, UCL3). The hottest and saltiest brine is found in the LCL (up to 67°C, 270 $g \cdot kg^{-1}$), which is separated from the successively colder and fresher layers above by extremely sharp vertical salt and temperature gradients.

The Atlantis II brine system is interpreted as a special case of a hydrothermal field at a mid-ocean ridge. In contrast to most hydrothermal areas, its hydrothermal fluid is not only the result of seawater reacting with basalts, but it also interacts with another geochemical reservoir, the Miocene evaporites underlying the entire Red Sea. According to a generally accepted model, sea water of normal salinity penetrates into the sub surface and circulates downward through evaporites, where it becomes strongly enriched in salt. The fluid moves horizontally along fissures through the newly formed oceanic crust and interacts with the young basalts. This model is consistent with various isotopic and chemical studies (e.g., Zierenberg and Shanks III, 1986; Anschutz et al., 1995). First evidence for interaction with basalts was the strong ^{3}He-MORB-excess transported by the discharging brines (Lupton et al., 1977). Subsequently, the hot fluid rises through fractures in the crust and is injected directly into the bottom of the southwest Atlantis basin (e.g., Hartmann, 1980; Monin et al., 1981).

However, in spite of numerous investigations of the hydrographic structure and its changes (e.g., Hartmann, 1980; Anschutz and Blanc, 1996; Anschutz et al., 1998; Hartmann et al., 1998a), little is known about the fluid history during hydrothermal sub sea floor circulation. In contrast to other hydrothermal systems, the hot fluid has never been sampled directly at the discharge site. Consequently, only indirectly derived information regarding the temperature and

the formation of the brines venting into the Atlantis II Deep is available. Whereas a wide range of discharge temperatures (200°- 400°C) is reported, most authors estimate venting temperatures in excess of 330°C (e.g., Monin and Plakhin, 1982; Oudin et al., 1984; Ramboz et al., 1988; Ramboz and Danis, 1990).
In recent years, boiling and phase separation have been verified as basic processes at mid-ocean ridge hydrothermal systems, e.g., at the Juan de Fuca Ridge (Butterfield et al., 1990; Butterfield et al., 1994, Butterfield et al., 1997, Von Damm et al., 1997). Evidence comes mainly from observation of non-volatile components, primarily large salinity variations, which are assumed to be the result of boiling (e.g., Delaney and Cosens, 1982; Bischoff and Pitzer, 1985). This approach is not feasible for the Atlantis II system, because a potential chloride variation due to boiling is masked by the extremely high salt concentration of the brine which is caused by the interaction with the evaporites.
For the Atlantis II system, fluid inclusions in anhydrite recovered from a sediment core provide mineralogical evidence for boiling within the sea floor (Ramboz et al., 1988). The fluid inclusions are interpreted to be precipitated from „successive boiling brine pulses“ at trapping temperatures of 390-403 C. However, the value of this method is limited as fluid inclusions are only secondary products of hydrothermal circulation.
Here, we present a more direct approach based on noble gas data from the brine itself offering the possibility to reevaluate the hypothesis of Ramboz et al. (1988). Due to their conservative nature in geochemical systems, noble gases represent an extremely useful tool to detect processes such as phase separation and to assess their effects on the gas composition of the hydrothermal fluid. In spite of their great potential, only one study applied atmospheric noble gases as tracers to hydrothermal vents (Kennedy, 1988).
For this study, water samples taken *in-situ* in the Atlantis II brine were analyzed for their noble gas composition. The data provide a unique opportunity to directly study the sub sea floor processes associated with the formation of the Atlantis II brine and to develop a conceptual model of the evolution of the hydrothermal fluid prior to injection into the Atlantis II basin.

2. Methods

During cruise 121 of RV SONNE in 1997 water samples for noble gas analysis were collected in copper tubes using a newly developed device to seal samples under *in-situ* conditions for post-cruise tracer analysis. The new sampler (Fig. 2) is based on the construction previously described by Weiss (1968) and Jean-Baptiste et al. (1994).
The sampler is directly attached to a standard Niskin bottle (piggyback method) and recovers water samples isolated at *in-situ* pressure in copper tubing. Closing of the sampler by two tampered pins at each end of the copper tube is activated when the Niskin bottle is triggered. After the closed Niskin bottle and sampler have been recovered on board the copper tube is finally sealed by closing the standard pinch-off clamps on both ends of the sampler. This procedure of sampling under *in-situ* conditions avoids degassing losses and fractionation due to pressure relaxation on the up-cast. Therefore, the data presented here reflect the undisturbed composition of the sampled brine layers.
For the noble gas mass spectrometric analysis, the samples were quantitatively degassed on a vacuum line. After purification and separation, the noble gases were measured in two statically operated 90° sector mass spectrometers. Experimental details of the analytical procedures can be found in Beyerle et al. (1999).

3. Results

The noble gas concentrations of the brine samples are summarized in Table 1. We assume that the initial noble gas composition of the circulating fluid is that of ambient Red Sea Deep Water (RSDW, T=21.5° C, S=40.6) in solubility equilibrium with the atmosphere (Weiss, 1970; Weiss, 1971; Weiss and Kyser, 1978; Smith and Kennedy, 1983) since it is commonly assumed that the overlying water column acts as the source for fluid recharge.
All the atmospheric noble gas concentrations (except Ne of sample #67) are depleted relative to RSDW. To discuss their depletion, Fig. 3 shows the obtained noble gas signatures expressed as ratio of observed and RSDW concentrations (i.e., $C/C_0 = 1$ represents RSDW). Sample # 407, drawn from the uppermost brine layer, closely resembles RSDW, whereas #261 from UCL1 shows a moderate depletion of about 10% compared to RSDW. The noble gas concentrations of the second sample from UCL1, #67, are significantly higher than those of #261, probably indicating a contamination by a small amount of air during the analytical procedure. The strongest depletion was observed for the three LCL samples #399, #357 and #385 obtained from different sub-basins of the Atlantis II Deep. Here, the noble gas concentrations were found to be 73-80 % of those expected for RSDW.
Accompanying helium and argon isotope analyses show extremely high helium enrichments as well as elevated $^{3}He/^{4}He$ and $^{40}Ar/^{36}Ar$ ratios which reflect the acquisition of a strong MORB signal. The strongest ^{3}He enrichment (up to a factor of 3200 with respect to RSDW) and highest argon isotope anomaly were observed in the LCL. The implications of these data in relation to mantle geochemistry will be discussed elsewhere.

4. Discussion

We focus on the noble gases of atmospheric origin (Ne, Ar_{atm}, Kr, Xe) and on the depletion effect observed in the Lower Convective Layer (LCL) which is thought to represent the hydrothermal fluid discharging into the Deep. The upper brine layers are generally explained as mixtures between the original hydrothermal fluid and RSDW (e.g., Hartmann, 1985). In the LCL, the noble gas concentrations were found to be ca. 73-80% of those expected for RSDW, without significant fractionation between the individual noble gases.
In the following, we discuss different processes which might have caused the observed depletion relative to the atmospheric signature of RSDW.
(1) None of the observed noble gas signatures in the brine layers can be interpreted as resulting from solubility equilibration with the atmosphere. For illustration, the equilibrium noble gas concentrations for the actual LCL brine conditions (67°C, 260 $g \cdot kg^{-1}$) are given in Table 1 and plotted in Fig. 3. They are significantly lower than the observed noble gas concentrations in the brine layers. Even more important, they show a significant fractionation relative to RSDW concentrations with the depletion increasing from Ne to Xe.
(2) Salt induced diffusion (Suckow and Sonntag, 1993) cannot be responsible for the noble gas loss because diffusive processes would lead to significant fractionation between the noble gases which is not observed.
(3) Degassing of the brines during sampling can be excluded as the copper tubes were closed under *in-situ* conditions preventing any contact with the atmosphere (see methods).
As these three potential processes can be ruled out, another process must be responsible for the observed gas loss relative to RSDW.

4.1 The boiling hypothesis

We propose that the observed depletion is the result of a boiling process and associated phase separation between a gas and a liquid phase. Red Sea deep water penetrates into the sea floor

and circulates through the hydrothermal system where it is heated and enriched in non-atmospheric noble gases, i.e., ^{3}He, ^{4}He and ^{40}Ar of mantle origin. As the hot fluid ascends it gradually reaches depth levels of lower hydrostatic pressure, causing it to boil and separate into a vapour phase and a residual liquid phase. The noble gases will preferentially partition into the lower density phase and consequently, the residual liquid phase is expected to be depleted in absolute gas concentrations relative to the pre-boiling liquid.

4.2 The boiling model

In order to evaluate this boiling hypothesis, we make an attempt to reconstruct the fluid's history. We present a simple boiling model which describes the partitioning of gases between the liquid and vapour phase and cross check its predictions with the data.
In principle, partitioning can be described by Henry's law. Two modes of phase separation may occur: (a) single-stage or (b) Rayleigh fractionation. Briefly, in a single-stage process, the vapour and liquid phases always remain in contact as the system evolves (closed system). In a Rayleigh process, the vapour is continuously removed from the liquid as boiling proceeds. The approach follows that of Mazor and Truesdell (1984) who applied these processes to a continental geothermal system.
For either system, the residual concentration of gas in the liquid phase can be calculated as a function of the boiling degree, for a single-stage separation

$$\frac{C_l}{C_0} = \frac{1}{F + \frac{1-F}{A}} \tag{1}$$

and for a continuous separation by

$$\frac{C_l}{C_0} = F^{(\frac{1}{A}-1)} \tag{2}$$

where C_l/C_0 is the ratio of the noble gas concentration in the remaining liquid to that in the initial one, F is the fraction of water remaining in the liquid phase after the fraction B:=1-F has been converted to vapour (in the following B is referred to as the degree of boiling), and A is the distribution coefficient C_{liquid}/C_{vapour}. The distribution coefficients are calculated from the Henry's Law constants K_H using the equation given by Ellis and Mahon (1977)

$$A = \frac{R\,T}{K_H\,V_{sp}} \tag{3}$$

where R is the gas constant, T the absolute temperature and V_{sp} the specific volume of vapour.
This model requires the knowledge of the solubilities. As there are very little experimental data on noble gas solubilities at high temperatures and pressures (Himmelblau, 1960; Potter II and Clynne, 1978; Crovetto et al., 1982), the quantitative assessment of the degree and exact process of phase separation is limited. In this study, we used the solubility data as given by Crovetto et al. (1982) for the temperature range of 30 to 330°C. Solubilities for temperatures up to 390°C were obtained by extrapolating their empirical equations. This causes uncertainties in the Henry's Law constants of as much as 40 %. An additional uncertainty arises because the „salting out effect" (i.e., lowering of the solubility due to addition of salt) is only known for temperatures below 60°C. According to Smith and Kennedy (1983) further extrapolation of the noble gas-brine solubility data is not feasible. Therefore, we refer to the extrapolated fresh water solubilities without corrections for salt effects.

It is important to state here that in spite of the uncertainties of noble gas solubility data at high temperatures the above cited experimental studies by Himmelblau (1960), Potter II and Clynne (1978) and Crovetto et al. (1982) agree in two main aspects
(a) whereas at low temperatures the noble gases are relatively insoluble, the noble gas solubilities increase (the Henry's Law constants decrease) rapidly with temperature by more than one order of magnitude
(b) whereas at low temperatures the solubilities are strongly element dependent, the solubilities for the different noble gases converge at high temperatures (> 550°C)
The initial boiling temperature can be estimated using the two-phase boundary curves for the system NaCl-H_2O derived by Bischoff and Pitzer (1985). In contrast to open ocean hydrothermal systems supercritical conditions do not have to be considered because the presence of large salt concentrations strongly elevates the critical point for the brine considered (540°C, 700 bar) relative to the critical point of pure sea water (407°C and 298.5 bars, (Bischoff and Rosenbauer, 1988)). In our model, the boiling temperature is taken to be 390°C, in agreement with fluid inclusion data by Ramboz et al. (1988).
We are fully aware of the uncertainties of the input parameters of our conceptual model. Nevertheless it allows us to determine the effect of phase separation and to study the basic features of the general trend of the noble gas evolution. Using Ne and Xe as examples, Fig. 4 shows the depletion of the atmospheric noble gases relative to the initial RSDW composition as a function of the boiling degree B for phase separation under closed and under open system conditions. Figure 4 clearly illustrates that there are - especially for low boiling degrees - only slight differences between the two scenarios and between the different noble gases, respectively.

4.3 Comparison of model results and observed noble gas patterns

4.3.1 Lack of mass-dependent fractionation

The model illustrates that the measured depletion pattern, namely the absence of a systematic mass-dependent fractionation pattern, is consistent with a boiling scenario at high temperatures where noble gas solubilities converge.

4.3.2 Extent of boiling

Our boiling model can be used to estimate the degree of boiling which is necessary to create the depletion observed in the LCL. The mean depletion of the Neon and Xenon concentration (C/C_0) of the three samples from the LCL is 0.73 and 0.81, respectively. In Fig. 4 the degree of boiling is given by the intersection with the depletion curves obtained from the model. The consistency of the two noble gas species is striking. For closed system conditions a boiling degree of 3.2 % (Ne) and 3 % (Xe) is obtained, for open-system conditions we find a boiling degree of about 2.6 % (Ne, Xe). This implies that a boiling process with about 3 % of the fluid converted to vapour - regardless of the mode of boiling - produces a residual fluid with an atmospheric noble gas depletion of about 25 % as observed in the LCL brine.
Compared to the 15-20 % boiling which has been suggested for oceanic hydrothermal fields at the Juan de Fuca Ridge (Butterfield et al., 1990) the boiling degree of 3 % reported here is significantly lower. Obviously, the Atlantis II brine system represents a relatively early stage of boiling, similar to those observed at continental geothermal systems of Wairakei, New Zealand (Mazor and Bosch, 1990) and in Mexico (Mazor and Truesdell, 1984).

4.3.3 Dilution trend

All noble gas ratios show a significant linear correlation indicating a mixture of two components. In Fig. 5, the Ar/Xe versus Kr/Xe ratio is shown as an example. In addition, we observe an anti-correlation between the atmospheric noble gases (Ne, Ar_{atm}, Kr, Xe) and the MORB-derived He concentration as we move up the water column through the brine layers (see Table 1). Since the boiling process occurs subsequent to the accumulation of the non-atmospheric signal and affects atmospheric and non-atmospheric noble gases alike, the observed anti-correlation excludes that the individual samples reflect different stages of boiling and also points to a two-component mixing: The residual liquid after boiling - the LCL endmember - which is still marked by a high MORB-^{4}He signal and strong depletion of the atmospheric noble gases is subsequently diluted with a RSDW-type component.

4.4 Evolution of the hydrothermal brine

This scenario is illustrated in Fig. 6: RSDW carrying atmospheric noble gases penetrates into the sediments. During the circulation through the Miocene evaporites it becomes strongly enriched in salt. Then the brine reaches a region of high temperatures, the hydrothermally active zone above the magma chamber, where it interacts with the hot young basalt and becomes enriched in MORB-components as He and Ar. As the fluid ascends, it progressively moves into regions of lower pressure and intersects the „boiling curve“: the fluid boils and separates into two phases, a residual noble gas-depleted liquid phase and a noble gas enriched vapour phase. All noble gases, the MORB-He excess as well as the atmospheric noble gases are depleted by boiling but note that the residual fluid still shows a strong He excess. Due to only small differences in the solubilities at high temperatures the different noble gas species are depleted approximately to the same degree relative to the initial conditions. The depleted residual liquid ascends rapidly to the sea floor and discharges into the brine pool. Substantial sub surface mixing with cold percolating sea water can be largely excluded with respect to the high venting temperatures. Thus, the LCL appears to basically represent the boiled fluid, whereby the upper brine layers are formed by subsequent mixing with RSDW.

If boiling and phase separation affects the Atlantis II brine then the question arises where the noble gas-enriched phase produced by phase separation moves. In this study, we only found the depleted liquid residual to phase separation but did not observe a phase enriched in noble gases. This could be explained either by local or temporal variability. The enriched phase may be found apart from the region sampled or phase separation may be a process occurring only in episodes. Our noble gas data prove that phase separation does occur, but not if it is occurring presently.

5. Conclusions

Our data and the simulation by the model imply that atmospheric noble gases are useful in reconstructing dynamic processes like phase separation in hydrothermal systems. The mass-independent noble gas depletion pattern of the Atlantis II brine is shown to be consistent with a phase separation process occurring during the hydrothermal circulation of the brine. Our results are consistent with a boiling scenario and indicate that boiling may be an important step in the formation of the Atlantis II brine. The data confirm a previous hypothesis of boiling in the Atlantis II brine system which was based on fluid inclusions (Ramboz et al., 1988). Furthermore, we conclude that the Red Sea brines are another oceanic hydrothermal system, in addition to the vent systems at sediment-free ridges, where boiling and phase separation play a key role in controlling the hydrothermal chemistry.

Acknowledgements - The authors thank U. Menet for preparing the drawing of the *in-situ* sampler. We also thank P. Schlosser, M. Stute and an anonymous reviewer for thoughtful comments which significantly improved the manuscript.

Table1. Noble gas composition of the brine samples

Sample	layer	depth	T [a]	Salinity [a]	N	He	Ne	Ar* [b]	Kr	Xe
						$[10^{-8}]$	$[10^{-7}]$	$[10^{-4}]$	$[10^{-8}]$	$[10^{-9}]$
		m	°C			$cm^3 \cdot g^{-1}$ (STP)				
407	Atlantis	2005	45.1	90	0.95	315	1.34	2.28	4.95	6.61
261	Atlantis	2024	56.4	147	0.89	626	1.32	2.19	4.82	6.53
67	Atlantis	2042	56.4	147	0.89	655	1.54	2.33	5.01	6.45
385	Atlantis LCL	2070	67.2	260	0.78	1240	1.01	1.79	3.98	5.44
357	Discovery	2085	45	260	0.78	1210	1.07	1.81	3.94	5.28
399	Atlantis LCL	2145	67.2	260	0.78	1260	1.12	1.85	4.02	5.47
	RSDW [c]		21.5	40.6	1	3.613	1.458	2.316	5.069	6.645
	LCL_{eq} [c]		67	260	0.78	1.143	0.412	0.355	0.566	0.553

To correct for the large salinity variation between the individual brine layers, the noble gas concentrations are reported as cm^3 STP per g RSDW. The measured noble gas concentrations in cm^3 STP per g brine were divided by the layer specific normalization factor N which is the mass fraction of RSDW in the brine.
The accuracy of the noble gas concentrations is ± 1% for He, Ne, Ar, Kr and ± 1.8 % for Xe.
[a] temperature and salinity data are from Hartmann et al. (1998a, 1998b).
[b] Ar* denotes the atmospheric Ar concentration after correcting for the amount of radiogenic Ar (≤ 3 %) present as indicated by the enhanced $^{40}Ar/^{36}Ar$ ratios (up to 305).
[c] RSDW and LCL_{eq} concentrations are determined as equilibrium concentrations for given T and salinity.

Figure captions

Fig.1 Location and bathymetric map of the Atlantis II Deep area after Anschutz and Blanc (1996).

Fig.2 Schematic drawing of one closing mechanism of the newly developed *in-situ* sampler. The spring is tensioned by a tripping lever that is connected to the trigger of the Niskin bottle. When the lever is tripped, the spring is released and the tampered pin seals the copper tube tightly. After recovery of the *in-situ* sampler, the copper tube is finally sealed by standard pinch-off clamps.

Fig.3 Atmospheric noble gas composition (Ne, Ar_{atm}, Kr, Xe) normalized to noble gas concentrations C_0 in RSDW. The samples were taken in different brine layers of the Atlantis II system, the Lower Convective Layer (LCL), the Upper Convective Layer 1 (UCL1) and the Upper Convective Layer 3 (UCL3). All atmospheric noble gases are depleted with respect to RSDW (except Ne of #67) without significant fractionation. For comparison, the noble gas concentrations determined for equilibrium conditions with actual LCL temperature (67°C) and salinity (260 $g \cdot kg^{-1}$) are added. These concentrations are much lower than those observed and show a stronger fractionation.

Fig.4 Model results, ratio of noble gas concentration in the residual fluid to initial RSDW noble gas concentration as a function of the boiling degree; depletion curves are shown for Ne (solid line) and Xe (dashed line), and for the two different processes, closed system conditions (thin) and open system conditions (Rayleigh, bold). Horizontal lines give the Ne and Xe depletion of the LCL (determined as mean values of the three samples) and intersect the depletion curves at the boiling degree of about 3-3.2 % for closed system conditions (thin) and 2.6 % for open system conditions (bold) as indicated by the vertical arrows.

Fig.5 Ar/Xe vs. Kr/Xe plot for the brine samples and RSDW. The linear correlation indicates a mixing trend of depleted LCL and RSDW.

Fig.6 Conceptual model of the evolution of the brine prior to injection into the Atlantis II Deep (see text).

References

Anschutz P. and Blanc G. (1996) Heat and salt fluxes in the Atlantis II Deep (Red Sea). *Earth Planet. Sci. Lett.* **142**, 147-159.

Anschutz P., Blanc G., and Stille P. (1995) Origin of fluids and the evolution of the Atlantis II deep hydrothermal system, Red Sea: Strontium isotope study. *Geochim. Cosmochim. Acta* **59**, 4799-4808.

Anschutz P., Turner J. S., and Blanc G. (1998) The development of layering, fluxes through double-diffusive interfaces, and location of hydrothermal sources of brines in the Atlantis II Deep: Red Sea. *J. Geophys. Res.* **103** (C12), 27809-27819.

Beyerle U., Kipfer R., Imboden D. M., Baur H., and Graf T. (1999) A mass spectrometric system for the analysis of noble gases from water samples. *Environ. Sci. Technol.*, in press.

Bischoff J. L. and Pitzer K. S. (1985) Phase relations and adiabats in boiling seafloor geothermal systems. *Earth Planet. Sci. Lett.* **75**, 327-338.

Bischoff J. L. and Rosenbauer R. J. (1988) Liquid-vapor relations in the critical region of the system NaCl-H_2O from 380 to 415°C: A refined determination of the critical point and two-phase boundary of seawater. *Geochim. Cosmochim. Acta* **52**, 2121-2126.

Blanc G. and Anschutz P. (1995) New stratification in the hydrothermal brine system of the Atlantis II Deep, Red Sea. *Geology* **23**, 543-546.

Butterfield D. A., Massoth G. J., McDuff R. E., Lupton J. E., and Lilley M. D. (1990) Geochemistry of hydrothermal fluids from Ashes Vent Field, Axial Seamount, Juan de Fuca Ridge: Subseafloor boiling and subsequent fluid-rock interaction. *J. Geophys. Res.* **95** (B8), 12895-12921.

Butterfield D. A., McDuff R. E., Mottl M. J., Lilley M. D., Lupton J. E., and Massoth G. J. (1994) Gradients in the composition of hydrothermal fluids from the Endeavour segment vent field: Phase separation and brine loss. *J. Geophys. Res.* **99** (B5), 9561-9583.

Butterfield D.A., Jonasson I.R., Massoth G.J., Feely R.A., Roe K.K., Embley R.E., Holden J.F., McDuff R.E., Lilley M.D., and Delaney J.R. (1997) Seafloor eruptions and evolution of hydrothermal fluid chemistry. *Phil. Trans. R. Soc. Lond. A* **355**, 369-386.

Crovetto R., Fernández-Prini R., and Japas M. L. (1982) Solubilities of inert gases and methane in H_2O and D_2O in the temperature range of 300 to 600K. *J. Chem. Phys.* **76**, 1077-1086.

Degens F. T. and Ross D. A. (1969) *Hot brines and recent heavy metal deposits in the Red Sea*. Springer-Verlag.

Delaney J. R. and Cosens B. A. (1982) Boiling and metal deposition in submarine hydrothermal systems. *Mar. Tech. Soc. J.* **16**, 62-66.

Ellis A. J. and Mahon W. A. J. (1977) *Chemistry and geothermal systems*. Academic Press.

Hartmann M. (1980) Atlantis II Deep geothermal brine system. Hydrographic situation in 1977 and changes since 1965. *Deep-Sea Res.* **21**, 161-171.

Hartmann M. (1985) Atlantis II Deep geothermal brine system. Chemical processes between hydrothermal brines and Red Sea Deep water. *Mar. Geol.* **64**, 157-177.

Hartmann M., Scholten J. C., Stoffers P., and Wehner F. (1998a) Hydrographic structure of brine-filled deeps in the Red Sea: new results from the Shaban, Kebrit, Atlantis II and Discovery Deep. *Mar. Geol.* **144**, 311-330.

Hartmann M., Scholten J. C. and Stoffers P. (1998b) Hydrographic structure of brine-filled deeps in the Red Sea: correction of Atlantis II deep temperatures. *Mar. Geol.* **144**, 331-332

Himmelblau D. M. (1960) Solubilities of inert gases in water: 0°C to near the critical point of water. *J. Chem. Eng. Data* **5**, 10-15.

Jean-Baptiste P., Messias M. J., Alba C., Charlou J. L., and Bougault H. (1994) A simple copper-tube sampler for collecting and storing seawater for post-cruise CFC measurements. *Deep-Sea Res.* **41**, 1361-1372.

Kennedy B. M. (1988) Noble gases in vent water from the Juan de Fuca Ridge. *Geochim. Cosmochim. Acta* **52**, 1929-1935.

Lupton J. E., Weiss R. F., and Craig H. (1977) Mantle helium in the Red Sea brines. *Nature* **266**, 244-246.

Mazor E. and Bosch A. (1990) The geothermal system of Wairakei, New Zealand: physical processes and age estimates inferred from noble gases. *Appl. Geochem.* **5**, 605-624.

Mazor E. and Truesdell A. H. (1984) Dynamics of a geothermal field traced by noble gases: Cerro Prieto, Mexico. *Geothermics* **13**, 91-102.

Miller A. R., Densmore C. D., Degens E. T., Hathaway J. C., Manheim F. T., McFarlin P. F., Pocklington R., and Jokela A. (1966) Hot brines and recent iron deposits in deeps of the Red Sea. *Geochim. Cosmochim. Acta* **30**, 341-359.

Monin A. S. and Plakhin E. A. (1982) Stratification and space-time variability of Red Sea hot brines. *Deep-Sea Res.* **29**, 1271-1291.

Monin A. S., Plakhin E. A., Podrazhansky A. M., Sagalevich A. M., and Sorokhtin O. G. (1981) Visual observation of the Red Sea hot brines. *Nature* **291**, 341-359.

Oudin E., Thisse Y., and Ramboz D. (1984) Fluid inclusion and mineralogical evidence for high-temperature saline hydrothermal circulation in the Red Sea metalliferous sediments: preliminary results. *Mar. Min.* **5**, 3-31.

Potter II R. W. and Clynne M. A. (1978) The solubility of the noble gases He, Ne, Ar, Kr and Xe in water up to the critical point. *J. Solution Chem.* **7**, 837-844.

Ramboz C. and Danis M. (1990) Superheating in the Red Sea? The heat-mass balance of the Atlantis II Deep revisited. *Earth Planet. Sci. Lett.* **97**, 190-210.

Ramboz C., Oudin E., and Thisse Y. (1988) Geyser-type discharge in Atlantis II Deep, Red Sea: Evidence of boiling from fluid inclusions in epigenetic anhydrite. *Can. Mineral.* **26**, 765-786.

Smith S. P. and Kennedy B. M. (1983) The solubility of noble gases in water and in NaCl brine. *Geochim. Cosmochim. Acta* **47**, 503-515.

Suckow A. and Sonntag C. (1993) The influence of salt on the noble gas thermometer. In *Isotope techniques in the study of past and current environmental changes in the hydrosphere and the atmosphere* IAEA-SM-329/64, Vienna, 307-318.

Von Damm K.L., Buttermore L.G., Oosting S.E., Bray A.M., Fornari D.J., Lilley M.D., Shanks W.C. III (1997) Direct observation of the evolution of a seafloor "black smoker" from vapor to brine. *Earth Planet. Sci. Lett.* **149**, 101-111.

Weiss R. F. (1968) Piggyback sampler for dissolved gas studies on sealed water samples. *Deep-Sea Res.* **15**, 695-699.

Weiss R. F. (1970) The solubility of nitrogen, oxygen and argon in water and seawater. *Deep-Sea Res.* **17**, 721-735.

Weiss R. F. (1971) Solubility of helium and neon in water and seawater. *J. Chem. Eng. Data* **16**, 235-241.

Weiss R. F. and Kyser T. K. (1978) Solubility of krypton in water and seawater. *J. Chem. Eng. Data* **23**, 69-72.

Zierenberg R. A. and Shanks III W. C. (1986) Isotopic constraints on the origin of the Atlantis II, Suakin and Valdivia brines, Red Sea. *Geochim. Cosmochim. Acta* **50**, 2205-2214.

Fig. 1

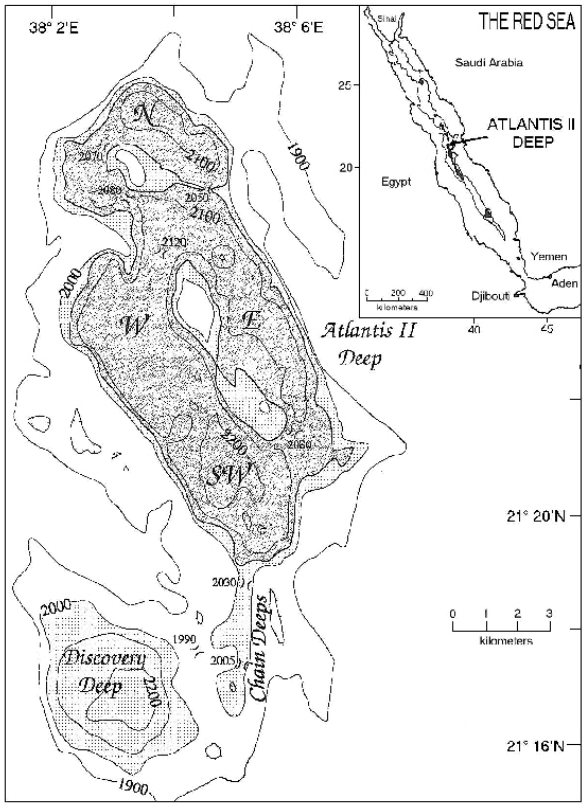
38° 2'E
38° 6'E
THE RED SEA
Saudi Arabia
ATLANTIS II
DEEP
Egypt
Yemen
Aden
Djibout
25
20
40
45
N
W
E
SW
Atlantis II
Deep
Discovery
Deep
Chain Deeps
1900
2000
2100
2120
2080
2070
2050
2030
1990
2005
21° 20'N
21° 16'N
0 1 2 3
kilometers

Fig. 2

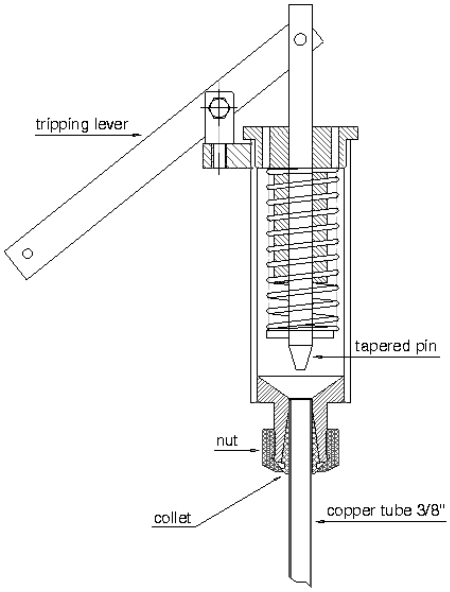

Fig. 3

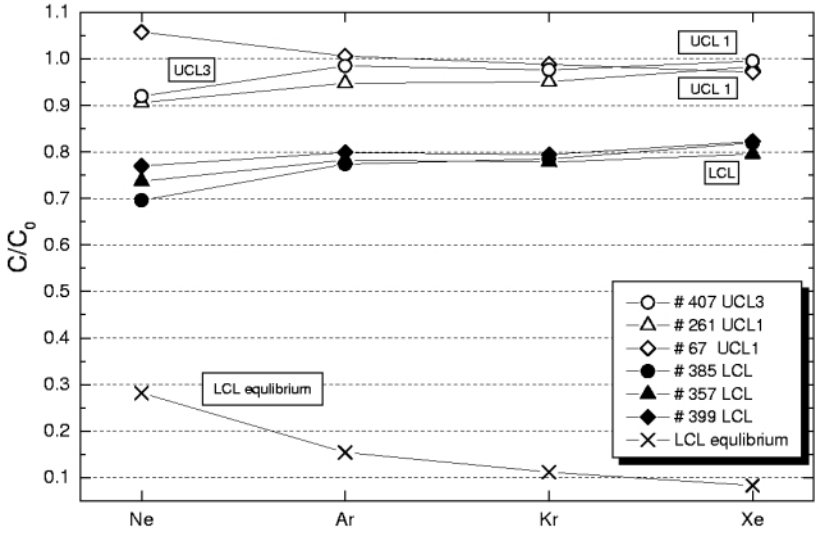
C/C0
UCL3
UCL 1
UCL 1
LCL
LCL equilibrium
407 UCL3
261 UCL1
67 UCL1
385 LCL
357 LCL
399 LCL
LCL equilibrium
Ne
Ar
Kr
Xe

Fig. 4

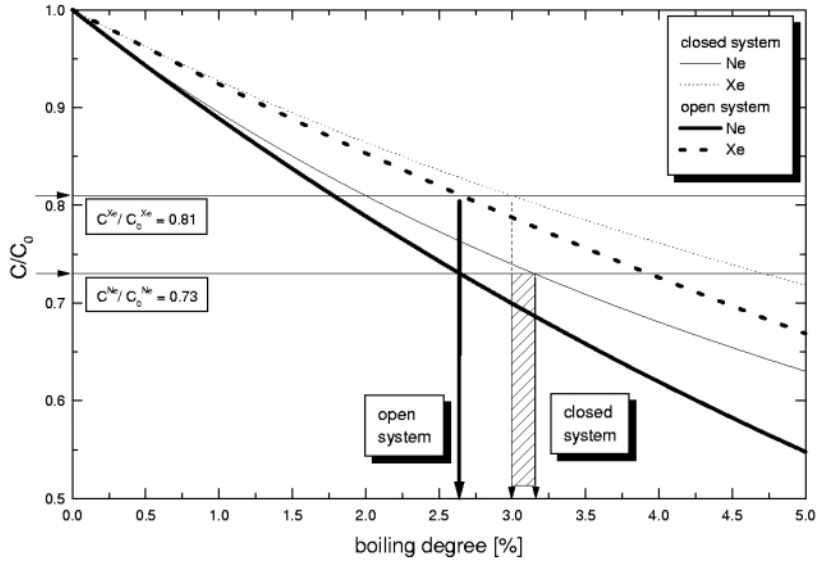
C/C0
closed system
Ne
Xe
open system
Ne
Xe
C^Xe / C0^Xe = 0.81
C^Ne / C0^Ne = 0.73
open system
closed system
boiling degree [%]

Fig. 5

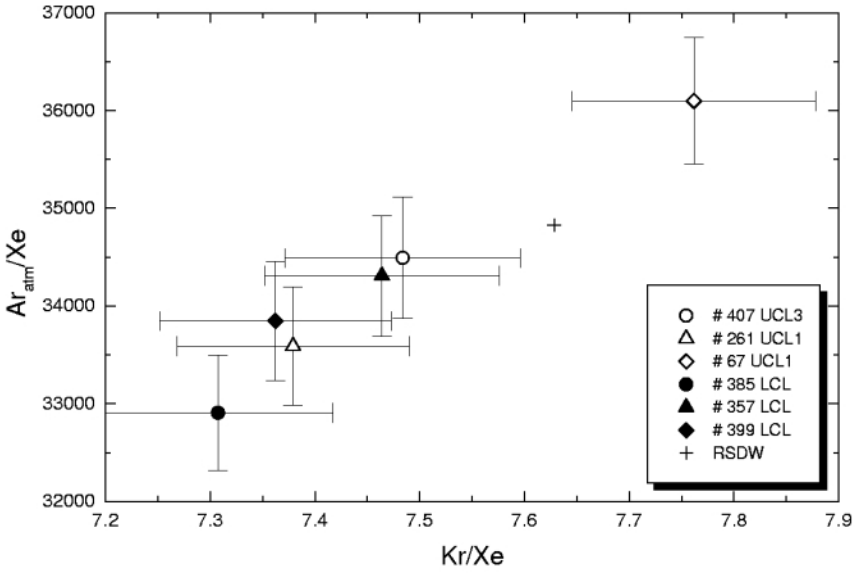
37000
36000
35000
34000
33000
32000
7.2
7.3
7.4
7.5
7.6
7.7
7.8
7.9
Ar_atm/Xe
Kr/Xe
407 UCL3
261 UCL1
67 UCL1
385 LCL
357 LCL
399 LCL
RSDW

Fig. 6

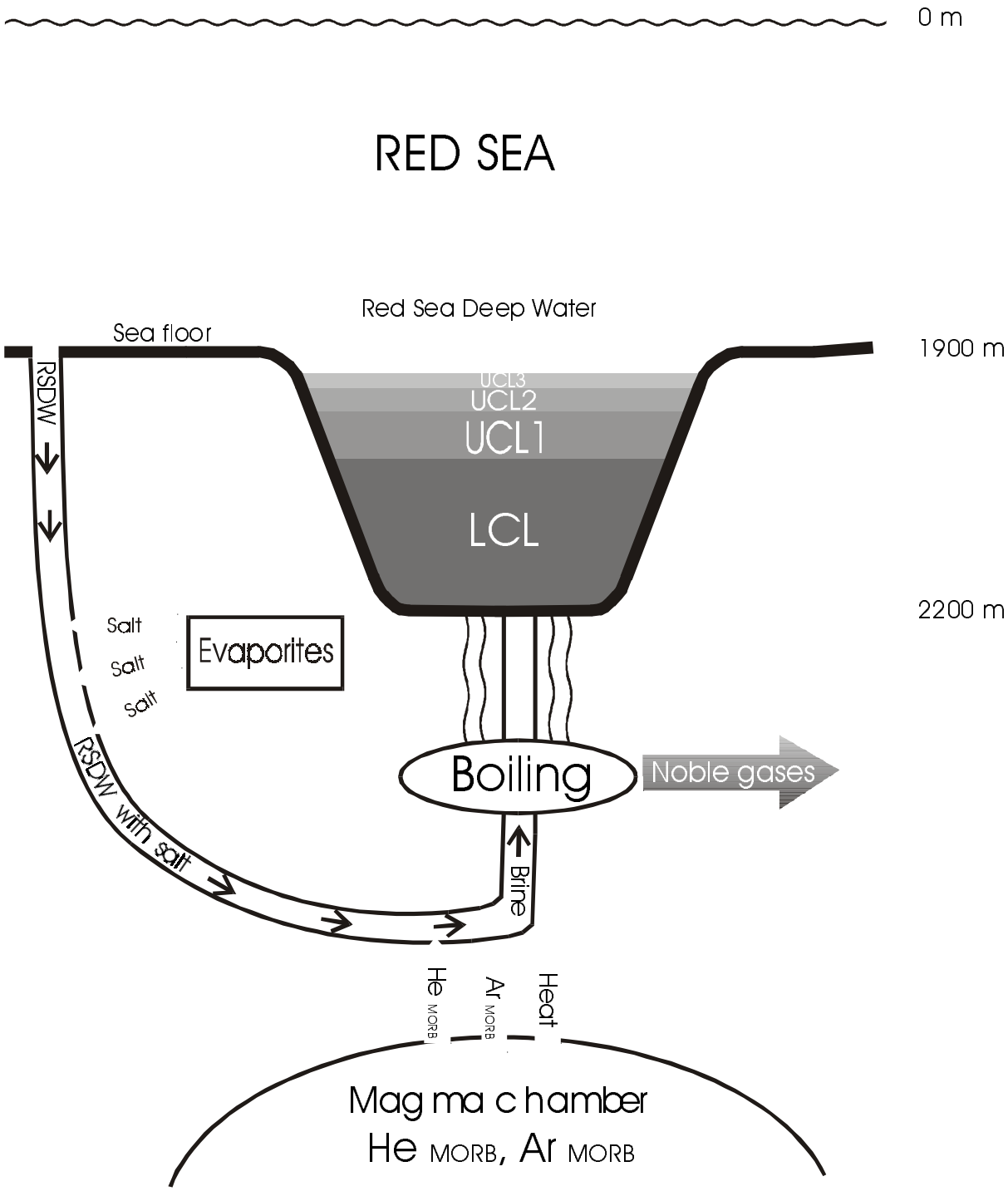
0 m
RED SEA
Red Sea Deep Water
Sea floor
1900 m
RSDW
UCL3
UCL2
UCL1
LCL
2200 m
Salt
Salt
Salt
Evaporites
Boiling
Noble gases
RSDW with salt
Brine
He MORB
Ar MORB
Heat
Mag ma c hamber
He MORB, Ar MORB

9. Geochemie der Massivsulfide aus dem Kebrit-Tief

Dietmar Schöps

Friedrich-Schiller-Universität Jena, Institut für Geowissenschaften,
Burgweg 11, 07749 Jena

Einleitung. Das Rote Meer gehört mit zu den wissenschaftlich interessantesten Nebenmeeren der Erde. Es ist das einzige Meer, in dem hydrothermale Aktivität in einem sterilen Milieu (anoxisch, heiß, salinar) auftritt und zu bedeutenden Erzablagerungen führt. Es stellt ein exzellentes Beispiel für den Übergang von einem kontinentalen zu einem ozeanischen Rift dar. Nach mehreren Riftphasen propagiert das Rote Meer seit etwa 3 Millionen Jahren langsam in Richtung Norden. Im Süden entsteht hingegen durch seafloor-spreading neue ozeanische Kruste. Die Spreizungsrate beträgt ca. 1-2 cm pro Jahr (Bäcker und Richter, 1973). Das Rote Meer gliedert sich in vier Regionen: (1) nördliche Region mit ausgedünnter kontinentaler Kruste (2) Übergangszone (3) Multi-Tief-Region (4) echte Rift-Zone mit ozeanischer Kruste aus Olivin-Tholeiiten (Abb. 1).

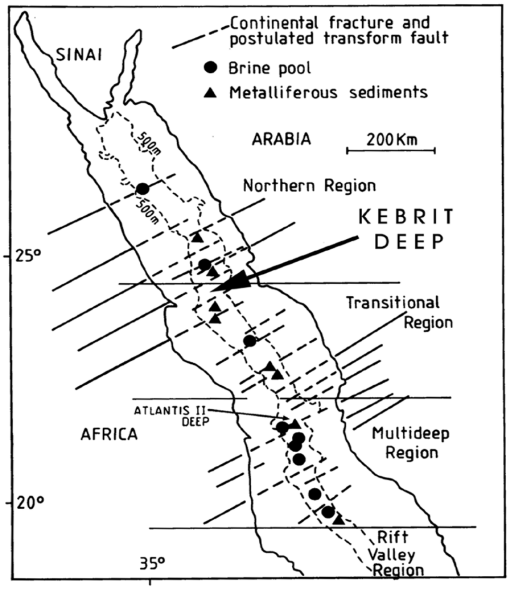

Abb. 1: Lokation des Kebrit-Tiefs im Roten Meer (modifiziert nach Bignell (1975))

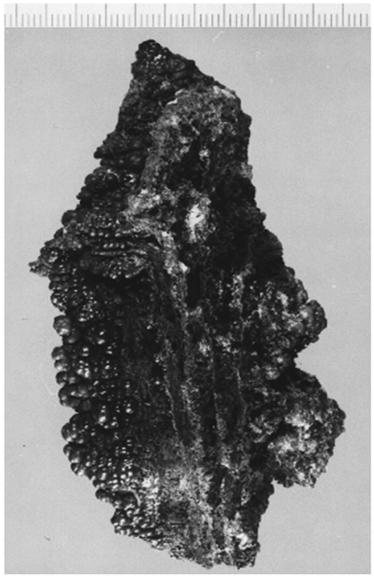

Abb. 2: Massivsulfid aus dem Kebrit-Tief

Mit zwei Expeditionen - 1995 mit FS Meteor und 1997 mit FS Sonne - wurde die insbesondere in den 60er und 70er Jahren erfolgreiche deutsche Erkundung des Roten Meeres fortgesetzt. Ziel dieser Fahrten ist u.a., den Zusammenhang zwischen Vulkanismus, Hydrothermalismus und Erzbildung im nördlichen Teil des Roten Meeres zu beleuchten. Massivsulfidfunde im

nördlich gelegenen Kebrit-Tief während SO-29 haben hierfür den Ausschlag gegeben (Blum und Puchelt, 1991).

Ergebnisse. Das Kebrit-Tief hat eine Ausdehnung von 2x2 km mit einer maximalen Tiefe von 1520 m. Es ist mit einer hochsalinaren Sole gefüllt, die bis 50 m oberhalb der maximalen Tiefe reicht. Die Meerwasser/Sole Grenze ist durch eine deutliche Farbänderung der Sedimente gekennzeichnet. Die Sedimente unterhalb der Meerwasser/Sole Grenze (anoxische Zone) erscheinen hellgrau und sind sehr feinkörnig. Im oxischen Bereich - oberhalb der Meerwasser/Sole Grenze - erscheinen die Sedimente hellbraun bis ockerfarben. Sowohl in der anoxischen als auch in den untersten ca. 30 m der oxischen Zone finden sich gelegentlich auf wenigen Quadratmetern Fläche Gruppen von inaktiven Sulfid-Chimneys (Abb. 3). Die Chimneys haben einen Durchmesser von maximal etwa 10 cm und erreichen maximal eine Höhe von 0,5 Metern. Die überwiegende Zahl der Chimneys ist kollabiert, nur selten ragen einzelne Stümpfe aufrecht stehend aus dem Sediment hervor.

Abb. 3: Stangenförmig ausgebildete Sulfid-Chimneys auf dem Grund des Kebrit-Tiefs. Wassertiefe: ca. 1500 m. Bildausschnitt: etwa 3x5 Meter.

Die Massivsulfide variieren in ihrem Aussehen von massiven und dichten Blöcken bis hin zu äußerst porösen, netzwerkartigen Strukturen, die von parallel verlaufenden Fluid- und/oder

Gaskanälen durchzogen sind (Abb. 2). Einige Sulfidproben sind dabei direkt auf einem karbonatischen Substrat aufgewachsen. In keinem Fall werden Gesteine als Substrate beobachtet. Als Erzminerale treten insbesondere Pyrit und Markasit auf, untergeordnet findet sich Sphalerit, Galenit und selten Chalkopyrit (Abb. 4). Pyrit kommt sowohl in kollomorpher als auch in framboidaler Ausbildung vor, wobei die Framboide isoliert oder in polyframboidalen Massen auftreten („Himbeerpyrit“). Röntgenographisch konnte in mehreren Proben auch elementarer Schwefel als Mineralphase nachgewiesen werden.

Abb. 4: Auflichtmikroskopische Aufnahme mit Galenit (Ga), Sphalerit (Sl) und Pyrit (Py). Der spät gebildete Sphalerit ummantelt die idiomorphen Galenit-Kristalle und verdrängt den Pyrit. Die untere Kantenlänge der Aufnahme beträgt 1,2 cm.

Röntgenfluoreszenzspektrometrische Untersuchungen der Massivsulfide spiegeln den auflichtmikroskopischen Befund wider und geben zusätzliche Hinweise auf das Vorhandensein von Spurenelementen in den Sulfiden (Tab. 1). So deuten Cd-Gehalte bis zu 1770 ppm in den Zn-reichsten Proben auf eine geringfügige Dotierung des Sphalerits mit Cd. Darüber hinaus treten in einigen Proben Mo-Gehalte bis zu 290 ppm auf, die sich jedoch nicht mit dem Auftreten eines Sulfidminerals korrelieren lassen. Bemerkenswert ist der in Probe 15 gefundene Tl-Wert von > 3000 ppm. Diese Probe zeigt auch als einzige einen nennenswerten Ni-Gehalt

von 530 ppm. Ein Tl-Mineral ist hier nicht zu beobachten, so daß dieses Element möglicherweise adsorptiv gebunden vorliegt. Dies könnte für Mo und Ni auch der Fall sein, da es weder eigenständige Minerale noch Hinweise darauf gibt, daß diese Elemente in die Fe-Sulfide eingebaut worden sind. Auch der Galenit ist frei von Spurenelementen; Ag oder Bi konnten energiedispersiv nicht nachgewiesen werden.

Tabelle 1: Ausgewählte röntgenfluoreszenzspektrometrische Analysen an Massivsulfiden aus dem Kebrit-Tief. Hauptkomponenten in Gew.%, Spurenelemente in ppm.

	SO-2 geschicht. Sulfid	SO-4 massive Kruste	SO-5 massives Sulfid	SO-6a alteriertes sulf. Mat.	SO-10b Markasit-Kugeln	SO-12 Sulfidplatte	SO-15 Smokerbruchstück
Fe	41,50	4,80	4,63	5,94	41,68	42,05	40,56
Zn	0,02	53,31	54,62	12,34	0,03	0,03	0,37
Pb	-	8,03	0,62	0,14	-	0,02	0,73
S	39,75	26,50	27,62	52,81	40,06	38,32	37,42
SiO_2	0,79	0,28	0,35	0,98	0,87	1,43	1,00
TiO_2	-	-	-	<<	<<	<<	-
Al_2O_3	0,71	0,19	0,02	0,47	0,63	0,75	0,60
MnO	0,27	0,03	0,17	0,03	0,51	0,02	0,35
MgO	<<	<<	<<	0,26	<<	0,10	0,24
CaO	0,39	0,18	0,53	0,39	0,43	0,59	0,53
Na_2O	0,45	-	-	-	0,20	0,30	1,05
K_2O	0,13	0,08	0,06	0,11	0,17	0,11	0,16
P_2O_5	-	0,01	0,42	0,01	0,01	0,05	0,01
Cl	0,24	1,57	1,41	4,13	0,19	0,29	0,85
		-	-	-	-	-	-
Ni	-	-	<<	-	-	-	530
Cu	<<	-	-	-	-	-	-
As	-	-	<<	-	<<	-	-
Br	-	-	-	40	-	-	90
Sr	-	-	<<	70	30	<<	-
Mo	-	-	290	220	-	180	-
Cd	-	1770	680	<<	-	-	-
Tl	-	-	-	-	-	-	3060

- = nicht nachweisbar; << = in Spuren vorhanden

Resumée. Die im Kebrit-Tief des Roten Meeres angetroffene polymetallische Mineralparagenese ist das Ergebnis einer relativ niedrigtemperierten hydrothermalen Aktivität in einem sterilen Milieu (vgl. auch Blum und Puchelt, 1991; T=110-130°C). Für niedrige Bildungstemperaturen der Sulfide spricht neben der Mineralparagenese auch die weitgehende Abstinenz von Spurenelementen in den vorhandenen Sulfidphasen. Teilweise in den untersuchten Proben auftretende erhöhte Gehalte an Tl, Mo und Ni sind wahrscheinlich auf eine adsorptiv Bindung dieser Elemente an eine bituminöse Phase oder an ein Fe-Sulfid-Gel (Jankovic, 1993) zurückzuführen.

Literatur:

Bäcker, H. und Richter, H. (1973). Die rezente hydrothermal-sedimentäre Lagerstätte Atlantis-II-Tief im Roten Meer. Geol. Rdsch. 62, 697-737.

Bignell, R.D. (1975). The geochemistry of metalliferous brine precipitates and other sediments from the Red Sea. Ph. D., University of London, London.

Blum, N. und Puchelt, H. (1991). Sedimentary-hosted polymetallic massive sulfide deposits of the Kebrit and Shaban Deeps, Red Sea. Mineral. Deposita 26, 217-227.

Jankovic, S.R. (1993). Metallogenic features of the Alšar epithermal Sb-As-Tl-Au deposit (The Serbo-Macedonian metallogenic province). N. Jb. Miner. Abh. 166, 25-41.

Lausmann, M. (1997). Geochemische und mineralogische Untersuchungen an Erzschlämmen (Atlantis-II-Tief) und Massivsulfiden (Kebrit-Tief) aus dem Roten Meer. Diplomarbeit RWTH Aachen, 86 S.

10. HYDROTHERMAL MINERALISATION IN THE RED SEA

J.C. SCHOLTEN[1+], P. STOFFERS[1] AND D. GARBE-SCHÖNBERG[1]
Institut für Geowissenschaften, Olshausenstr. 40, D- 24098 Kiel

1. Introduction

First reports of metalliferous deposits from the Red Sea date back to the last century. During the Austrian expedition with the research vessel POLA (1897) red-brown mud was sampled from the Red Sea. Especially in the 1960´s many research expeditions were undertaken (Tab. 1); but most of the work concentrated on the Atlantis-II-Deep area, where, as will be described below, the most important deposits were found. The major results of these expeditions were published by Degens and Ross,[1] Bäcker and Richter,[2] Bignell,[3] and Bignell et al.[4] In order to explore for comparable deposits, research in the 1980´s concentrated on the northern part of the Red Sea. Although no hydrothermal deposits comparable to the Atlantis II-Deep were found there, the most spectacular finding was the recovery of massive sulfides from the Kebrit Deep in 1984 which, at that time, was one of the first examples of formation of massive sulfide deposits at a slow spreading ridge.[5]

2. Tectonic setting

The remarkable fit of opposite coastlines led Alfred Wegener (1927) to propose the hypothesis that the Red Sea is an example of the early stage of a continental drift (Fig. 1). Since this first observation a lot of evidence has been gathered to show that the Red Sea represents an ocean "in statu nascendi", evolving from continental rifting to seafloor spreading. It was in the late Oligocene when the first phase of the Red Sea formation started with the break-up of the Arabian plate from Africa, accompanied by intense magmatic activity and continental rifting. Seafloor spreading started in the early Miocene.[9] Whereas it is generally accepted that in the last 5 million years seafloor spreading formed a mid-oceanic ridge in the southern Red Sea there is a lively debate about the nature of crust in the marginal regions of the Red Sea. Thick Miocene evaporates sedimented in the Red Sea depression which makes the identification of a clear ocean-continent boundary difficult. Based on the good match of the African and Arabian coastlines one hypothesis assumes seafloor spreading to have formed oceanic basement in the entire Red Sea in Miocene times.[9-11] Accordingly, most of the Red Sea basement is supposed to be of basaltic composition. This model, however, cannot explain the existence of continental crust in the Southern Red sea and the Afar Triangle.[12] An alternative model postulates diffuse thinning and stretching of the continental crust and assumes the Red Sea basement to be composed of some kind of intermediate crust.[13-15] These models may explain the outcrops of Precambrian basement off the coast such as at Zabarged Island and basaltic intrusions found in Miocene evaporates.[16,17]

During the past 4 to 5 million years a spreading rate of about 1 cm/yr formed a continuous oceanic rift with a 1500m to 2000m deep axial graben in the Southern Red Sea.[18] Towards the north-west the axial zone narrows and the age of the oceanic crust gets younger.[19] North of about 21°N no continuous rift is present, and isolated deeps alternate with smooth intertrough zones. Oceanic basement, basaltic intrusions and magnetic anomalies suggest these deeps to be nucleation points for oceanic rifts. As rifting propagates the more or less regularly spaced deeps could join to form a continuous axial rift valley.[20]

2. Hydrothermal convection

More than 100 sites of submarine hydrothermal activity have been identified at seafloor spreading centers.[21,22] The close relationship between the formation of young oceanic crust and hydrothermal activity is due to a subsurface magma chamber which, on the one hand fuels the basalt flow at the rim of the divergent plate boundaries, and on the other hand is the driving force for subsurface circulation of seawater.

When seawater enters the crust, its chemical composition gradually changes due to chemical reactions with the rocks. Alteration of the rocks caused by fixation of alkali elements, oxidation - e. g. formation of iron oxides - and fixation of Mg^{++} are the main chemical reactions in this recharge zone. As the seawater penetrates downwards, the temperature increases, and oxygen content and pH drop. The solution is now capable of mobilising certain chemical elements from the host rocks, e. g. metals like copper, zinc, iron and manganese (reaction zone). Estimates of temperature and pressure in the reaction zone range from 340-465°C and 350-550 bars, which are conditions near the critical point of seawater.[22] Near this point physical properties of the seawater drastically change causing an upflow of hydrothermal solutions. This upflow may either be "focused", and active vents at the seafloor are an example of such a channelled flow. Alternatively the upflow may be "diffuse", the hydrothermal fluids not reaching the seafloor or diffusing through it over a wide area as on the flanks of the mid-ocean ridges. Subsurface mixing of these hydrothermal solutions with seawater may result in stockwork-like mineralisations.[22]

When hydrothermal fluids mix with cold oxygen rich seawater at the seafloor the mineral load of the fluids rapidly precipitates resulting in the formation of massive sulfides, black smokers and/or hydrothermal sediments. The type of deposit formed on the seafloor depends on various factors: chemical composition of rocks which interact with the hydrothermal fluids, fluid/rock ratios, temperature of fluids, water depth and tectonic setting of the plate boundary.

Throughout much of the 1960´s and early 1970´s the Red Sea hydrothermal system was thought to be unique. It was not until more recently that it came to be realised that it is a special case of a mid-ocean ridge type hydrothermal system. Unlike at mid-oceanic ridges, the special conditions in the Red Sea facilitate the formation of unusual hydrothermal deposits. First, the formation of oceanic crust in the Red Sea is focused on small deeps; due to their structure these basins act as a trap for the discharging hydrothermal fluids and prevent their distribution over large areas. Thus, when hydrothermal precipitates are formed, they are concentrated within relatively small areas. The second factor facilitating the formation of hydrothermal deposits is highly saline brines which fill about 25 deeps in the Red Sea.[23] The environment in the brine pool, especially the lack of oxygen, favours the formation and preservation of hydrothermal deposits.[6]

The formation of the brines is related to evaporites which were deposited in the entire Red Sea during the Miocene. Leaching of Miocene evaporites, which sometimes outcrop at the flanks of the deeps, is one of the brine forming processes especially in those deeps of the Red Sea, e. g. Valdivia-Deep, which are less affected by hydrothermal activity.[24,25] In the case of hydrothermally driven circulation, e. g. in the Atlantis-II-Deep, three major reservoirs strongly influenced the brine composition: seawater, marine sediments (including evaporites and black shales) and oceanic basalt.[25-29]

3. Sediment facies

About 25 deeps in the Red Sea have been explored and investigated for hydrothermal activity and related deposits. As one result, a variety of hydrothermal sediments have been found. On the basis of their lithology, mineralogy and geochemistry, Bignell et al.[30] and Bäcker and Richter[2] classified several hydrothermal sediment facies types which were further subdivided into subfacies groups. These facies types are frequently intermixed due to several ore forming processes operating at the same time within one area.[30]

3.1 Normal Red Sea sediments

Normal Red Sea sediments form the main sediment facies not influenced by hydrothermal processes. They are of light-brown to grey-brown colour and are predominantly composed of biogenic and inorganic carbonates and terrigenous material. Calcite, Mg-calcite, quartz, feldspars and clays are the main mineralogical constituents. Foraminifera, pteropods and nannofossils are the prominent biogenic material. The composition of normal Red Sea sediments changed during glacial times in that the concentrations of magnesian calcite, dolomite and inorganically precipitated aragonite increased.[31,32] Furthermore, the abundance of planktonic foraminifera decreased resulting in a so-called aplanktonic zone. These changes in the sediment composition was attributed to glacial-interglacial contrasts of salinity in the Red Sea which was due to lowering of sea level. This caused a separation of the Red Sea from the Golf of Aden and subsequently increased evaporation and changes of the ventilation of Red Sea deep waters.[33] Geochemically the normal Red Sea sediments are characterised by low Fe, Mn, Zn, and Cu content and are high in CaO and SiO_2 (Tab. 2)

3.2 Oxide facies

The oxide facies is subdivided into the goethite, lepidocrocite, hematite, magnetite and manganite facies.

The most common iron oxide facies in the Red Sea is the orange-yellow goethite facies. It occurs as pure monomineralic layers or it is intermixed with other iron facies types. The goethite facies is enriched in Fe and Zn and also in Cu in the Atlantis-II-Deep (Tab. 3). Bischoff[35] related the goethite formation to dehydration of amorphous iron oxides. Chukrov[38] suggested a reaction of Fe^{++}-solutions with ferrihydrite (x-ray amorphous iron oxide, $5Fe_2O_3*9H_2O$). Detailed laboratory studies indicated that maximum amounts of goethite with traces of hematite form via ageing of ferrihydrite at a pH 4 and pH12.[39] A comparable paragenesis, i. e. goethite with trace amounts of hematite and ferrihydrite, was found by means of Mössbauer analyses in the goethite facies from the Thetis-Deep.[40]

The lepidocrocite facies is a further iron oxide facies which can be observed as orange-brown, sometimes monomineralic layers in Red Sea sediments. Apart from Fe this facies is enriched in Cu and Zn (Tab. 4a). Lepidocrocite is believed to be formed by rapid oxidation of Fe^{++}-solutions forming a Fe^{2+}/Fe^{3+} complex, the so-called green rust.[41] Further oxidation in neutral to alkaline pH causes the formation of lepidocrocite.

The hematite facies is characterised by red coloured layers in the Atlantis-II-Deep probably in the vicinity of the incoming brines and in the Thetis and Nereus deeps.[30] It is also a common component in other oxide facies types. High Cu and Zn characterises the hematite facies (Tab. 4b). Bischoff[35] ascribes the formation of hematite to a dehydration of goethite. Detailed laboratory studies showed, however, that ageing of ferrihydrite at a pH of about 7-8 is the major pathway for hematite formation[39].

In the Atlantis-II-Deep, magnetite replaces hematite pseudomorphically with increasing sediment depths.[43] The magnetite facies occurs as almost pure black layers in the Thetis and Nereus deeps. They are characterised by high concentrations in Fe, Zn and Cu (Tab. 5a). Slow oxidation of Fe^{2+}-solutions and green rust is believed to be the major formation pathway.[41]

Brown manganite facies is present in the Atlantis-II, Thetis, Nereus, Chain, and Shagara deeps. It is characterised by high Mn and Zn content and, depending on the amounts of intermixed normal Red Sea sediments, variable CaO content (Tab. 6). Bischoff[35] describes well-crystallised and coarse grained manganite, but most common in the Red Sea deeps are poorly crystallised manganese phases (groutite, woodruffite). The manganese facies is believed to be

formed by oxidation of dissolved Mn^{2+}. Because of the reducing conditions in the brine, manganite is not stable in the Atlantis-II-Deep and precipitates at the rim of the basin.

3.3 Silicate facies

A variety of silicates have been described from the Atlantis-II-Deep.[45-47] They are found as x-ray amorphous silicates in the upper sediment layers of the Atlantis-II-Deep or as green-olive layers rich in nontronite and sulfides. The formation of the nontronite is thought to occur by sorption of silica supplied by the incoming hydrothermal solutions on Fe-oxyhydroxide. High silica and trace metal contents characterise these facies type (Tab. 5b).

3.4 Sulphide and Sulphate facies

With respect to the trace metal content and the economic value of hydrothermal deposits the sulphide facies represents the most interesting deposit in the Red Sea deeps. Trace metal content up to 10.9% Zn and 2.22% Cu have been reported from the sulphide facies from the Atlantis-II-Deep (Tab. 7). Here two distinct subfacies, the monosulphide and the pyrite facies, can be found. The violet-gray monosulfide facies is mainly composed of sphalerite, pyrite, chalcopyrite and manganosiderite, whereas the black pyrite facies is predominantly composed pyrite and manganosiderite with only traces of sphalerite. Traces of sulphides were also reported from the Gypsum and Erba deeps. In the Thetis Deep traces of sulphides are found in the magnetite facies.

Sulphates as anhydrite and barite occur in the Atlantis-II and Thetis deeps; gypsum is found in the Kebrit and Gypsum deeps. Anhydrite forms up to 1 m thick layers in the Atlantis-II-Deep and is believed to precipitate from the incoming hydrothermal solutions which mix with seawater.[2]

The chemical composition of the hydrothermal facies types described above varies between the different Red Sea deeps. This is due to the regional differences in the extent of hydrothermal activity, the influence of brines in ore forming processes, and the amount of sedimentation of normal Red Sea sediments. A comparison of the average content of Fe/Mn (for oxide mineralisations), Ca/Al (representing normal Red Sea sediments) and Cu/Zn (for sulfide mineralisation) in sediments indicates (Fig. 2) that apart from the Atlantis-II-Deep the sediments from the Thetis, Nereus, Gypsum and Vema deeps contain significant amounts of metalliferous mineralisations.

4. Atlantis-II Deep

The Atlantis-II-Deep is an elongated basin with a maximum water depth of about 2200m. It can be subdivided into four basins which are separated by bathymetric highs: the N-basin, E-basin, W-basin and the SW-basin. Towards the south, a sill at about 2030m water depths parts the SW-basin from the neighbouring Chain Deep. The Atlantis-II-Deep is filled by a layered brine pool. The several layers are characterised by distinct temperatures and salinities, which are nearly constant within the layers due to thermo-haline convection.[48] The "lower convective layer" (LCL, depth of surface at about 2046 m) covers an area of about 57 km^2 with a volume of about 3.94 km^3.[49] Investigations of the brine between 1965 and 1977 revealed above the LCL one "upper convective layer" (UCL) which results from diffusive mixing of two endmembers, the LCL and normal seawater.[50] The UCL is followed by a transition zone where the temperature gradually decreases to that of Red Sea Deep Water. However, according to observations of Anschutz and Blanc[51] in 1992 the UCL had split into 3 sections (UCL1, UCL 2, UCL 3) but investigations in 1995 and 1997 showed that the UCL 3 had changed to a transition zone with a temperature gradient to that of normal Red Sea bottom water.[23,52]

Although the brine pool spreads throughout the Atlantis-II-Deep differences in the brine temperature between the N- and the SW-basin can be observed. Whereas the UCL shows similar temperature and salinity distribution in the entire Atlantis-II-Deep the LCL is different in each basin. In the SW-basin the temperature of the LCL is constant with depth but in the N-basin the temperature decreases with depth from 66.0°C to 60°C.[52] This suggests that the connection of the LCL to the N-basin is restricted.[23] The N-basin is separated from the other basins of the Atlantis-II-Deep by a sill which has approximately the same depth as that of the LCL surface. Therefore, entry of the LCL into the north basin is restricted, and the LCL present in the north basin may represent an older brine having a lower temperature.

The brine pool has low pH and is, relative to seawater, enriched in Na, K, Ca, Cl, and depleted in Mg, SO_4^{2-},I ,F and NO_3^-.[53-55] High amounts of Fe, Mn, Zn, Pb, Si and Zn are found in solution. The absence of H_2S indicates that these metals are in excess of H_2S and that the input of sulphur is the limiting process controlling sulfide precipitation rather than the metal content in the discharging fluids.

The general precipitation processes in the brine pools are shown in Fig. 3. In the LCL, low Eh and the lack of oxygen favour the formation of sulfides. Ca, Mn, Fe and some Cu and Zn diffuse from the LCL to the UCL, and anhydrite is formed at the LCL/UCL boundary due to diffusion of SO^{-4} into the LCL.[50] Iron and manganese oxihydroxides form in the UCL and deposit on the flanks of the deep or re-dissolve when sinking back to the LCL layer.

Since the Atlantis-II-Deep has been studied over a long period of time it is one of the very few cases in marine geoscience where long term observation of a hydrothermal system has been possible and thus its time-dependent variability may be investigated. Hartmann[57] compared the chemical compositions of the LCL and UCL between 1966 and 1977 and observed only minor changes in the concentrations of Ca, Cl^-, Fe, Mn and Zn, but concentrations of Cu decreased by about a factor of 1000 in a period of 11 years (Tab. 8). He assumed that this decrease was due to an increase in supply of sulphur causing the precipitation of copper sulfides which have very low solubility in comparison to other sulfides. There seems to have been a slight increase in Mn and Fe in the LCL as well as Mn in the UCL in the past 18 years (1977-1995) which suggests an increased supply of these elements from the hydrothermal vents. The comparison of chemical data over the period of about 29 years is, however, complicated by the differences in the analytical methods used. For instance, the first measurements by Brooks et al.[58] were performed using an organic extraction method whereas modern analytical facilities (e. g. High Resolution ICP-MS) allow a direct measurement of the elements in the solution. Therefore, some of the chemical trends described above may be partly an artefact of analytical techniques.

The most striking evidence for temporal changes in the Atlantis-II-Deep brine system comes from temperature measurements which show in the LCL an increase from 55.9°C in 1965 to 67.2°C in 1997 (Fig. 4). In about the same period the UCL1 temperature changed from 44.3 to 56.3.[52,62] This continuous increase in temperatures suggests a steady increase of hydrothermal activity.[23] Almost all heat and salt which has been supplied to the brine since 1965 has been confined to the deep and has not been dispersed into the overlying seawater. The average flow rate of the hydrothermal solution has been 670-1000 kg/s, estimations based on a salt and heat balance of the brine.[49]

Although many investigations have been focused on the hydrothermal activity in the Atlantis-II-Deep, active vents have not yet been found and, therefore, the endmember composition of the fluids is still not known. Suggestions that venting takes place in the SW-basin are based on the isotope composition of the brine, the brine temperature and the geochemistry of surface

sediments (Fig. 5). The steeper gradient of temperature increase of the UCL between 1976 and 1984 in comparison to the LCL (Fig. 4) and isotopic data point to an outlet of the hydrothermal solutions on the flanks of the SW-basin above the LCL.[27,52] Detailed temperature measurements of the brine in the SW-basin during the SONNE cruise SO 121 in 1998 showed, however, a clear temperature maximum at the upper edge of the LCL brine which points to hydrothermal fluids which upwell from the bottom of the basin and spread laterally at the top of the LCL.[52] Anhydrite veins within the sediments of the SW-basin are further indications of fluids discharging from the bottom there.

4.1 Metalliferous sediments in the Atlantis-II-Deep

Over 600 cores have been taken from the Atlantis-II-Deep and this is why this area is one of the best investigated marine hydrothermal deposits. Bäcker and Richter[2] established a general lithostratigraphy (Fig. 6) and define five lithostratigraphic units - four units in the SW-basin-, which have been recently modified based on mineralogical data.[27,51]

The oldest sediments (25.000 to 28.000 years) in the Atlantis-II-Deep which overlay basalt are those from the detrital-oxide-pyrite zone (DOP). They consist of biogenic-detrital marl with several limonitic and manganitic layers, which indicate the first occurrence of hydrothermal activity in the Atlantis-II-Deep. Based on the thickness of limonitic mineralizations Bäcker and Richter[2] suggested that the main hydrothermal activity was situated in the northern part of the basin during the formation of the DOP facies.

About 15.000 years ago the formation of the lower sulfidic zone (SU1) indicates the establishment of a stable brine pool.[2] This finding is based on the mineralogical composition of the SU1 zone which is composed of dark-red brown Fe-rich clays with layers of sulfides, mainly pyrite but also chalcopyrite and sphalerite. Red coloured silicate layers with iron oxides mark the change from the SU1 zone to the central oxidic zone (CO) which is composed of limonite, hematite and manganite facies. The variable layering of these facies and slumping structures indicate a less stable brine pool. Anhydrite at the top of the CO zone characterises the gradual change to the upper sulfidic zone (SU2). This zone is similar in most characteristics to SU1, but the silicates of this zone are, in contrast to the red-brown silicates from the SU1 zone, green coloured. The youngest lithostratigraphic unit which is presently still being formed, is the amorphous-silicate zone (AM). This is a very soft (about 94% brine content) homogeneous marl containing x-ray amorphous Fe-oxides and silicates, and only in the lower part of this unit goethite layers can be observed.

In the SW-basin slightly different lithostratigraphic units can be observed, most probably due to the vent area being situated in this part of the Atlantis-II-Deep since the formation of the CO zone. The CO zone in the SW-basin overlays basalt and consists of coarse grained hematite and goethite facies sometimes in monomineralic layers. This zone is followed by a 2-5m thick sulfidic-oxidic-anhydrite zone (SOAN), which is characterised by disturbed layering and alternate sequences of metal-rich sulphides, hematite, anhydrite and silicate facies. The colour of this zone varies according to the facies between red-brown and olive-green. The oxidic-anhydritic zone (OAN) on top of the SOAN is characterised by breccias and turbiditic layering and consists of hematite, anhydrite, and silicates with fragments of sulfides and silicates. Veins filled with anhydrite can also be observed. The uppermost unit in the SW-basin consists of an about 4.5m thick sulfidic-amorphous-silicate-zone (SAM). It is characterised by a sulfide layer at the base having a high content of sphalerite. The facies generally has a high brine content (>90%), and sulfides, silicates and anhydrite are the main mineralogical phases which have been identified in it.

Several authors have tried to specify the temperatures and other environmental conditions of mineral precipitation by studying the mineral parageneses of the sediments. Missak et al.[63]

described two parageneses in their sediment core from the SW-basin: a) intermediate solid solutions (also described as chalcopyrrhotite) with sphalerite encrustations and intergrowths and b) intermediate solid solution free of sphalerite. They suggested that differences in the sulfide mineralogy are due to changes in the composition of ore forming fluids and a change in the sulphur fugacity. The presence of exsolved chalcopyrite lamellae in intermediate solid solutions indicate slow cooling of the fluids with a temperature < 450°C. Veins in sediments filled with mineral assemblages of pyrrhotite, cubic cubanite, high iron sphalerite and anhydrite suggests a disequilibrium between H_2S and SO_4^{-2} in the hydrothermal fluids.[64] This may be caused by a mixing of two fluids, one having a relatively low temperature (<250°C and SO_4< H_2S), the other a hot fluid rich in H_2S. A precipitation temperature of between 200° and 250°C is indicated by the paragenesis of cubic cubanite, chalcophyrite and monoclinic pyrrhotite. Based on fluid inclusions thermometry of anhydrite crystals, exit temperatures of between 240°C and 400°C have been estimated for the venting fluids.[64-66]
The composition of the sediments in the Atlantis-II-Deep is very variable and differs even when sediment cores were retrieved at very close distances from each other. Therefore, estimates of fluid composition and temperatures based on mineral paragenesis depends very much on the sediments investigated. A summary of published temperature estimates of the hydrothermal fluids is shown in Table 9.

The great variability in the composition of the sediments, as already mentioned above, causes the chemistry of the facies types to vary from core to core which is why the various investigators cited in tables 2-7 give different values for the chemical composition of Atlantis-II-Deep sediments. Because of the variability in the chemical composition of Atlantis-II-Deep sediments, their economic potential has been judged differently by different authors. Hackett and Bischoff [73] estimated the mass of Zn to be $32.2*10^5$ tons with $8.1*10^5$ tons of copper. Based on chemical analyses of 628 cores having a total length of about 4 km, Guney et al.[74] estimated that the Deep contains the following: zinc $18,9*\ 10^5$ tons, copper $4,25*10^5$ tons, silver 3.750 tons, gold 47 tons, and cobalt 5.369 tons. Because of the high economic value of the Atlantis-II-Deep deposits, a pre-pilot mining test using the drill ship Sedco 445 was conducted in 1979 which was the first time that hydrothermal deep sea deposits were recovered for economic purposes. Because the metal grades of the wet sediments are very low (0.5 % for Zn and about 0.07 % for Cu) pre-concentration of the metals on board the ship was necessary.[6] About $15.000m^3$ of metalliferous mud was pumped from the Atlantis-II-Deep through a 2.200m long pipe string and subjected to separation by flotation on-board. The results of the mining test suggested that recovery of the hydrothermal deposits in the Atlantis-II-Deep is, in principle, possible and would take a period of about 16 years to complete.[74]
Although the economic potential of the Atlantis-II-Deep deposits seems to be enormous, the consequences for the biological environment in the Red Sea have not yet been fully explored. Separation of the metal sulfides on-board the ship will result in flotation produced tailings. These tailings contain iron oxides, silicates and also traces of sulfides. Release of the tailings in surface waters, or even at 800m depth as suggested by Bäcker [6], could have enormous ecological effects on the environment in the Red Sea unless mitigated.

5. Hydrothermal sediments outside the Atlantis-II-Deep area
Apart from the Atlantis-II-Deep significant hydrothermal deposits are found in the Thetis, Nereus, Vema and Gypsum deeps.

The Thetis Deep is divided into several subbasins. Hydrothermal sediments occur only in the NE basin, which is 10 km long and 3 km wide and up to 1780 m deep. The sediments consist of various types of iron oxide facies (hematite, goethite, magnetite) sometimes forming monomineralic layers. The sulfide paragenesis suggests that primarily two distinct

hydrothermal solutions, one rich in zinc (major elements Cu, Fe, Zn, S) the other depleted in it (major elements: Cu, Fe, S) were active.[75]
Detailed investigation by Scholten et al.[36] showed that the sediments in the Thetis Deep are comparable to the CO zone facies types in the Atlantis-II-Deep. In contrast to the Atlantis-II-Deep, however, no brine fills the Thetis-Deep. Nevertheless, a strong fractionation between Fe and Mn in the sediments suggests that the Thetis-Deep is an example of intermittent brine filling of a deep. Timing of the hydrothermal deposition in the Thetis-Deep seems to correlate with similar events in the Atlantis-II-Deep and it may be that major tectonic events in the Red Sea may possibly trigger hydrothermal activity.[36]

The Nereus Deep has an overall width of 12 km and is 40 km in length. It is divided along its length by a saddle into an east and a west basin, the latter one being filled by a brine pool. Whereas sediments in the west basin mainly consist of normal Red Sea sediments, the most concentrated hydrothermal sediments have been found in a round depression in the south eastern part of the basin. The deposits consist of an up to 4 m thick sequence of manganite, goethite and hematite facies types.[76]

The 24 km long and 6 km wide Vema Deep (1608m water depth) does not contain a brine pool but the two cores recovered during the Valdivia cruise in 1972 recovered an up to 3 m thick sequence of relatively pure goethite mud with high concentrations of Fe and Zn. A sharp boundary between the base of the hydrothermal sequence and the underlying normal Red Sea Sediments mark the beginning of hydrothermal activity in this area.[30]

The Gypsum deep was named after large idiomorphic gypsum crystals which were recovered from the sediments. Morphologically the deep is more like a depression with a maximum water depth of 1196m. In the upper 2m of sediments two Fe-rich layers occurred in which goethite, lepidocrocite and siderite are the dominant minerals. Below the upper Fe-rich layer a fine grained pyrite mud rich in Ca, Fe, Cu and Zn was observed.[30]

6. Massive sulfides from the Kebrit Deep

The Kebrit-Deep (kebrit = Arabic sulphur) was first explored during the Valdivia cruise in 1971 and consists of a single basin of about 1 by 2.5 km in size. The basin has a maximum depth of 1549m and is filled by a 84m thick oxygen-free brine. Over the past 23 years the temperature has increased slightly from 23.24°C to 23.34°C, but chlorinity (154‰ Cl) has remained unchanged.[23] The strongly reducing brine has a sulphur content of 12 to 14 mg S/l. In the deeper brine section 100µg/l Fe is present whereas just below the seawater/brine interface Fe concentrations < 1000 µg/l were reported.[23] These differences are probably due to dynamic precipitation and resolution processes between the O_2-rich seawater and the brine. Such processes were observed during SONNE cruise 121 (1997)[52] using TV. Plate a) shows the contact of the brine/seawater interface with the sediments. Three zones can be distinguished: the ligh-gray coloured zone is the brine and the transition to more dark-gray colours mark the boundary between the reducing conditions of the brine and a zone where Fe-oxides precipitate due to mixing with seawater. More distal from the brine, a black coloured zone indicates precipitation of Mn-oxides.

During the Valdivia cruise in 1972 no indications of active hydrothermal venting were found, but dredging during research cruise Sonne 29 (1984) recovered massive sulfides. Detailed sampling and exploration during Meteor (1995)[77] and Sonne 121 (1997)[52] cruises suggests that most of the sulfides are situated in a narrow band near the brine/seawater interface. The sulfides are very porous, fragile and most of them have a cauliflower structure. They have a

chimney-like shape; also spindle type chimneys up to 1 m height were observed (Plates b,c,f). The most common sulfides are massive aggregates which are covered by sediments (Plates d,e). On steep slopes of the basin, outcrops of these sulfides can be frequently observed. Sometimes encrustations and impregnations of consolidated sediments are found. Some of the sulfides recovered are impregnated with tar and asphalt.

6.1 Mineralogy

According to investigations by Blum and Puchelt[78] and by Missak[75], the massive sulfides from the Kebrit Deep can be separated into two different groups, here called type I and type II deposit.

Type I

Type I consists of pyrite, marcasite, bravoite, sphalerite, digenite, chalcocite, jarosite, and minor amounts of galena. Pyrite is the most common sulphide mineral and is found either as cellular aggregates or in globular masses. It often alternates with various concentric layers of bravoite, marcasite and spalerite. This sequence of rhythmic banding points to pH variations during precipitation.[78] The colloform texture suggests a low temperature formation of pyrite.

Marcasite is less abundant than pyrite in the type I deposit and is mainly found as fine elongated radial crystals and as fine euhedral to subhedral grains included in pyrite. The composition of marcasite is characterised by a Zn content of between 2-2.5 wt%, Mn content in between 1-3.2wt%, and As between 0.01-0.05 wt%. No Cu could be detected.[75]

Bravoite is found in two different forms, mainly with colloform texture in alternating layers with pyrite, marcasite, sphalerite, and as fine crystals of 0.1-0.05 mm in size. Bravoite seems to be formed at a low temperature; its upper stability limit is, according to Kullerud,[79] 135°, and its formation is typical of euxinic sedimentary environments.

Sphalerite exhibits a colloform banding of different shades of gray which is attributed to differences in Fe content (1.2-5.5 wt%). In layers with low Fe the original ZnS phase is supposed to be wurtzite which later transformed to sphalerite. The Zn content of sphalerite ranges from 56.9 to 62.5 wt% and Mn is between 0.02 and 0.09 wt%. The FeS content of < 10 mol% indicates a low temperature formation.

Galena is only present in sphalerite as euhedral fine grains (0.2-0.25mm in diameter). Subhedral crystals form along sphalerite bands with one side curved and banded with the banding curves of sphalerite whereas the outer free surface is euhedral. The banding curves indicate that crystallisation took place while the gel was still mobile and before the next zone was precipitated. Galena is also found in skeletal forms which is indicative of low temperature formation.[80] It is free of Bi and Ag; Sb content is <0.09 wt%.

Type II

The second group of massive sulfides consists almost exclusively of pyrite and traces of marcasite. Pyrite is found in colloform bands and as framboids. Pyritization of fossils (foraminifers, radiolarians) is a common feature.

6.2 Chemical composition

The mineralogical differences between the massive sulfides from the Kebrit Deep is also evident from their total chemical composition (Tab. 10). The type I sulfides are characterised by Zn and Pb concentrations of up to 50.9% and 0.69%, respectively, whereas type II is poor in these metals. In both types Cu and Ni are low and Fe is between 8.6% and 43.6%.

Massive sulfide deposits with Cu and Zn enrichments have been described from various slow spreading ridges like those at the TAG field at the Mid-Atlantic Ridge.[21] The Kebrit Deep differ from those areas in that no basement rocks outcrop in the Kebrit area. Therefore, the Kebrit sulfides can be grouped in with sediment-hosted sulfide deposits like those from the Escanaba Trough and Guaymas Basin which also formed at sediment-covered spreading

centers. These deposits differ from the volcanic-hosted massive sulfides in that Zn and Cu concentrations are often lower whereas their Pb content is higher (Tab. 10). These differences are interpreted as being due to the interaction of the hydrothermal fluids with the sediments which leads to a buffering of the solutions, increase in pH, decrease in temperature and precipitation of Cu and Zn sulfides within the sediment complex. Cu is more mobile in hydrothermal solutions at temperatures > 300°C whereas Pb and Zn-sulfides preferentially form at low temperatures (120°C and 300°C).[83] The lack of significant Cu-mineralisations in the massive sulfides from the Kebrit Deep may thus be due to low temperatures of the hydrothermal solutions. Evidence for low formation temperatures are found in the mineralogical and microprobe analyses of Kebrit massive sulfides described above. Blum and Puchelt[78] postulated that Cu-bearing phases may be found in deeper stockwork under the Kebrit deposit.

A common feature of sediment-hosted sulfide deposits is the generation of hydrocarbons. Circulation of hydrothermal fluids through sediments causes thermal alteration of sedimentary organic matter. In the Guaymas Basin liquid hydro-carbon-bearing inclusions occur in hydrothermal minerals of sulfide chimneys[84]. Massive sulfides in the Kebrit Deep are often impregnated with asphalt. Based on the distribution of bio-markers, Michaelis et al.[85] suggested the hydrothermal organic compounds were derived from the underlying Miocene evaporites. They explained the high asphalt content of the massive sulfides by a condensation effect of hydrothermal fluids transporting petroleum-like substances to the surface.
Further indications of an interaction of hydrothermal fluids in the Kebrit Deep with the sediments leading to the concentrations of metals found in the massive sulfides are provided by lead isotope data.[78] In a diagram of $^{206}Pb/^{204}Pb$ versus $^{208}Pb/^{204}Pb$ the lead isotope ratios of the Kebrit sulfides plot near the values for detrital and metalliferous sediments from the Nereus Deep and Atlantis-II-Deep (Fig. 7). In these deposits two sources of the lead have been proposed, a basaltic end-member source and a detrital source.[29,86] The lead isotope signature of the detrital component may derive from a more radiogenic source like igneous and metamorphic rocks of Precambrian or Phanerozoic age. Stratiform massive sulfide deposits located at the Egyptian coast which underlay Miocene evaporites may be a further end-member source for the Pb-isotope in the sediments.

Although extensive sampling of massive sulfides was conducted during Meteor cruise M31/2 (1995) and Sonne cruise 121 (1997) in the Kebrit Deep, no sulfides with high Zn and Pb contents (type I) were retrieved. This indicates that the type I sulfides are of minor importance in the total volume of the Kebrit sulfide deposits. Uranium-thorium disequilibrium dating suggests the age of type II sulfides to be between 20,000 and 28,000 years, whereas type I sulfides are much younger (< 5,000 years; unpublished data). The age differences suggest different periods of hydrothermal activity during which there were different physical and chemical properties of the discharging hydrothermal fluids. In the Thetis Deep, which is situated about 250 km south of the Kebrit Deep, two periods of hydrothermal activity have also been deduced from the record of metalliferous sediments.[36] The first occurred between 23,000 years and 14,000 years ago and the second started about 10,000 years ago with increased intensity in between 2,700 and 1,200 years ago. Like in the case of the Kebrit deposits, there was obviously a change in the composition of the hydrothermal fluids in the Thetis-Deep. The first period of hydrothermal activity was characterised by high Zn-content whereas the second was almost Zn free. Whether or not the timing of hydrothermal activity in the Kebrit Deep is connected to that observed in the Thetis-Deep and Atlantis-II-Deep by tectonic activity, can only be a matter of speculation until more detailed information about the occurrences of hydrothermal activity in the Kebrit Deep is available.

7. Conclusions

The formation of hydrothermal deposits in the Red Sea is a result of the divergent movement of the African and Arabian continental plates. These deposits are unique in comparison with other metalliferous mineralisations at divergent plate boundaries in that they have high ore concentrations. This is caused by the fact that discharging hydrothermal solutions are trapped in isolated basins, and that these deeps are often filled with high-saline, oxygen-free brines which favour the preservation of hydrothermal mineralisations. Variations of both, hydrothermal activity and composition of hydrothermal fluids as well as differences in the physicochemical conditions in the brine pools have resulted in the formation of oxides, sulphides, sulphates and silicates. Outside the well-investigated Atlantis-II-Deep deposits, the most highly metalliferous sediments have been found in the Thetis, Nereus, Gypsum and Vema deeps. In the brine-filled Kebrit Deep massive sulfides were recovered comparable with the Guaymas type deposits. The chemical and mineralogical composition of the Kebrit Deep massive sulfides points to a low temperature formation; and lead isotope data suggested that the source of the metals in the hydrothermal fluids have derived from basaltic and detrital components. It is believed that in deeper stockwork under the Kebrit Deep deposits Cu-bearing sulfide phases may be found.

As in the cases of the Atlantis-II-Deep and the Thetis Deep two major periods of extensive hydrothermal activity at roughly the same time can be observed in the Kebrit Deep. Further research is necessary to investigate any possible connection of hydrothermal activity in the Red Sea with e.g. large scale tectonic events.

8. References

1 Degens, E. T., and Ross, D. A., *Hot brines and recent heavy metal deposits in the Red Sea*, Springer Verlag, New York, 1969, 600 pp.

2 Bäcker, H. and Richter, H., Die rezente hydrothermal-sedimentäre Lagerstätte Atlantis II-Tief im Roten Meer, *Geol. Rundschau*, 62, 697, 1973.

3 Bignell, R. D., *The geochemistry of metalliferous brine precipitates and other sediments in the Red Sea*, Ph.D. Thesis, University of London, 1975.

4 Puchelt, H. and Laschek, D., Marine Erzvorkommen im Roten Meer, *Fridericiana, Zeitschrift der Universität Karlsruhe*, 34, 3, 1984.

5 Thisse, Y., Guennoc, P., Poult, G. and Nawab, Z., The Red Sea: a natural geodynamic and metallogenic laboratory, *Episodes*, 3, 3, 1983.

6 Bäcker, H., Metalliferous sediments of hydrothermal origin from the Red Sea, in *Marine mineral deposits*, Halbach, P. and Winter, P., Eds., Verlag Glückauf, Essen, 102, 1982.

7 Bäcker, H., Marchig, V., von Stackelberg, U., Stoffers, P., Puteanus, D. and Tufar, W., Hydrothermale Aktivität auf dem Meeresboden, *Geol. Jb.*, D93, 103, 1991.

8 Girdler, R. W., Problems concerning the evolution of oceanic lithosphere in the Northern Red Sea, *Tectonophysic*, 116, 109, 1985.

9 Girdler, R. W, and Styles, P., Two stage Red Sea floor spreading, *Nature*, 330, 716, 1974.

10 McKenzie, D. P., Davies, D. and Molnar, P., Plate tectonic of the Red Sea and East Africa, *Nature*, 226, 243 et al., 1970.

11 Makris, J., Rihm, R., Shear-controlled evolution of the Red Sea: pull apart model, *Tectonophysics*, 198, 441, 1991.

12 Cochran, J. R., A model for the development of the Red Sea, *Bull. Am. Assoc. Pet. Geol.*, 67, 41, 1983.

13 Wernicke, B., Uniform sense normal simple shear of the continental lithosphere, *Can. J. Sci*, 22, 108, 1985.

14 Le Pichon, X. and Gaullier, J. M., The rotation of the Arabia and Levant Fault System, *Tectonophysics*, 153, 271, 1988.

15 Bonatti, E. and Seyler, M., Crustal underplating and evolution in the Red Sea rift: uplifted gabbro/gneiss crustal complexes on Zarbargad and Brothers Islands, *J. Geophys. Res.*, 92, 12803, 1987.

16 Lowell, J. D. and Genik, G. J., Sea floor spreading and structural evolution of the southern Red Sea, *Am. Assoc. Pet. Geol. Bull.*, 56, 247, 1972.

17 Bäcker, H., Lange, K. and Richter, H., Morphology of the Red Sea Central Graben between Subair Islands and Abul Kizaan, *Geol. Jahrb.*, D13, 79, 1975.

18 Izzeldin, Y. A., Seismic, gravity and magnetic surveys in the central part of the Red Sea; their interpretation and implications for the structure and evolution of the Red Sea, *Tectonophysics*, 143, 269, 1987.

19 Bonatti, E., Punctiform initiation of seafloor spreading in the Red Sea during transition from a continental to an oceanic rift, *Nature*, 316, 33, 1985.

20 Rona, P. A. and Scott, S. D., Preface to special issue on seafloor hydrothermal mineralisation: New Perspectives, *Econ. Geol.*, 88, 1935, 1993.

21 Herzig, P. M. and Hannington, M. D., Polymetallic massive sulfides at the modern seafloor: A review, *Ore Geol. Reviews*, 10, 95, 1995.

22 Alt, J. C., Subseafloor processes in mid-ocean ridge hydrothermal systems, in *Seafloor hydrothermal systems*, Humphris, S. E., Zierenberg, R. A., Mullineaux, L. S. and Thomson, R. E., Eds., Geophysical Monograph, 91, 85, 1995.

23 Hartmann, M., Scholten, J. C., Stoffers, P. and Wehner, F., Hydrographic structure of brine-filled deeps in the Red Sea – new results from the Shaban, Kebrit, Atlantis II, and Discovery Deep, *Mar. Geol.*, 144, 311, 1998.

24 Manheim, F. T., Red Sea geochemistry, in *Initial Reports of the Deep Sea Drilling Project*, Whitmarsh, R. B., Weser, O. E., Ross, D. A., Eds., U. S. Government Printing Office, Washington, 23, 975, 1974,

25 Zierenberg, R. A. and Shanks, W.C., Isotopic constraints on the origin of the Atlantis II, Suakin and Valdivia brines, Red Sea, *Geochim. Cosmochim. Acta*, 50, 2205, 1986.

26 Anschutz. P., Blanc, G. and Stille, P., Origin of fluids and the evolution of the Atlantis II deep hydrothermal system, Red Sea, *Geochim. Comochim. Acta*, 59, 4799, 1995.

27 Blanc, G., Boulegue, J. and Michard, A., Isotope composition of the Red Sea hydrothermal end-member, *C. R. Acad. Sci. Paris*, 320, 1187, 1995.

28 Schoell, M. and Stahl, W.,The carbon isotopic composition and the concentration of the dissolved anorganic carbon in the Atlantis II deep brines (Red Sea), *Earth Planet. Sci. Lett.*, 15, 206, 1972.

29 Dupré, B., Blanc, G., Boulegue, J. and Allegre, C. J., Metal remobilisation at a spreading centre studied using lead isotopes, *Nature*, 333, 165, 1988.

30 Bignell, R. D., Cronan, D. S. and Tooms, J. S., Red Sea metalliferous brine precipitates, *Geol. Ass. Canada*, no. 14, 147, 1976.

31 Milliman, J. D,, Ross, D. A., and Ku, T., Precipitation and lithification of deep sea carbonates in the Red Sea, *J. Sed. Petr.*, 39, 724, 1969.

32 Stoffers, P., Botz, R., Carbonate crusts in the Red Sea, in *Facets of modern Biogeochemistry*, Ittekkot, V., Kempe, S., Spitzy, A., Eds., Springer Verlag, Berlin, 1990, 242.

33 Thunell, R. C., Locke, S. M., Williams, D. F., Glacio-eustatic sea-level control on Red Sea salinity, *Nature*, 334, 601, 1988.

34 Bäcker, H., Fazies und chemische Zusammensetzung rezenter Ausfällungen aus Mineralquellen im Roten Meer, *Geol. Jb.*, D 17, 151, 1976.

35 Bischoff, J. L., Red Sea geothermal brine deposits: Their mineralogy, chemistry, and genesis, in , in *Hot brines and recent heavy metal deposit*, Degens, E. T., and Ross, D. A., Eds., Springer, New York, 368, 1969.

36 Scholten, J., Stoffers, P., Walter, P. and Plüger, W., Evidence for episodic hydrothermal activity in the Red Sea from composition and formation of hydrothermal sediments, Thetis-Deep, *Tectonophys.*, 190, 109, 1991.

37 Bignell, R. D., Timing, distribution and origin of submarine mineralisations in the Red Sea, *Inst. Mining Metallurgy Trans.*, 84, 1, 1975.

38 Chukrov , F., Ferrihydrite, *Inter. Geol. Review*, 16, 1131, 1974.

39 Schwertmann, U., and Murad, E., Effect of pH on the formation of goethite and hemetatite from ferrihydrite, *Clay and Clay Min.*, 31, 277, 1983.

40 Haxel, C., ZU Anwendung der Mößbauer-Spekroskopie aud asugewählte Mineralien und Fragestellungen zu deren Genese, *Heidelberger Geowiss, Abhandl.*, 9, pp.268, 1987.

41 Murray, J. W., Iron oxyd, *Marine Minerals*, Barns, R. G., Ed., Min. Sic. Am. Short Course Notes, 6, 47, 1979.

42 Jedwab, J., Blanc, G., and Boulegue, J., Vanadiferous minerals from the Nereus Deep, Red Sea, *Terra Nova*, 1, 188, 1989.

43 Zierenberg, R. A. and Shanks, W. C. Mineralogy and geochemistry of epigenetic features in metalliferous sediments, Atlantis-II-Deep, Red Sea, *Econ. Geol.*, 78, 57, 1983.

44 Weber-Diefenbach, K., Geochemistry and diagenesis of recent heavy metal ore deposits at the Atlantis-II-Deep (Red Sea), in *Time- and strata-bound ore deposits*, Klemm, D. D. and Schneider, H.-J., Eds., Springer, Berlin, 419, 1977.

45 Cole, T. G., Oxygen isotope geothermometry and origin of smekites in the Atlantis-II-Deep, *Earth Planet. Sci. Lett.*, 66, 166, 1983.

46 Singer, A., and Stoffers, P., Mineralogy of a hydrothermal sequence in a core from the Atlantis-II-Deep, Red Sea, *Clay Miner.*, 22, 251, 1987.

47 Schneider, W., and Schumann, D., Tonminerale in Normalsediment, hydrothermal beeinflußten Sedimenten und Erzschlämmen des Roten Meeres, *Geol. Rundsch.*, 68, 631, 1979.

48 Turner, J. S., Double-diffusive phenomena, *Ann. Rev. Fluid Mech.*, 6, 37, 1974.

49 Anschutz, P. and Blanc, G., Heat and salt fluxes in the Atlantis II Deep (Red Sea), *Earth Planet. Sci. Lett.*, 141, 147, 1996.

50 Hartmann, M., Atlantis II-Deep geothermal brine system: Hydrographic situation in 1977 and changes since 1965, *Deep Sea Research*, 127, 161, 1980.

51 Anschutz, P. and Blanc, G., New stratification in the hydrothermal brine system of the Atlantis II Deep, Red Sea, *Geology*, 23, 543, 1995.

52 Stoffers, P., Moammar, M. and Scientific Party, Cruise Report Sonne 121 Red Sea, *Reports, Geol.-Paläont. Inst Univ. Kiel*, 88, p.107, 1998.

53 Brewer, P. G., Densmore, C. D., Munns, R. and Stanley, R. J., Hydrography of the Red Sea brines, in *Hot brines and recent heavy metal deposits in the Red Sea*, Degens, E. T. and Ross, D. A., Eds., Springer, New York, 138, 1969.

54 Miller, A. R., Densmore, C. D., Degens, E. T., Hathaway, J. C., Mannheim, F. T., McFarlin, P. F., Pocklington, R. and Jokela, A., Hot brines and recent iron deposits in deeps of the Red Sea, *Geochim. Cosmochim. Acta*, 30, 341, 1966.

55 Brewer, P. G. and Spencer, D. W., A note on the chemical composition of the Red Sea brines, in *Hot brines and recent heavy metal deposit*, Degens, E. T., and Ross, D. A., Eds., Springer, New York, 174, 1969.

56 Bäcker, H., Rezente hydrothermal-sedimentäre Lagerstättenbildung, *Erzmetall*, 26, 544, 1973.

57 Hartmann, M., Atlantis-II-Deep geothermal brine system. Chemical processes between hydrothermal brines and Red Sea deep water, *Marine Geol.*, 64, 157, 1985.

58 Brooks, R. R., Kaplan, I. R. and Peterson, M. N. A., Trace metal composition of the Red Sea geothermal brines and interstitial water, in *Hot brines and recent heavy metal deposit*, Degens, E. T., and Ross, D. A., Eds., Springer, New York, 180, 1969.

59 Hartmann, M., Untersuchungen von suspendiertem Material in den Hydrothermallaugen des Atlantis-II-Tiefs, *Geol. Rundsch*, 62, 742, 1973.

60 Danielsson, L.-G., Dyrsson, D. and Granéli, A., Chemical Investigations of Atlantis II and Discovery brines in the Red Sea, *Geochim. Cosmochim. Acta*, 44, 2051, 1980.

61 Post, H., Changes in the Red Sea hydrothermal activities between 1964-1984, unpublished manuscript, p. 5, 1985.

62 Hartmann, M., Scholten, J. C. and Stoffers, P., Hydrographic structure of the brine-filled deeps in the Red Sea – correction of the Atlantis Deep temperatures, *Mar. Geology*, 144, 331, 1998.

63 Missack, E., Stoffers, P. and El Goresy, A., Mineralogy, parageneses and phase relations of copper-iron sulfides in the Atlantis II-Deep, Red Sea, *Mineral Deposita*, 24, 82, 1989.

64 Pottorf, R. J. and Barnes, H. L., Mineralogy, geochemistry, and ore genesis of hydrothermal sediments from the Atlantis-II-Deep, Red Sea, *Econ. Geol.*, 5, 198, 1983.

65 Ramboz, C., Oudin, E. and Thisse, Y., Geyser-type discharge in Atlantis II Deep , Red Sea: Evidence of boiling from fluid inclusions in epigenetic anhydrite, *Canad. Mineral.*, 26, 765, 1988.

66 Oudin, E., Thisse, Y. and Ramboz, C., Fluid inclusion and mineralogical evidence for high temperature saline hydrothermal circulation in the Red Sea metalliferous sediments: preliminary results, *Mar. Mining*, 5, 3, 1984.

67 Brewer, P. G., Wilson, T. R. S., Murray, J. W., Munns, R. G. and Densmore, C. D., Hydrographic observations on the Red Sea brines indicate a marked increase in temperature, *Nature*, 231, 37, 1971.

68 Ross, D. A., Red Sea hot brine area: Revisited, *Science*, 175, 1455, 1972.

69 Sakai, H., Osaki, S. and Tsukagishi, M., Sulfur and oxygen isotopic geochemistry of sulfate in black ore deposits of Japan, *Geochim Jour. (Japan)*, 4, 27, 1970.

70 Schoell, M., The hydrogen and carbon isotopic composition of methane from natural gases of various origins, *Geochim. Cosmochim. Acta*, 44, 649, 1980.

71 Truesdell, A. H., Summary of section II: Geochemical techniques in exploration, *United Nations symposium on the development and use of geothermal resources*, San Francisco, Proc., 1, liii, 1975.

72 Ramboz, C. & Danis, M., Superheating in the Red Sea? The heat-mass balance of the Atlantis II deep revisited, *Earth Planet. Sci. Lett.*, 97, 190, 1990.

73 Hackett, J. P. Jr., and Bischoff, J. L., New data on the stratigraphy, extent and geologic history of the Red Sea geothermal deposits, *Econ. Geol.*, 68, 553, 1973.

74 Guney, M., Nawab, Z. and Marhoun, M. A., Atlantis-II-Deep´s metal reserves and their evaluation, *Offshore Technology Conf. Houston*, 3, 33, 1984.

75 Missak, E. A., Mineralogy and phase relation of the massive sulphides and metalliferous sediments of the axial rift valley, Red Sea, *Heidelberger Geowiss. Abhandl.*, 23, pp. 213, 1988.

76 Bignell and Ali, S. S., Geochemistry and stratigraphy of Nereus Deep, Red Sea, *Geol. Jahrb. D* , 17, 173, 1976.

77 Hemleben, Ch., Roether, W. and Stoffesr, P., Östliches Mittelmeer, Rotes Meer, Arabisches Meer, Cruise No. 31, 30 December 1994- 22 March 1995, Meteor Berichte, Universität Hamburg, 96-4, pp. 282, 1996.

78 Blum, N. and Puchelt, H., Sedimentary-hosted polymetallic massive sulphide deposits of the Kebrit and Shaban Deeps, Red Sea, *Mineral Deposita*, 26, 217, 1991.

79 Kullerud, G., Sulfide studies, in *Researches in geochemistry*, Abelso, P. H., Ed., John Wiley and Sons, New York, 474, 1967.

80 Ramdohr, P., The ore minerals and their intergrowth, *Oxford, Pergamon Press*, pp. 1174, 1969.

81 Koski, R. A., Shanks III, W. C., Bohrson, W. A. and Oscarson, R. L., The composition of massive sulfide deposits from the sediment-covered floor of Escanaba Trough, Gorda Ridge: Implications for depositional processes, *Canad. Mineral.*, 26, 655, 1988.

82 Koski, R. A., Lonsdale, P. F., Shanks, W. C., Berndt, M. E. and Howe, S. S., Mineralogy and geochemistry of a sediment-hosted hydrothermal sulfide deposit from the southern trough of Guaymas Basin, Golf of California, *J. Geophys. Res.*, 90, 6695, 1985.

83 Scott, S. D., Seafloor polymetallic sulfides: Scientific curiosities or mines in future?, in *Marine Minerals: Resource assesment strategies*, Teleki, P. G., Dobon, M. R., Moore, J. R., von Stackelberg, U., Eds., Proc. NATO Advanced Research Workshop, Series C, Reidel, Boston, 87, 1987.

84 Peter, J. M., Simoneit, B. R. T. and Kawaka, O. E., Liquid hydrocarbon-bearing inclusions in modern hydrothermal chimneys and mounds from the southern trough of Guaymas Basin, Gulf of Californnia, *Appl. Geochem.*, 5, 51, 1990.

85 Michaelis, W., Jenisch, A. and Richnow, H.H., Hydrothermal petroleum generation in Red Sea sediments from the Kebrit and Shaban deeps, Applied Geochem., 5, 103, 1990.

86 Bosch, D., Lancelot, J. and Boulegue, J., Sr, Nd and Pb isotope constraints on the formation of the metalliferous sediments in the Nerus Deep, Red Sea, *Earth Planet. Sci. Lett.*, 123, 299, 1994.

87 Volker, F., McCulloch, M. T. and Altherr, R., Submarine basalts from the Red Sea: New Pb, Sr, and Nd isotopic data, *J. Geophys. Res.*, 20, 927, 1993.

88 Stacey, J. S., Doe, B. R., Roberts, R. J., Delevaux, M. H. and Gramlich, J. W., A lead isotope study of mineralization in the Saudi Arabien Shield, *Contr. Mineral. Petrol,* 74, 175, 1980.

Table and figure captions

Table 1: History of research cruises to the Red Sea (data compiled from Thisse et al. [5], Bäcker [6] and unpublished data).

Table 2: Geochemical composition of the normal Red Sea sediment facies; 1 Bäcker,[34] normal Red Sea sediments north of 19.5°; 2 Bischoff,[35] average of 43 samples; 3 Scholten et al.[36] average of 2 samples; 4 Bignell et al.[30;] n.m. = not measured.

Table 3. Geochemical composition of the goethite facies, 1 Bäcker,[34] average of 100 samples from the SW basin of the Atlantis-II-Deep; 2 Bäcker[34], average of 22 samples; 3 Bischoff, [35] average of 43 samples; 5 Scholten et al.,[36] average of 10 samples; 6 Bignell et al.[30]; 7 Bignell[37].

Table 4: Geochemical composition of the lepidocrocite (a) and hematite facies(b). 1 Bignell et al.[30]; 2 Scholten et al.,[36] average of 12 samples; 3 Bignell[37]; 4 Bäcker,[34] average of 5 samples; 5 Scholten et al.[36], average of 7 samples; 6 Jedwab et al.[42].

Table 5: Geochemical composition of the magnetite (a) and silicate facies (b). 1 Scholten et al.[36], average of 6 samples; 2 Jedwab et al.,[42]; 3 Bäcker,[34] average of 20 samples; 4 Bäcker,[34] average of 43 samples from the green silicate facies; 5 Bignell et al.,[30] green silicate; 6 Bignell et al.,[30].

Table 6: Geochemical composition of the of the manganite facies; 1 Bäcker,[34] average of 34 samples; 2 Weber-Diefenbach[44], average of 3 samples; 3 Bischoff,[35] average of 2 samples; 4 Scholten et al.,[36] average of 27 samples; 5 Bignell et al.,[30] average of two cores; 6 Bignell[37].

Table 7: Geochemical composition of the sulfide facies. 1 Bäcker,[34] average of 64 samples from various sulfide layers; 2 Bischoff,[35] average of 42 samples; 3 Bignell et al.,[30] average of two sulfide layers; 4 Weber-Diefenbach,[44] average of 16 samples; 5 Bignell et al.,[30].

Table 8: Metal content of brines in the Atlantis-II-Deep in mg/kg; a) Brooks et al.[58]; b) Hartmann,[57,59] c) Danielsson et al.,[60]; d) Hartmann;[57] e) unpublished data (0.4 µm filtered); - not measured.

Table 9: Summary of temperature estimates of hydrothermal deposits from the Atlantis-II-Deep; a) Brewer et al.,[67]; b) Ross,[68]; c) Sakai et al.,[69]; d) Schoell,[70]; e) Truesdell,[71]; f) Pottorf and Barnes,[64]; g) Missak et al.,[63]; h) Ramboz et al., [65]; i) Ramboz and Danis,[72]; j) Anschutz and Blanc,[49].

Table 10: Geochemistry of massive sulfides from the Kebrit Deep and comparison with deposits from Escanaba Trough, Guaymas Basin and volcanic-hosted mid-ocean ridge deposits; a) Blum and Puchelt,[78]; b) massive sulfide samples from Meteor cruise (1995), chemical data from Puchelt (pers. comm.); c) pyrrhotite-rich sulfides, average of 5 samples, Koski et al.,[81]; d) polymetallic sulfides, average of 2 samples, Koski et al.,[81]; e) Koski et al.[82]; f) Herzig and Hannington,[21].

Figures

Figure 1: The Red Sea with the location of the deeps. (after Bäcker [7]; reproduced by permission of the Geologische Jahrbuch, Hannover)

Figure 2: Relationships between Ca+Al, Fe+2Mn and 50(Zn+Cu) in sediments from various deeps of the Red Sea. Ca+Al is the endmember of biogenic-detrital sediments, Fe+2Mn represents iron-manganese deposits and 50(Zn+Cu) is the endmember of sulfide deposits. Apart from the Atlantis-II-deep the most concentrated hydrothermal sediment deposits in the Red Sea occur in the Thetis, Gypsum, Nereus and Vema deeps (Bäcker[7]; reproduced by permission of the Geologische Jahrbuch, Hannover)

Figure 3: Principles of hydrothermal convection and formation of hydrothermal deposits in the Atlantis-II-Deep. Seawater percolates through Miocene sedimentary deposits and

fissures in basaltic basement; heating of the fluids due to proximity of a magma chamber; fluid interaction with sediments and basalts in the recharge zone changing the physical and chemical characteristics of the fluids; when the hydrothermal solutions discharge into the basin metalliferous sediments precipitate (modified after, Bignell[3] and Bäcker[56]).

Figure 4: Temperature increase of LCL (Lower Convective Layer) and UCL (Upper Convective Layer) between 1965 and 1997 (compiled after Post[61] and Hartmann et al.[62]).

Figure 5: Ratio of Fe and Mn in sediments of the Atlantis-II-Deep based on about 600 sediment cores from which the average Fe/Mn covering all facies types were taken. Whereas Fe precipitates near the hydrothermal vents as Fe-silicates and sulfides, Mn diffuses to areas more distal from the vent sites. The high Fe/Mnx5 ratios indicate that the hydrothermal vents discharge in the SW-Basin of the Atlantis-II-Deep (Bäcker [7]; reproduced by permission of the Geologische Jahrbuch, Hannover)

Figure 6: Lithostratigraphic units of the sediments in the Atlantis-II-Deep (Bäcker and Richter;[2] reproduced with permission of the authors)

Figure 7: Plot of $^{206}Pb/^{204}Pb$ versus $^{208}Pb/^{204}Pb$ in sulfides, sediments and basalts from the Red Sea area. The ratios in the massive sulfides from the Kebrit Deep plot near to those of detrital and metalliferous sediments. The isotopic data indicate the source of the metals in the hydrothermal fluids, which formed the massive sulfides in the Kebrit Deep, to be derived from mixing between basaltic and detrital components.

Plates

a) Transition zone between the brine pool and normal seawater in the Kebrit Deep. The light-gray coloured zone is the brine and the transition to dark-gray colours mark the boundary between the reducing conditions in the brine and a zone where Fe-oxides precipitate due to mixing with seawater. More distal from the brine a black coloured zone indicates precipitation of Mn-oxides. White organisms surround a sulfide chimney in the upper part of the plate.

b) Chimneys of massive sulfides within the brine pool of the Kebrit Deep

c) Spindle type chimneys, which stick out of the sediments on the flank of the Kebrit Deep above the brine pool; anthropogenic pollution is indicated by the plastic cups

d) Massive sediment-covered sulfides, which outcrop on the flanks of the Kebrit Deep

e) Massive sulfide recovered during Meteor cruise in 1997 on the flanks of the Kebrit Deep. The sulfides almost exclusively consist of pyrite; often they are impregnated with tar.

f) Chimney-like massive sulfide recovered during Sonne cruise 29 (1984). The sulfides are very fragile and porous.

Year	Ship	Investigations
1881 - 83	Vityaz (U.S.S.R.)	First measurements of temperature and salinity in Red Sea Waters, sediments
1897	Pol (Austria)	
1898	Valdivia (GER)	
1948	Albatross (S)	Discovery of anomalously high temperature and salinity values around 21°N
1959	Atlantis (U.S.A.)	
1963	Atlantis II (U.S.A.)	
1963	Discovery (U.K.)	
1964	Discovery (U.K.)	
1964 - 65	Meteor (GER)	
1965	Atlantis II (U.S.A.)	Discovery of the deeps, dredging, coring of metalliferous muds
1965	Meteor (GER)	
1966	Chain (U.S.A.)	
1966	AK.S. Vavilov (U.S.S.R.)	
1967	Discovery (U.K.)	
1967	Oceanographer (U.K.)	
1969	Wando River (U.S.A.)	
1970 -71	Nereus (Saudi Arabia)	
1971	Valdivia (GER)	
1969	Chain (U.S.A.)	
1972	Glomar Challenger (U.S.A.)	
1976	AK. Kurchatov (U.S.S.R.)	
1977 - 78	Sonne (GER) - COMMISSION I (SO - 01)	Saudi-Sudanese Red Sea Commision program devoted to evaluation of the economic interest of muds and ecological impact of an exploitation
1977 - 78	Sonne (GER.) - MESEDA I (SOI - 02)	
1979	Valdivia (GER.) - MESEDA II (Va 22)	
1979	Sedco 445 - Pre Pilot Mining Test	
1980 - 81	Valdivia (GER.) - MESEDA III (Va 29)	
1981	Marion-Dufresnes (France) - COMMAR I	
1978	Melville (France)	
1979	Jean-Charcot (France) - MEROU -	Bathymetric survey (Seabeam)
1980	AK. Kurchatov(U.S.S.R.) Pr. Chotkman BRS Agnarrante	Study of 18°N axial area and diving in the Atlantis-II-Deep area
1980 - 83	Sonne – MENOR I +II (GER)	Metal exploration of the northern Red Sea
1981	Marion-Dufresnes (France)	Atlantis-II-Deep, Nereus-Deep
1984	Sonne (GER) SO 29	Deeps in the northern Red Sea
1986	Meteor (GER)	Hydrography Atlantis-II-Deep
1985	Marion-Dufresnes (France)	Atlantis-II-Deep
1992	Marion-Dufresnes (France)	Atlantis-II-Deep
1995	Meteor (GER)	Deeps in the northern Red Sea
1997	Sonne (GER) SO 121	Deeps in the northern Red Sea

Table 1

Normal Red Sea facies				
%	**Average [1]**	**Atlantis-II-Deep [2]**	**Thetis Deep [3]**	**Kebrit Deep [4]**
SiO_2	n.m	24.4	n.m.	
Al_2O_3	5.20	1.70	n.m.	
CaO	27.00	23.6	37.9	35.00
MgO	3.60	n.m.	1.70	n.m
Fe	4.00	4.50	1.50	3.50
Mn	0.35	0.40	0.70	0.12
Zn	0.03	0.06	0.04	0.02
Cu	0.007	0.007	0.01	0.004

Tab. 2:

Goethite facies								
%	**Atlantis-II-Deep [1]**	**Atlantis-II-Deep [2]**	**Atlantis-II-Deep [3]**	**Atlantis-II-Deep [4]**	**Thetis-Deep[5]**	**Kebrit-Deep[6]**	**Nereus-Deep[6]**	**Gypsum Deep [7]**
SiO_2	n.m	n.m.	8.70	n.m.	2.57	n.m.	n.m.	n.m.
Al_2O_3	n.m	n.m	1.10	1.93	0.09	2.76	0.92	0.84
CaO	0.90	2.30	3.40	0.42	0.41	20.9	0.49	2.20
MgO	0.60	0.90	n.m.	n.m.	1.31	4.64	0.50	1.65
Fe	51.3	50.1	44.9	63.2	50.2	30.8	54.6	50.7
Mn	1.10	0.60	0.80	0.26	0.51	0.17	0.45	0.35
Zn	0.27	0.27	0.56	0.15	0.17	0.10	0.66	0.24
Cu	0.19	0.05	0.24	0.01	0.02	0.03	0.006	0.01

Tab. 3..

Lepidocrocite facies					***Hematite facies***			
%	**Atlantis-II-Deep [1]**	**Thetis-Deep[2]**	**Nereus-Deep [3]**	**Gypsum-Deep[3]**	**Atlantis-II-Deep [4]**	**Atlantis-II-Deep [1]**	**Thetis-Deep[5]**	**Nereus-Deep[6]**
SiO_2	n.m.	0.73		n.m.	n.m	n.m.	7.91	8.10
Al_2O_3	0.67	0.26	1.20	0.66	n.m	1.03	2.66	1.00
CaO	2.00	0.55	14.2	1.63	1.00	8.22	15.5	3.00
MgO	n.m.	1.18	n.m.	n.m.	1.10	n.m	4.59	0.80
Fe	63.16	48.97	35.00	54.35	49.1	35.29	19.9	65.4
Mn	0.26	0.45	2.00	0.19	1.10	0.29	6.89	0.69
Zn	0.15	0.15	0.10	0.18	0.16	0.12	0.35	0.24
Cu	0.01	0.15	0.09	0.03	0.27	0.74	0.08	0.16

Tab. 4:

Magnetite facies			*Silicate facies*			
%	**Thetis-Deep[1]**	**Nereus-Deep[2]**	**Atlantis-II-Deep[3]**	**Atlantis-II-Deep[4]**	**Atlantis-II-Deep[5]**	**Thetis-Deep[6]**
SiO_2	2.60	3.50	23.7	n.m.	n.m.	n.m.
Al_2O_3	1.21	0.20	1.50	n.m.	0.10	4.00
CaO	1.20	8.00	6.00	4.00	2.50	1.96
MgO	2.00	1.00	1.00	1.50	n.m.	n.m.
Fe	54.5	56.9	28.7	27.2	3.57	39.5
Mn	0.23	0.39	1.20	0.70	0.04	0.72
Zn	0.14	1.52	1.93	2.52	0.004	0.14
Cu	0.41	1.51	0.51	0.47	0.02	0.11

Tab 5

Manganite facies							
%	**Atlantis-II-Deep [1]**	**Atlantis-II-Deep [2]**	**Atlantis-II-Deep [2]**	**Thetis Deep[4]**	**Nereus Deep[5]**	**Chain Deep[6]**	**Shagara Deep[6]**
SiO_2	n.m.	5.70	7.50	4.81	n.m.	n.m.	n.m.
Al_2O_3	n.m	4.90	0.70	2.83	0.63	1.07	2.56
CaO	3.60	11.8	2.90	11.1	5.78	4.77	21.8
MgO	1.90	1.06	n.m.	3.66	n.m.	n.m.	n.m.
Fe	15.3	19.6	21.3	13.0	30.8	12.9	3.89
Mn	32.7	29.4	27.5	14.1	17.9	35.8	15.6
Zn	0.64	0.19	1.12	0.58	1.33	1.22	0.21
Cu	0.09	0.01	0.08	0.08	0.04	0.13	0.01

Tab 6:

Element	**Sulphide facies**					
%	**Atlantis-II Deep [1]**	**Atlantis-II Deep[2]**	**Atlantis-II Deep[3]**	**Atlantis-II Deep[4]**	**Erba Deep[5]**	**Gypsum Deep[5]**
SiO_2	n.m	24.7	n.m	21.4	n.m	n.m.
Al_2O_3	n.m.	1.5	2.27	4.9	10.6	29.1
CaO	4.2	2.5	9.37	3.6	7.15	4.07
MgO	1.69	n.m.	n.m	1.3	n.m.	n.m.
Fe	23.8	17.0	18.0	25.5	26.6	29.1
Mn	1.3	0.8	1.96	1.94	0.51	0.09
Zn	5.93	9.76	8.12	4.5	0.34	0.05
Cu	1.26	3.6	1.78	1.06	0.06	0.67
Cd	0.02	n.m.	0.03	n.m	0.001	0.004
S	8.8	16.8	n.m	12.9	n.m.	n.m.

Tab 7:

	1966 a)	1971b)	1976 c)	1977 d)	1995 e)
UCL brine					
Fe	1-3	6-8	6.5 ± 2	7.3 ± 0.2	2 ± 2
Mn	79 ± 2	78 ± 1	71.5 ± 1	75 ± 2	101 ± 8
Cu	0.1 ± 0.6	0.03-0.04	0.022	0.0005-0.001	-
Zn	2-8	1.1-2	1.6	1.61 ± 0.05	2.7
LCL brine					
Fe	90 ± 8	86 ± 5	81 ± 4	75-81	88 ± 2
Mn	87 ± 5	82 ± 6	82 ± 4	81 ± 2	100 ± 1
Cu	0.15 -0.6	0.03-0.12	0.021	0.0005	-
Zn	7 ± 2	2-5	3.0	3.0 ± 1	4.2

Tab. 8:

Temperature	Technique	Reference
110°	Measured volume and temperature changes of the lower brine from mixing with the hydrothermal fluid	a,b
> 210°	Measured volume and temperature changes of the lower brine from mixing with the hydrothermal fluids	d
> 108°	Silica solubility	e
> 158°	Na, K, Ca, geothermometer	e
250°	oxygen isotope geothermometry, SO_4^{-2},H_2O pair	c
261°	oxygen isotope geothermometry, SO_4^{-2}, H_2O pair	e
> 210°	minimum thermal stability of cubic cubanite	f
210-251	cubic cubanite+chalcophyrite+monocline pyrrhotite assemblage	f
> 334	cubic cubanite+chalcophyrite+pyrite assemblage	f
238	homogenisation temperature on vein anhydrite	f
< 450°	exsolved chalcopyrite lamellae in intermediate solid solutions	g
390-403°	homogenisation temperature of anhydrite from sediments from the SW-basin	h)
432-353°	heat-mass balance of the Atlantis-II-Deep brine	i)
195-310°	heat and salt mass balance	j)

Tab. 9

Sample	Fe (%)	Zn (%)	Pb (ppm)	Cu (ppm)	Ni (ppm)	no. of samples
DC 354 75/0	22.1	26.4	6200	<5	<20	1 [a)]
DC 354 75/1	16.5	35.9	6900	0.5	3	1 [a)]
DC 354 75/2a	8.6	50.9	3700	2.6	<10	1 [a)]
DC 354 75/2b	40.2	5.5	590	2.9	3	1 [a)]
DC 354 75/3a	20.3	31.7	3800	<5	4	1 [a)]
DC 354 75/3b	42.5	1.4	150	1.1	6	1 [a)]
DC 354 75/4a	22.4	31.8	3700	3.6	3	1 [a)]
DC 354 75/4b	41.9	1.8	140	2.7	7	1 [a)]
DC 352	43.6	<0.1	<100	5	<20	1 [a)]
17006-6	38.9	0.38	n.a.	n.a.	27	1 [b)]
17006-7	29.4	0.04	n.a	n.a	n.d.	2 [b)]
17006-9	28.5	0.35	n.a	n.a	41	7 [b)]
Escanaba Trough	41.5	1.1	2800	16500	n.a	5 [c)]
Escanaba Trough	25.0	31.8	44000	10000	n.a.	2 [d)]
Guaymas Basin	33.5	3.9	3400	5900	n. a.	9 [e)]
volcanic-hosted mid-ocean ridges	23.6	11.7	0.2	43000	n.a	890 [f)]

Table 10

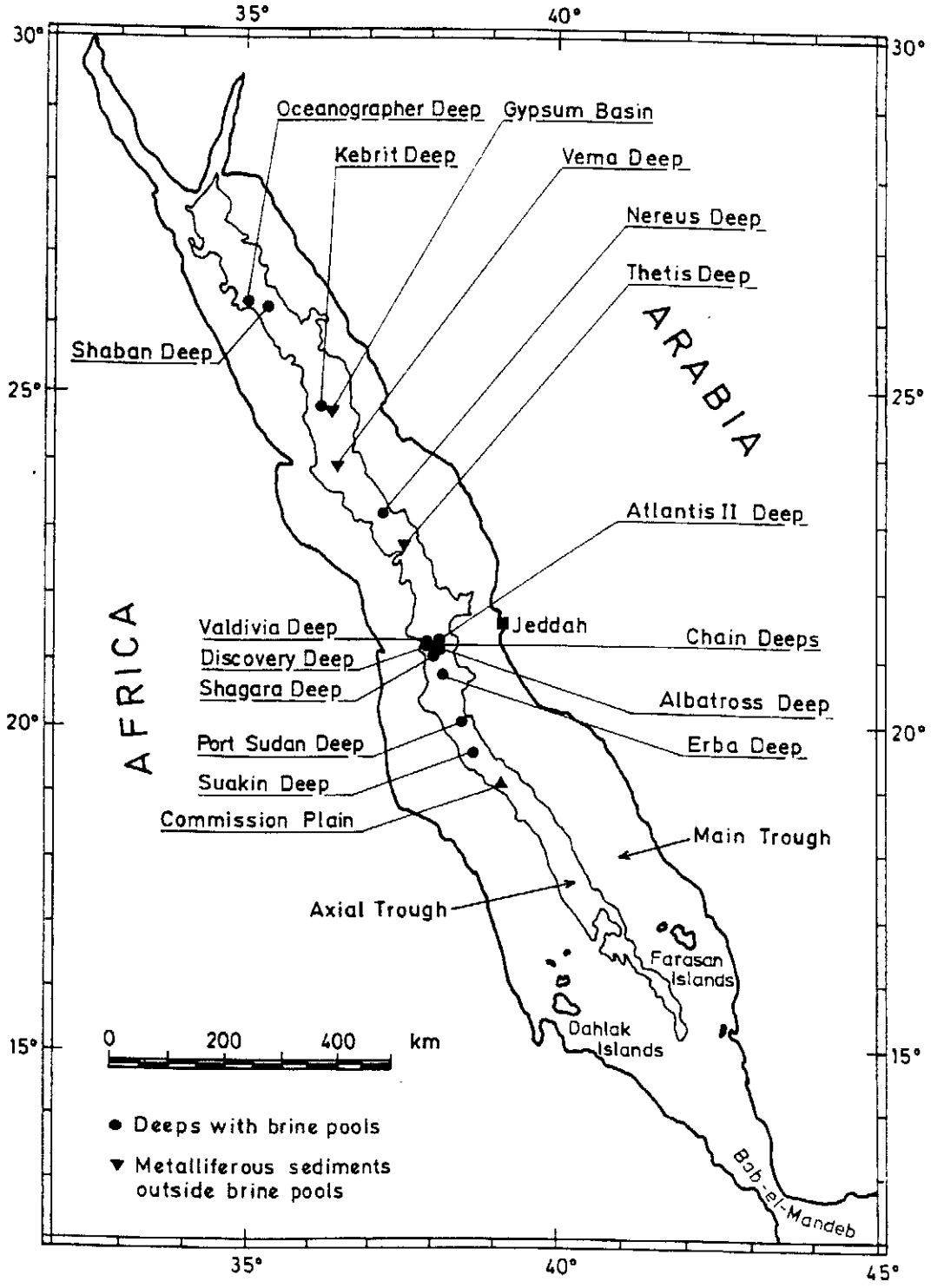
35°
40°
30°
25°
20°
15°
45°
Oceanographer Deep
Gypsum Basin
Kebrit Deep
Verna Deep
Nereus Deep
Thetis Deep
Shaban Deep
ARABIA
Atlantis II Deep
AFRICA
Valdivia Deep
Jeddah
Chain Deeps
Discovery Deep
Shagara Deep
Albatross Deep
Erba Deep
Port Sudan Deep
Suakin Deep
Commission Plain
Main Trough
Axial Trough
Farasan Islands
Dahlak Islands
0
200
400
km
Deeps with brine pools
Metalliferous sediments outside brine pools
Bab-el-Mandeb

Fig. 1

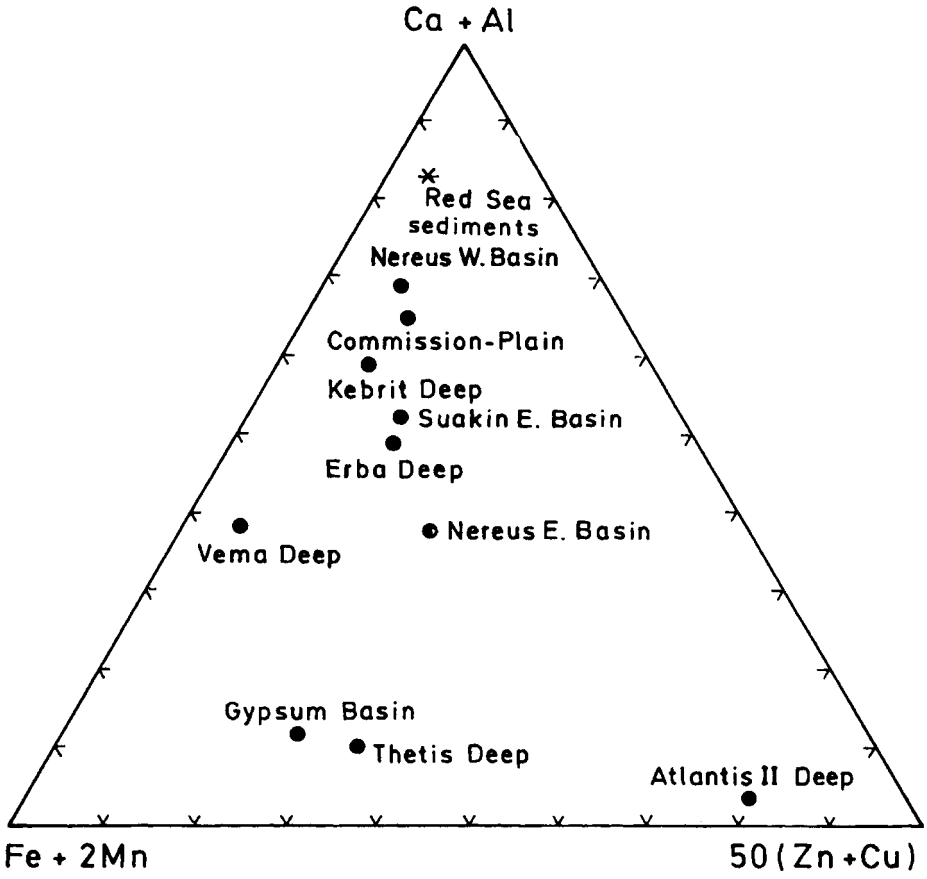
Ca + Al
Red Sea sediments
Nereus W. Basin
Commission-Plain
Kebrit Deep
Suakin E. Basin
Erba Deep
Nereus E. Basin
Vema Deep
Gypsum Basin
Thetis Deep
Atlantis II Deep
Fe + 2Mn
50 (Zn + Cu)

Fig. 2

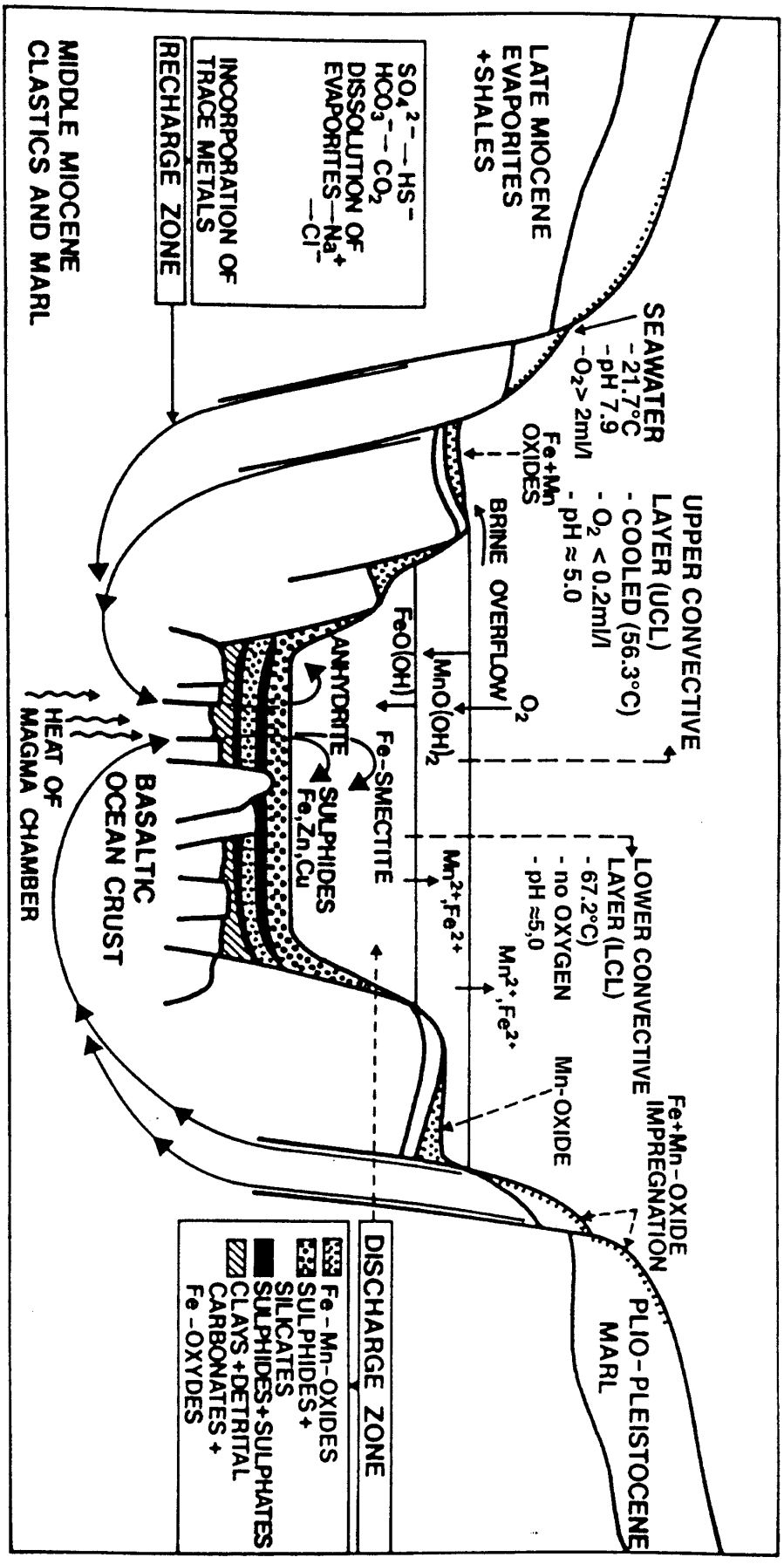
SEAWATER
-21.7°C
-pH 7.9
-O2> 2ml/l
LATE MIOCENE
EVAPORITES
+SHALES
UPPER CONVECTIVE
LAYER (UCL)
- COOLED (56.3°C)
- O2 < 0.2ml/l
- pH ≈ 5.0
Fe+Mn
OXIDES
BRINE OVERFLOW
O2
FeO(OH)
MnO(OH)2
Fe-SMECITE
ANHYDRITE
SULPHIDES
Fe,Zn,Cu
Mn2+,Fe2+
LOWER CONVECTIVE
LAYER (LCL)
- 67.2°C)
- no OXYGEN
- pH ≈5,0
Mn2+,Fe2+
Mn-OXIDE
Fe+Mn-OXIDE
IMPREGNATION
PLIO-PLEISTOCENE
MARL
SO4 2- — HS-
HCO3- — CO2
DISSOLUTION OF
EVAPORITES—Na+
—Cl-
INCORPORATION OF
TRACE METALS
RECHARGE ZONE
MIDDLE MIOCENE
CLASTICS AND MARL
HEAT OF
MAGMA CHAMBER
BASALTIC
OCEAN CRUST
DISCHARGE ZONE
Fe-Mn-OXIDES
SULPHIDES+
SILICATES
SULPHIDES+SULPHATES
CLAYS+DETRITAL
CARBONATES+
Fe-OXYDES

Fig. 3

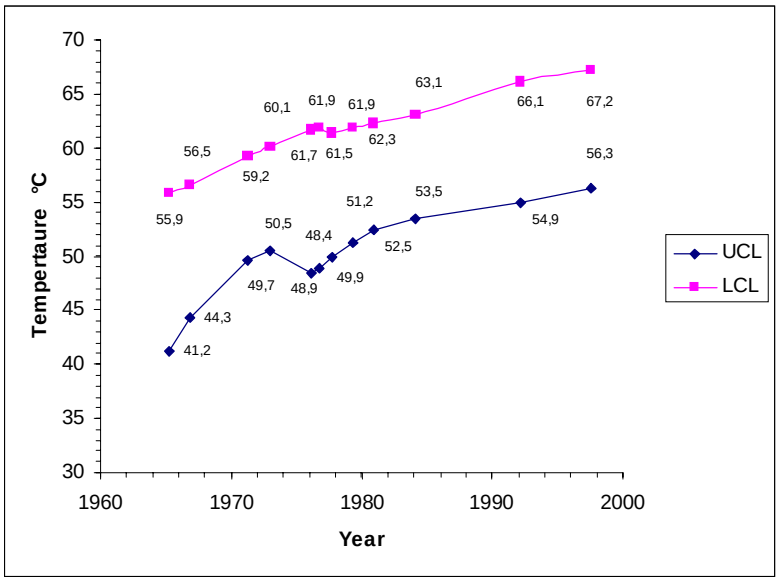

Fig. 4

ATLANTIS-II DEEP

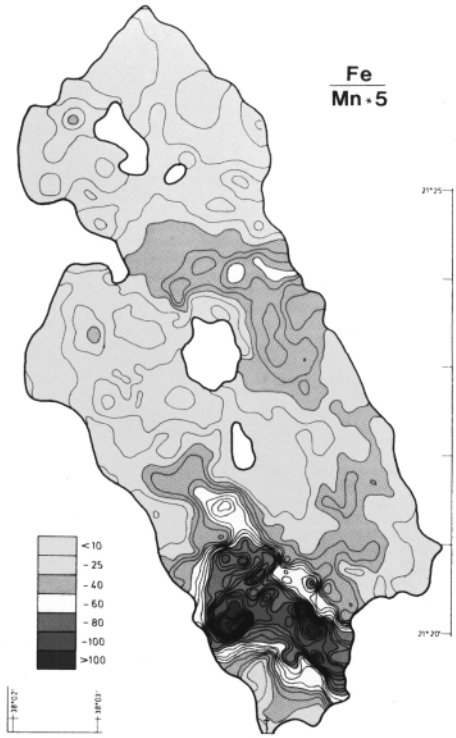

Ratio of Fe to Mn in sediments cores
(after Bäcker et al., 1991)

Fig. 5

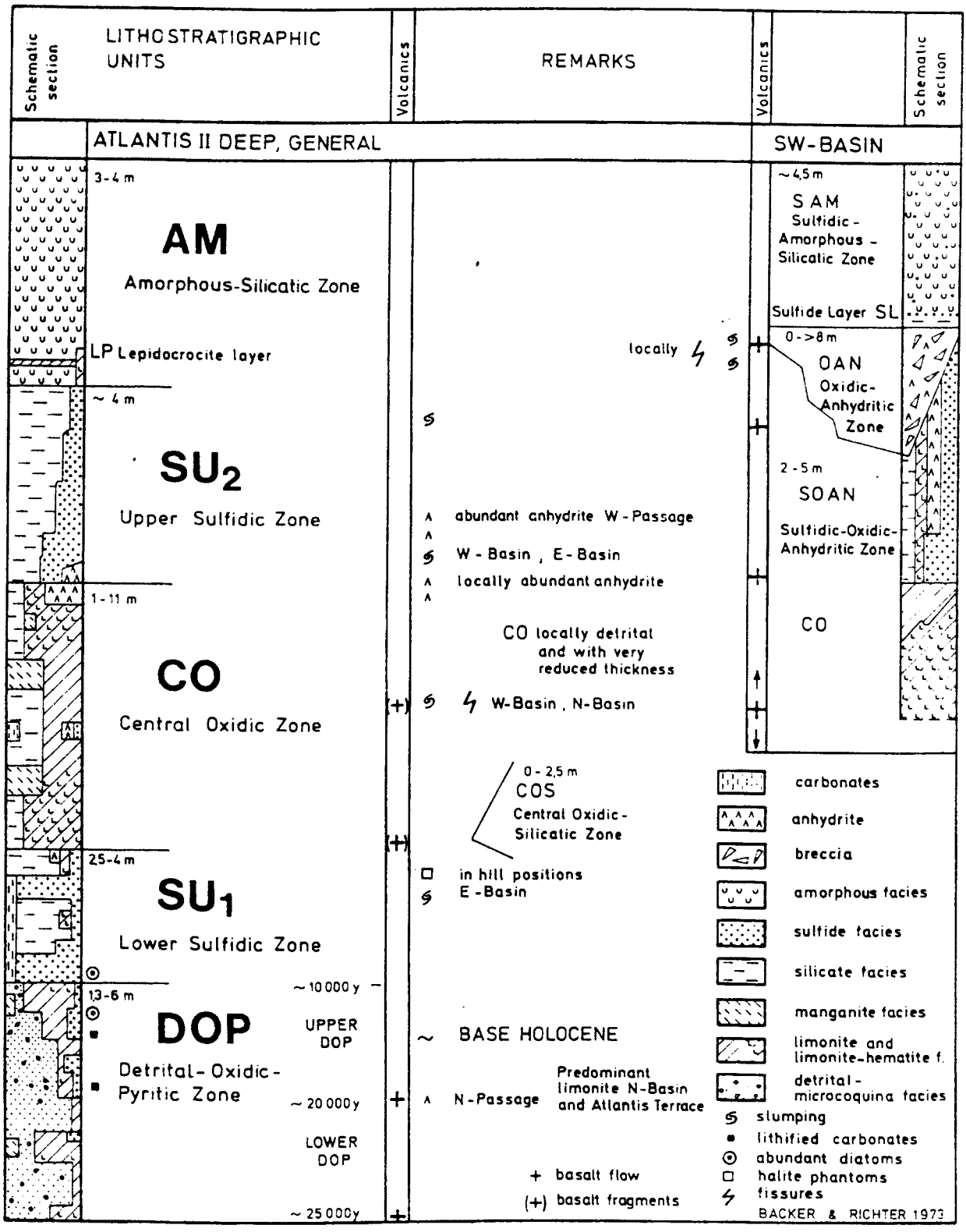
Schematic section
LITHOSTRATIGRAPHIC UNITS
Volcanics
REMARKS
Volcanics
Schematic section
ATLANTIS II DEEP, GENERAL
SW-BASIN
3-4 m
AM
Amorphous-Silicatic Zone
LP Lepidocrocite layer
~ 4 m
SU2
Upper Sulfidic Zone
1-11 m
CO
Central Oxidic Zone
2.5-4 m
SU1
Lower Sulfidic Zone
1.3-6 m
DOP
Detrital-Oxidic-Pyritic Zone
~ 10 000 y
UPPER DOP
~ 20 000 y
LOWER DOP
~ 25 000 y
locally
abundant anhydrite W-Passage
W-Basin, E-Basin
locally abundant anhydrite
CO locally detrital and with very reduced thickness
W-Basin, N-Basin
0-2,5 m
COS
Central Oxidic-Silicatic Zone
in hill positions
E-Basin
BASE HOLOCENE
N-Passage
Predominant limonite N-Basin and Atlantis Terrace
basalt flow
basalt fragments
~4,5 m
SAM
Sulfidic-Amorphous-Silicatic Zone
Sulfide Layer SL
0->8 m
OAN
Oxidic-Anhydritic Zone
2-5 m
SOAN
Sulfidic-Oxidic-Anhydritic Zone
CO
carbonates
anhydrite
breccia
amorphous facies
sulfide facies
silicate facies
manganite facies
limonite and limonite-hematite f.
detrital-microcoquina facies
slumping
lithified carbonates
abundant diatoms
halite phantoms
fissures
BACKER & RICHTER 1973

Fig. 6

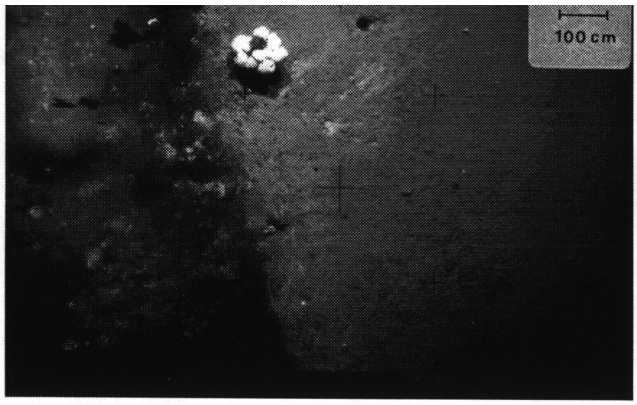

Plate a

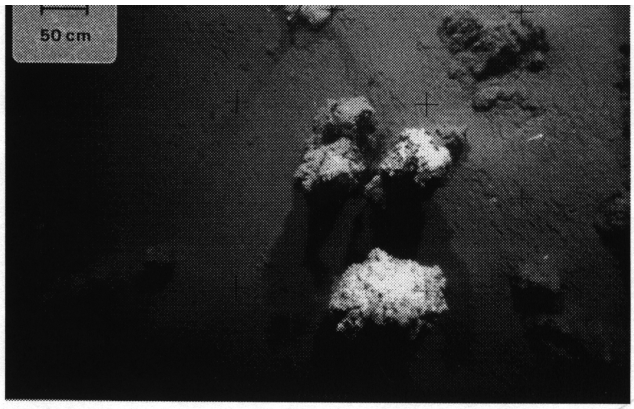

Plate b

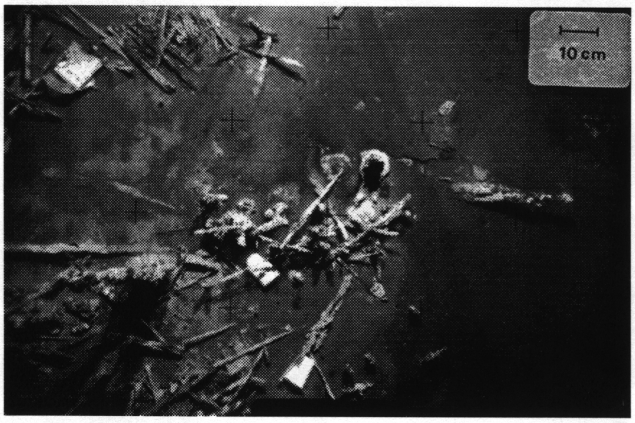

Plate c

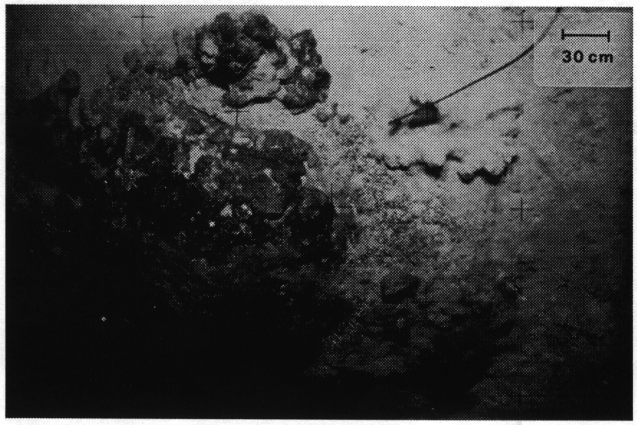

Plate d

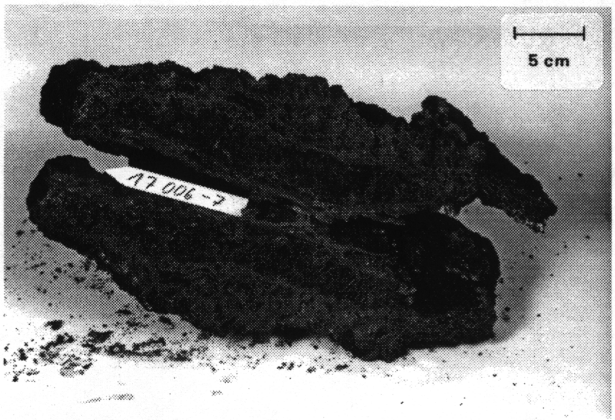

Plate e

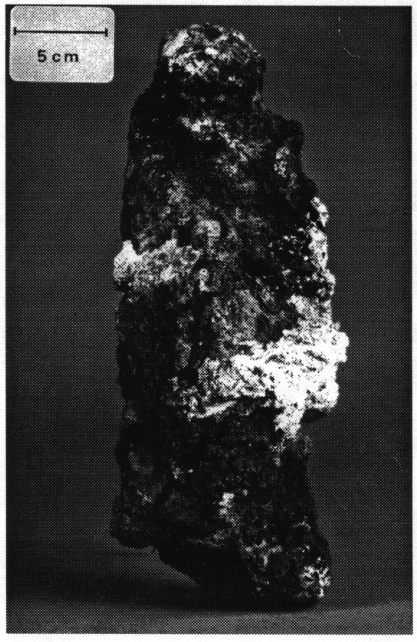

Plate f

Fig. 7

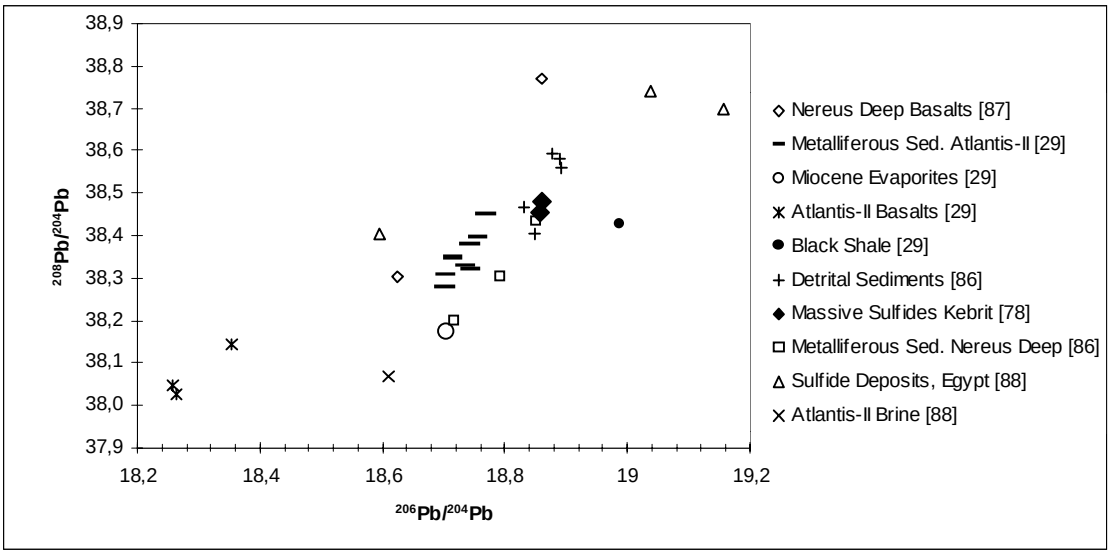
38,9
38,8
38,7
38,6
38,5
38,4
38,3
38,2
38,1
38,0
37,9
208Pb/204Pb
18,2
18,4
18,6
18,8
19
19,2
206Pb/204Pb
Nereus Deep Basalts [87]
Metalliferous Sed. Atlantis-II [29]
Miocene Evaporites [29]
Atlantis-II Basalts [29]
Black Shale [29]
Detrital Sediments [86]
Massive Sulfides Kebrit [78]
Metalliferous Sed. Nereus Deep [86]
Sulfide Deposits, Egypt [88]
Atlantis-II Brine [88]

Fig. 8

11. Novel 16S rRNA gene sequences retrieved from highly saline brine sediments of Kebrit Deep, Red Sea

Wolfgang Eder, Wolfgang Ludwig, Robert Huber

Introduction

In geological time scales, the Red Sea is an ocean *in statu nascendi* forming during the past 20 million years due to the divergent movement of the Arabian and African continental plates (Girdler and Styles 1974). This movement is accompanied by the formation of new oceanic crust, which can be observed in the southern Red Sea as a 1500-2000 m deep axial graben. Towards the north, the graben narrows and north of 21°N only isolated deeps are found, reflecting a punctiform emplacement of oceanic crust (Fig. 1; Bonatti et al. 1985). About 25 of these deeps are filled with highly saline brines, formed due to the dissolution of Miocene evaporites (Zierenberg and Shanks 1986; Hartmann et al. 1998).

The Kebrit Deep (Fig. 1) is a roundish basin of about 1 km in diameter, with sides falling steeply to a maximum depth of 1549 m from the surrounding, topographically smooth seafloor (Bignell et al. 1976; Pautot 1983). The basin is filled by a 84 m thick anaerobic, slightly acidic brine (about pH 5.5), with a high salinity of 26% (chlorinity: 154‰ Cl^-) and a temperature of 23.3°C (Bäcker and Schoell 1972; Hartmann et al. 1998; D. Garbe-Schönberg, personal communication). The brine has a high gas content, made up largely of CO_2 and H_2S (12-14 mg S/l), and small amounts of N_2, CH_4 and C_2H_6 (Bäcker and Schoell 1972; Hartmann et al. 1998). Since the discovery of the deep during Valdivia cruise VA03 in 1971, no significant changes in temperature and salinity have been observed (Schoell 1974; Hartmann et al. 1998; Stoffers et al. 1998).

In recent years, new molecular techniques were developed, enabling a phylogenetic assignment of prokaryotic assemblages in natural ecosystems (Olsen et al. 1986; Pace et al. 1986). Using the 16S rRNA gene as a molecular marker, bacterial and archaeal communities have been studied in different biotopes including hot springs, soils, coastal sediments, marine picoplankton and water samples from the Pacific and Atlantic Ocean (DeLong 1992; Liesack and Stackebrandt 1992; Barns et al. 1994; DeLong et al. 1994; Fuhrman and Davis 1997; Ludwig et al. 1997; Massana et al. 1997; Munson et al. 1997; Hugenholtz et al. 1998). To date, the microbial communities of the extremely saline, anaerobic environment of the Kebrit Deep have not been investigated and are therefore unknown. In order to look for the existence of potential extremophiles, we took a highly saline brine sediment sample in a depth of 1515 m in the Kebrit Deep and assayed 16S rRNA genes as indicators of procaryotic life. For the first time we report here on the existence of unique 16S rRNA gene sequences, suggesting the presence of novel anaerobic, high salt and high pressure communities.

Materials and Methods

Collection of samples

During RV *Sonne* expedition SO 121 in 1997, sediment sample KT 5 (total volume: 120 ml) was taken by a multicorer in a depth of 1515 m (determined by echo sounding) from the Kebrit Deep brine, Red Sea (station no.: 17032-2; position: 24°43.95'N, 36°16.40'E; Fig. 1). Sample KT 5 from the upper sediment layer (1-3 cm) was composed of soft greyish-green material and smelled strongly of H_2S; the salinity was 24.2% (hand refractometer, A.S.T., Japan), the original temperature 23.3°C (Stoffers et al. 1998), and the original pH 6.5 (Neutralit, Merck,

Darmstadt, Germany). The sample was transported to the laboratory by air at ambient temperature and was stored at 4°C.

DNA extraction

Nucleic acids were extracted from 30 ml of the Kebrit Deep sediment sample KT 5 by the freeze-thaw lysis procedure of Barns et al. (1994). The mixture was extracted with an equal volume of phenol (pH 7.5; AquaPhenol, Appligene, Illkirch, France), followed by extraction with phenol-chloroform-isoamylalcohol, 24:24:1 (by volume). Nucleic acids were precipitated with 0.1 volume of 3 M (wt/vol) sodium acetate and 2 volumes of 96% (wt/vol) ethanol, washed with 70% (wt/vol) ethanol and dried. For further purification, the nucleic acids were dialyzed at 4°C against 10 mM Tris/HCl (pH 8.3) and precipitated.

PCR amplification of rRNA genes

rRNA genes were PCR amplified with standard primers (Tab. 1) from 1 to 20 ng of bulk DNA in reaction mixtures containing (as final concentrations) 1x PCR buffer II (Perkin Elmer, Foster City, California), 1.5 mM $MgCl_2$, 4 x 200 µM deoxynucleoside triphosphates, 1 ng each forward and reverse primer, and 0.05 U of Ampli Taq or AmpliTaq LD (Perkin Elmer) per µl. Reaction mixtures were incubated in a model PE 9600 thermal cycler (Perkin Elmer) for an initial denaturation at 96°C for 90 s, followed by 10 cycles of 96°C for 30 s, 60°C for 30 s, and 72°C for 1 min, 25 cycles of 94°C for 20 s, 60°C for 30 s, and 72°C for 1 min (+2 s for each further cycle), and a final incubation at 72°C for 10 min (= standard protocol).

Purification and cloning of PCR products

Amplified DNA from 5 to 10 reaction mixtures was pooled, purified through a 1% (wt/vol) low-melting point agarose gel (Appligene), excised and extracted from the melted agarose (42°C) with glass milk using Geneclean II Kit (Bio 101, Vista, California). The purified 16S rRNA gene fragments were cloned into the pAMP1 vector (Life Technologies, Gaithersburg, USA) according to the manufacturer's instructions and the resulting ligation products were used to transform *Escherichia coli* DH5α cells. The presence of inserts of the appropriate size in the transformants was identified by direct PCR screening without plasmid extraction. For this method, 40 to 50 clones were randomly choosen and a small amount of each colony was used in a PCR reaction with the standard protocol (see above). Amplified inserts were identified by gel electrophoresis and an aliquot of each insert was used for digestion with a combination of the four restriction endonucleases AluI, HinfI, HhaI and RsaI (Life Technologies, Gaithersburg, USA; Rudolph 1998).

Sequencing of rRNA gene clones

Based on the fingerprinting pattern of the rRNA gene clones representative transformants were selected, and the corresponding plasmid DNAs were obtained using the QIAprep 8 Turbo Miniprep kit (Quiagen, Hilden, Germany). The plasmid templates were sequenced with an ABI 377 DNA Sequencer (PE Applied Biosystems, Foster City, California), using the ABI Prism BigDye terminator cycle sequencing ready reaction kit (Perkin Elmer) at the Institute for Medical Microbiology and Hygiene, clinical hospital of the University of Regensburg. Bacterial sequences were determined using a combination of the primers 8bF, 518uF and 1513uR, archaeal sequences using the primers 8aF, 344aF and 1406uR (Tab. 1).

Phylogenetic analyses

For the analyses, an alignment of about 10,000 homologous full and partial primary sequences available in public databases (ARB project, Ludwig and Strunk; Ludwig 1995) was used. The new bacterial and archaeal 16S rRNA gene sequences (about 1269 to 1481 nucleotides) were fitted in the 16S rRNA alignment by using the respective automated tools of the ARB software package (Ludwig and Strunk). Distance matrix (Jukes and Cantor correction), maximum parsimony and maximum likelihood (fastDNAml) methods were applied for tree reconstruction as implemented in the ARB software package. Although the application of alternative treeing methods allows reliable evaluation of tree topologies, in addition resampling techniques were used to estimate the significance of branching patterns (Ludwig et al. 1998). Each sequence was submitted to the CHECK_CHIMERA program of the Ribosomal Database Project (RDP) (Maidak et al. 1999) to detect the presence of possible chimeric artefacts.

Nucleotide sequence accession numbers

The sequences of the archaeal and bacterial rDNA clones have been deposited in the EMBL nucleotide sequence database under the accession no. AJ133615 to AJ133625.

Results and Discussion

A sediment sample from the Kebrit Deep was analysed for the presence and diversity of procaryotes in anaerobic highly saline brines of the Red Sea (Fig. 1). After extraction of the nucleic acids from the sediment and subsequent dialysis, PCR reactions with specific archaeal or bacterial forward primers and universal reverse primers were performed (Tab. 1). However, using the standard PCR protocol for amplification, no PCR products could be identified on agarose gels. Therefore, a modified PCR protocol was used. In the first step, ten PCR cycles according to the standard protocol were performed. From this PCR reaction mixture, 2 µl were added to a new 50 µl PCR mixture and 35 PCR cycles were carried out in a second step. Amplification products with the expected size could be visualized on agarose gels. Bacterial PCR products were obtained with primers 8bF and 1513uR, archaeal PCR products with 8aF and 1406uR (Tab. 1). After cloning, the 16S rRNA gene fragments were further characterized by restriction endonucleases digestion. Based on a comparison of the restriction patterns on agarose gels, five different archaeal and six different bacterial groups were identified (Tab. 2). From a representative of each restriction pattern group, the 16S rRNA gene sequence was determined and aligned with 16S rRNA sequences derived from the ARB database (Ludwig and Strunk). The analysis of the clone sequences showed, that the majority of the identified sequences did not show higher sequence similarities to sequences of cultivated microorganisms or to sequences from environmental samples.

Using three different tree construction methods (see Materials and Methods), the analysis of the bacterial sequences showed, that they cluster together and form the new KB1 sequence group (KTK 14, KTK 27, KTK 32, KTK 36, KTK 41 and KTK 42) in the 16S rRNA tree (Fig. 2). The G+C content of the rRNA gene sequences range from 0.55 to 0.58 mol%. The KB1 group form a deep phylogenetic branch between the *Aquificales* and the *Thermotogales* (Huber et al. 1992; Huber and Stetter 1992). Its branching point (Fig. 2) was supported by all three methods of constructing phylogenetic trees (not shown). The unique phylogenetic position is strenghtened by large evolutionary distance values of the KB1 group to the *Aquificales* (26.8%), *Thermotogales* (26.5%), and clone sequences obtained from environmental samples of hot springs (19-31%, Fig. 2; Hugenholtz et al. 1998; Yamamoto et al. 1998) and by bootstrap values of 98% and higher (maximum parsimony and distance matrix).

Phylogenetic analysis of the archaeal 16S rRNA gene sequences showed that they belong to the kingdom of the *Euryarchaeota*. No close phylogenetic similarity to cultivated members of

the *Euryarchaeota* could be identified. Interestingly, sequence clones KTK 4A, KTK 9A and KTK 31A from the highly saline brine sediment cluster with a clade of sequences obtained from environmental samples with salt concentrations typical for sea water, including the marine planktonic group II and marine group III euryarchaeota sequences (Fig. 3; DeLong 1992; DeLong et al. 1994; Fuhrman and Davis 1997; Massana et al. 1997; Munson et al. 1997). Representatives of this sequence clade have been detected recently in samples from the Antarctic and the Atlantic and Pacific Ocean, where they may be important components of the ecosystems (DeLong 1992; DeLong et al. 1994). Our results show that highly divergent members of this clade are also present in the Red Sea. Sequence clone KTK 4A may be the representative of a new branch, due to a sequence identity to existing rRNA gene sequences of less than 83%. The remaining sequence clones KTK 18A and KTK 28A did not show high similarity to known sequences. Separate branching points for the sequence clones KTK 18A and KTK 28A (Fig. 3) were supported by all tree construction methods (not shown). According to the results of our analyses these two sequences do not significantly cluster with others, due to the lack of closer related 16S rRNA gene sequences. The G+C content of the new archaeal rRNA gene sequences range from 0.53 to 0.56 mol%. These relatively low G+C contents (Woese et al. 1991) indicate that the corresponding organisms are active at the constant environmental temperature (23°C).

Our investigations show that novel groups of archaea and bacteria may thrive in the extreme environment of the Kebrit Deep in the northern Red Sea (Fig. 1). A far less probable possibility is that the 16S rRNA gene sequences were derived from detritus of procaryotic material that settled down from the upper sea water. Therefore, the origin of the sequence-predicted organisms is still a riddle and only cultivation experiments in the laboratory will give us information on their natural environment. The results presented in this paper are the prerequisite for culture attempts as we have described recently, employing enrichment cultures, phylogenetic staining and "optical tweezers" (Huber et al. 1995; Huber et al. 1998). To date, first enrichment cultures were obtained under anaerobic cultivation conditions growing under the extreme environmental conditions of the Kebrit Deep, like high salt and sulfide concentrations and high pressure.

ACKNOWLEDGMENTS

We are greatful to K.O. Stetter for stimulating and critical discussions. Furthermore, we thank H. Huber for discussions. The highly valuable help of the Gelogical Institute of the University of Kiel, P. Stoffers, and of the crew on board of RV *Sonne* (SO 121 cruise) is appreciated. This work was financially supported by the BMBF under grant 03G0121B and the Fond der Chemischen Industrie.

References

Barns SM, Fundyga RE, Jeffries MW, Pace NR (1994) Remarkable archaeal diversity detected in a Yellowstone National Park hot spring environment. Proc. Natl. Acad. Sci. U.S.A. 91:1609-1613

Bäcker H, Schoell M (1972) New deeps with brines and metalliferous sediments in the Red Sea. Nature Physical Science 240:153-158

Bignell RD, Cronan DS, Tooms JS (1976) Red Sea metalliferous brine precipitates. Special paper - Geological Association of Canada 14:147-179

Bonatti E (1985) Punctiform initiation of seafloor spreading in the Red Sea during transition from a continental to an oceanic rift. Nature 316:33-37

Brosius J, Dull TJ, Sleeter DD, Noller HF (1981) Gene organization and primary structure of a ribosomal RNA operon from *Escherichia coli*. J. Mol. Biol. 148:107-127

Burggraf S, Stetter KO, Rouviere P, Woese CR (1991) *Methanopyrus kandleri*: An archaeal methanogen unrelated to all other known methanogens. System. Appl. Microbiol. 14:346-351

Burggraf S, Olsen GJ, Stetter KO, Woese CR (1992) A phylogenetic analysis of *Aquifex pyrophilus*. System. Appl. Microbiol. 15:352-356

Burggraf S, Huber H, Stetter KO (1997) Reclassification of the crenarchaeal orders and families in accordance with 16S ribosomal RNA sequence data. Int. J. Syst. Bacteriol. 47:657-660

DeLong EF (1992) Archaea in coastal marine environments. Proc. Natl. Acad. Sci. U.S.A. 89:5685-5689

DeLong EF, Wu KY, Prézelin BB, Jovine RVM (1994) High abundance of Archaea in Antarctic marine picoplankton. Nature 371:695-697

Fuhrman JA, Davis AA (1997) Widespread Archaea and novel Bacteria from the deep sea as shown by 16S rRNA gene sequences. Marine Ecology Progress Series 150:275-285

Girdler RW, Styles P (1974) Two stage Red Sea floor spreading. Nature 247:7-11

Hartmann M, Scholten JC, Stoffers P, Wehner F (1998) Hydrographic structure of brine-filled deeps in the Red Sea - new results from the Shaban, Kebrit, Atlantis II, and Discovery Deep. Marine Geology 144:311-330

Huber R, Stetter KO (1992) The order *Thermotogales*. In: Balows A, Trüper HG, Dworkin M, Harder W, Schleifer KH (eds) The Prokaryotes. Springer Verlag, New York, pp 3809-3815

Huber R, Wilharm T, Huber D, Trincone A, Burggraf S, König H, Rachel R, Rockinger I, Fricke H, Stetter KO (1992) *Aquifex pyrophilus* gen.nov. sp.nov., represents a novel group of marine hyperthermophilic hydrogen-oxidizing bacteria. System. Appl. Microbiol. 15:340-351

Huber R, Burggraf S, Mayer T, Barns SM, Rossnagel P, Stetter KO (1995) Isolation of a hyperthermophilic archaeum predicted by *in situ* RNA analysis. Nature 376:57-58

Huber R, Eder W, Heldwein S, Wanner G, Huber H, Rachel R, Stetter KO (1998) *Thermocrinis ruber* gen. nov., sp. nov., a pink-filament-forming hyperthermophilic bacterium isolated from Yellowstone National Park. Appl. Environ. Microbiol. 64:3576-3583

Hugenholtz P, Pitulle C, Hershberger KL, Pace NR (1998) Novel division level bacterial diversity in a Yellowstone hot spring. J. Bacteriol. 180:366-376

Lane DJ (1991) 16S/23S rRNA sequencing. In: Stackebrandt E, Goodfellow M (eds) Nucleic acid techniques in bacterial systematics. John Wiley & sons, Chichester, England, pp 115-175

Liesack W, Stackebrandt E (1992) Occurrence of novel groups of the domain *Bacteria* as revealed by analysis of genetic material isolated from an australian terrestrial environment. J. Bacteriol. 174:5072-5078

Ludwig W (1995) Sequence databases (3.3.5). In: Akkermans ADL, Van Elsas JD, De Bruijn FJ (eds) Molecular microbial ecology manual. Kluwer Academic Publishers, Dordrecht, Netherlands, pp 1-22

Ludwig W, Strunk O ARB: a software environment for sequence data. http://www.mikro.biologie.tu-muenchen.de/pub/ARB/documentation/arb.ps

Ludwig W, Bauer SH, Bauer M, Held I, Kirchhof G, Schulze R, Huber I, Spring S, Hartmann A, Schleifer KH (1997) Detection and in situ identification of representatives of a widely distributed new bacterial phylum. FEMS Microbiol. Lett. 153:181-190

Ludwig W, Strunk O, Klugbauer S, Klugbauer N, Weizenegger M, Neumaier J, Bachleitner M, Schleifer, KH (1998) Bacterial phylogeny based on comparative sequence analysis. Electrophoresis 19:554-568

Maidak BL et al. (1999) A new version of the RDP (Ribosomal Database Project). Nucleic Acids Res. 27:171-173

Massana R, Murray AE, Preston CM, DeLong EF (1997) Vertical distribution and phylogenetic characterization of marine planktonic *Archaea* in the Santa Barbara channel. Appl. Env. Microbiol. 63:50-56

Munson MA, Nedwell DB, Embley TM (1997) Phylogenetic diversity of *Archaea* in sediment samples from a coastal salt marsh. Appl. Env. Microbiol. 63:4729-4733

Olsen GJ, Lane DJ, Giovannoni SJ, Pace NR, Stahl DA (1986) Microbial ecology and evolution: a ribosomal RNA approach. Annu. Rev. Microbiol. 40:337-365

Pace NR, Stahl DA, Lane DJ, Olsen GJ (1986) The analysis of natural microbial populations by rRNA sequences. Adv. Microbiol. Ecol. 9:1-55

Pautot G (1983) Les fosses de la Mer Rouge: approche géomorphologique d'un stade initial d'ouverture océanique réalisée à l'aide du Seabeam. Oceanologica Acta 6:235-244

Rudolph C (1998) Weiterführende Untersuchungen zur Mikrobenpopulation der Schwefelquellen des Sippenauer Moors. Thesis, Universität Regensburg, Germany

Schoell M (1974) Valdivia VA 01/03, Hydrographie II und III. Bundesanstalt f. Bodenforschung, Hannover, Germany

Stoffers P et al. (1998) Cruise report SONNE 121, Red Sea. Hydrography, hydrothermalism and palaeoceanography in the Red Sea. Nr.88. Geologisch-Paläontologisches Institut der Universität Kiel, Kiel, Germany.

Woese CR, Achenbach L, Rouviere P, Mandelco L (1991) Archaeal phylogeny: reexamination of the phylogenetic position of *Archaeoglobus fulgidus* in light of certain composition-induced artifacts. System. Appl. Microbiol. 14:364-371

Yamamoto H, Hiraishi A, Kato K, Chiura HX, Maki Y, Shimizu A (1998) Phylogenetic evidence for the existence of novel thermophilic bacteria in hot spring sulfur-turf microbial mats in Japan. Appl. Environ. Microbiol. 64:1680-1687

Zierenberg RA, Shanks WC (1986) Isotopic constraints on the origin of the Atlantis II, Suakin and Valdivia brines, Red Sea. Geochim. Cosmochim. Acta 50:2205-2214

LEGEND TO THE FIGURES

Fig. 1: Distribution of brine pools in the northern Red Sea. The topographical map was generated with the Online Map Creation program, Geomar, Kiel (http://www.aquarius.geomar.de).

Fig. 2: 16S rRNA gene based phylogenetic tree of the bacterial domain and bacterial 16S rDNA sequences (KB1 clone group) from the Kebrit Deep, northern Red Sea. The topology of the tree is based on results of a maximum parsimony analysis. Reference sequences were chosen to represent the broadest diversity of *Bacteria*. Only sequence positions which share identical residues of 50% or greater of all available bacterial 16S rRNA sequences were included for tree construction. The scale bar represents a 10% estimated difference in nucleotide sequences.

Fig. 3: Dendrogram of 16S rRNA relatedness between the *Archaea* and archaeal 16S rDNA sequences from the Kebrit Deep, northern Red Sea. The tree was inferred by maximum parsimony analysis. Reference sequences were chosen to represent the broadest diversity of *Archaea*. Only sequence positions which share identical residues of 50% or greater of all available archaeal and euryarchaeotal 16S rRNA sequences were included for tree construction. The scale bar represents a 10% estimated difference in nucleotide sequences.

Table 1. Oligonucleotide primers used for PCR amplification and sequencing reactions of bacterial and archaeal 16S rRNA genes. The target site are based on the *Escherichia coli* sequence numbering according to Brosius et al. (1981)

Oligonucleotide	**Target site**	**Sequence (5' → 3')**	**Specifity**	**Source**
8aF	8-23	TCYGGTTGATCCTGCC	archaea	Burggraf et al., 1991
8bF	8-26	GRGTTTGATCCTGGCTCAG	bacteria	Burggraf et al., 1992
344aF	344-363	CGGGGYGCASCAGGCGCGAA	archaea	Burggraf et al., 1997
518uF	518-535	CAGCMGCCGCGGTAATAC	universal	Burggraf et al., 1997
1406uR	1390-1406	ACGGGCGGTGTGTRCAA	universal	Lane, 1991
1513uR	1493-1513	ACGGHTACCTTGTTACGACTT	universal	Lane, 1991

Table 2. Bacterial and archaeal clone restriction groups identified by fingerprinting using different restriction endonucleases.

Bacterial restriction groups	KTK 14	KTK 27	KTK 32	KTK 36	KTK 41	KTK 42
number of clones (%)	30	35	22	9	2	2
Archaeal restriction groups	KTK 4A	KTK 9A	KTK 18A	KTK 28A	KTK 31A	
number of clones (%)	67	20	7	3	3	

Fig. 1

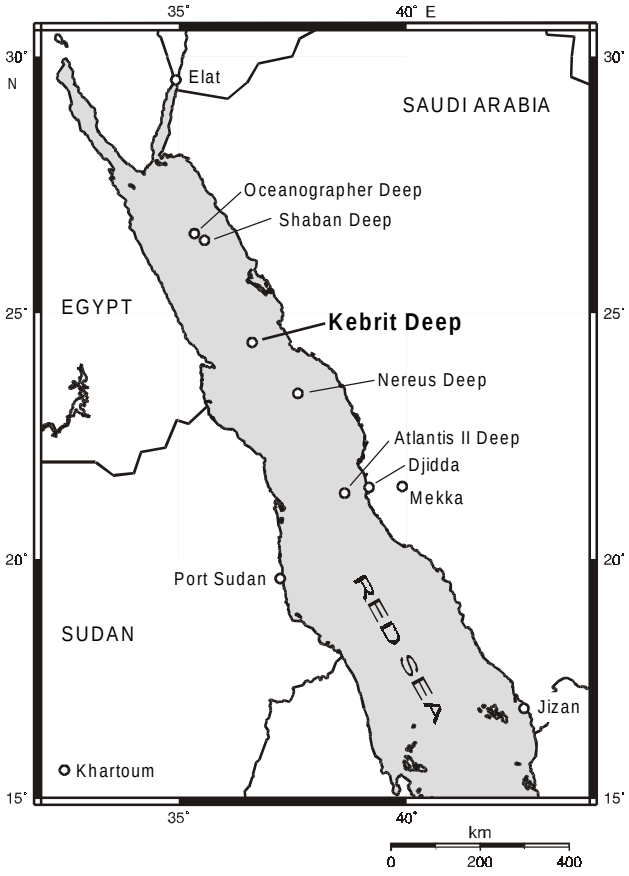

Fig. 2

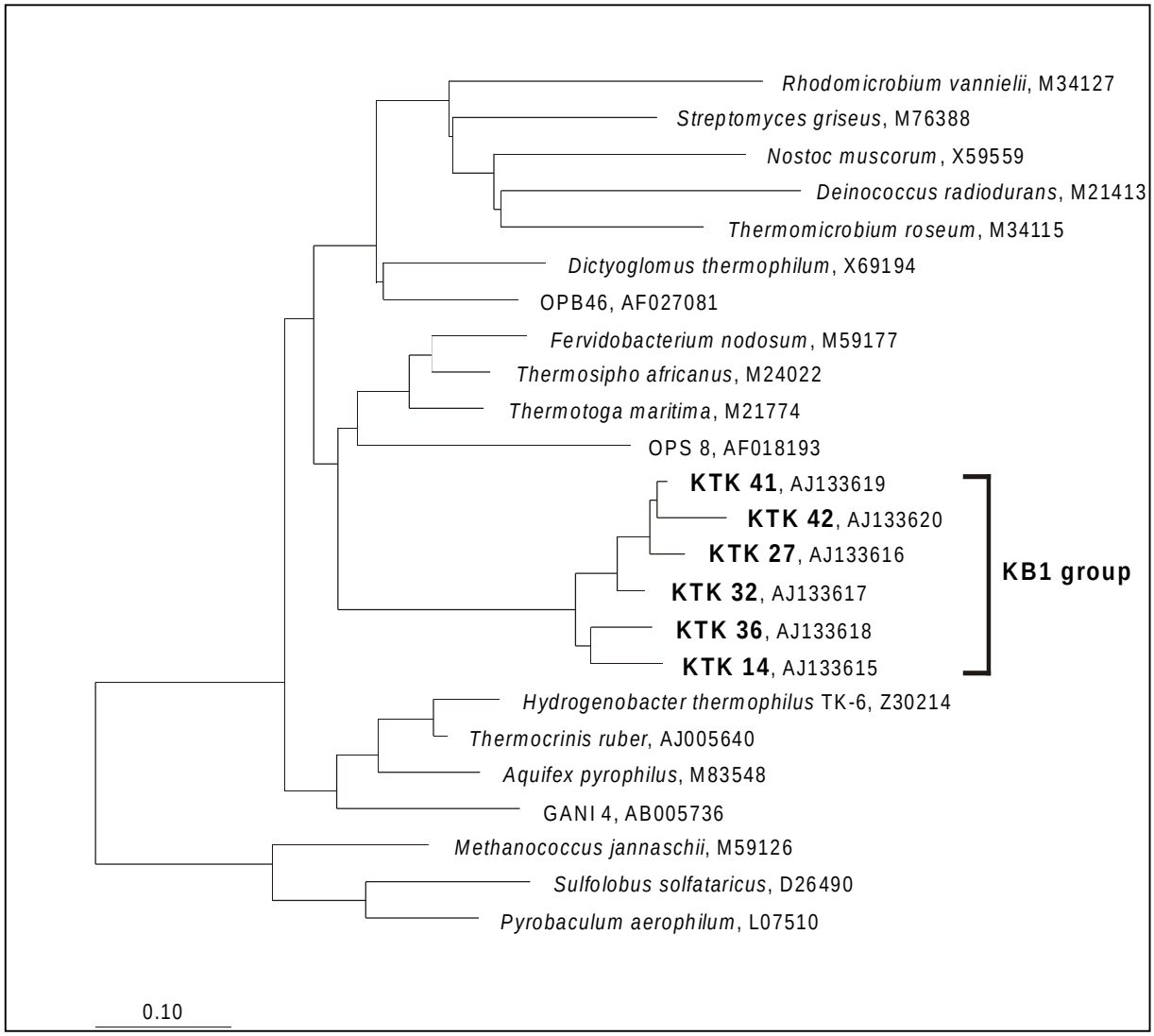
Rhodomicrobium vannielii, M34127
Streptomyces griseus, M76388
Nostoc muscorum, X59559
Deinococcus radiodurans, M21413
Thermomicrobium roseum, M34115
Dictyoglomus thermophilum, X69194
OPB46, AF027081
Fervidobacterium nodosum, M59177
Thermosipho africanus, M24022
Thermotoga maritima, M21774
OPS 8, AF018193
KTK 41, AJ133619
KTK 42, AJ133620
KTK 27, AJ133616
KTK 32, AJ133617
KTK 36, AJ133618
KTK 14, AJ133615
KB1 group
Hydrogenobacter thermophilus TK-6, Z30214
Thermocrinis ruber, AJ005640
Aquifex pyrophilus, M83548
GANI 4, AB005736
Methanococcus jannaschii, M59126
Sulfolobus solfataricus, D26490
Pyrobaculum aerophilum, L07510
0.10

Fig. 3

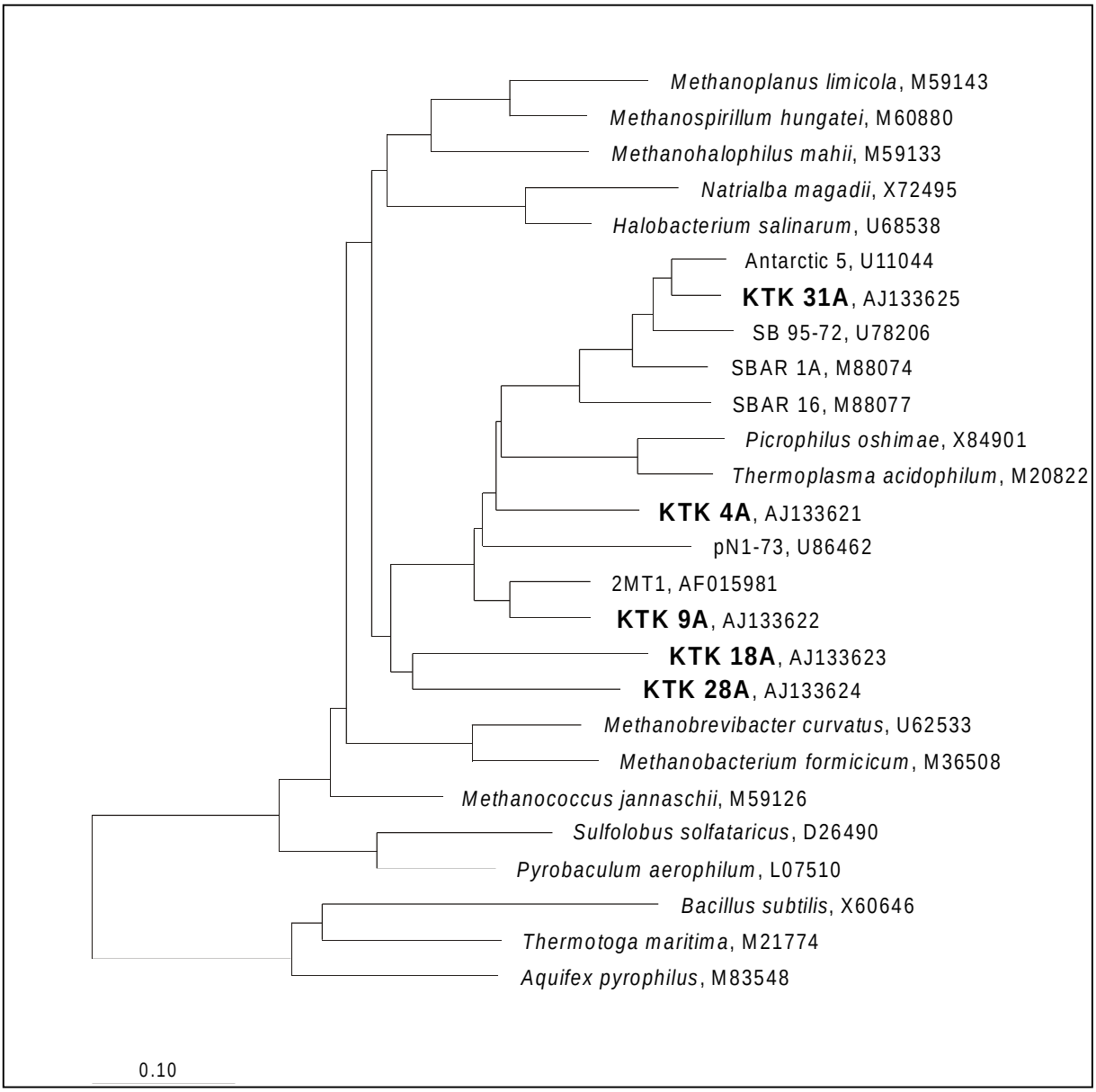
Methanoplanus limicola, M59143
Methanospirillum hungatei, M60880
Methanohalophilus mahii, M59133
Natrialba magadii, X72495
Halobacterium salinarum, U68538
Antarctic 5, U11044
KTK 31A, AJ133625
SB 95-72, U78206
SBAR 1A, M88074
SBAR 16, M88077
Picrophilus oshimae, X84901
Thermoplasma acidophilum, M20822
KTK 4A, AJ133621
pN1-73, U86462
2MT1, AF015981
KTK 9A, AJ133622
KTK 18A, AJ133623
KTK 28A, AJ133624
Methanobrevibacter curvatus, U62533
Methanobacterium formicicum, M36508
Methanococcus jannaschii, M59126
Sulfolobus solfataricus, D26490
Pyrobaculum aerophilum, L07510
Bacillus subtilis, X60646
Thermotoga maritima, M21774
Aquifex pyrophilus, M83548
0.10

12. Organic geochemistry of sediments of brine-filled Red Sea basins

Walter Michaelis, Sabine Beckmann, Stefan Boldt, Angela Jenisch –Anton, Richard Seifert

Institut für Biogeochemie und Meereschemie, Universität Hamburg

Introduction

Main objective of our contribution to the project SO 121 was to enhance our knowledge on the sources and the generation processes of hydrothermally altered organic matter in Red Sea brine habitats. First and extensive information on this subject could be acquired within a former study (SO 29, Michaelis et al., 1990). Unfortunately, petroleum impregnated sediments and asphalt containing massive sulphides alike those recovered and investigated then could not be obtained during this campaign. It was therefore not possible to meet al scientific targets primarily envisioned. Samples obtained derive from the Kebrit Deep, the Atlantis II Deep and the Umm Laij Deep. This includes sediments, pore waters and samples of the water column.

Results

Sedimentary carbon and nitrogen

Sediments of the Kebrit Deep (Table 1) revealed total carbon (TC) contents in the range between 5 and 8.3 wgt.% most of which was contributed by carbonate carbon. Ccarb concentrations from 4.29 up to 7.25 wgt.% show that about 50% of the sedimentary matter generally consists of carbonates. Organic carbon (Corg) represents between 0.4 and 1.28 wgt.% of the dry sediment (Fig. 1). While higher values have been determined for various horizons of the upper sediment column, all samples from below 3.5 mbsf (meter below sea floor) revealed Corg values of about 0.5 wgt.%. Nitrogen was measured in the range from 0.02 to 1 wgt.%, resulting in molar ratios between Corg and N between 8.6 and 47. High ratios are associated to samples of elevated Corg content (Fig. 2).

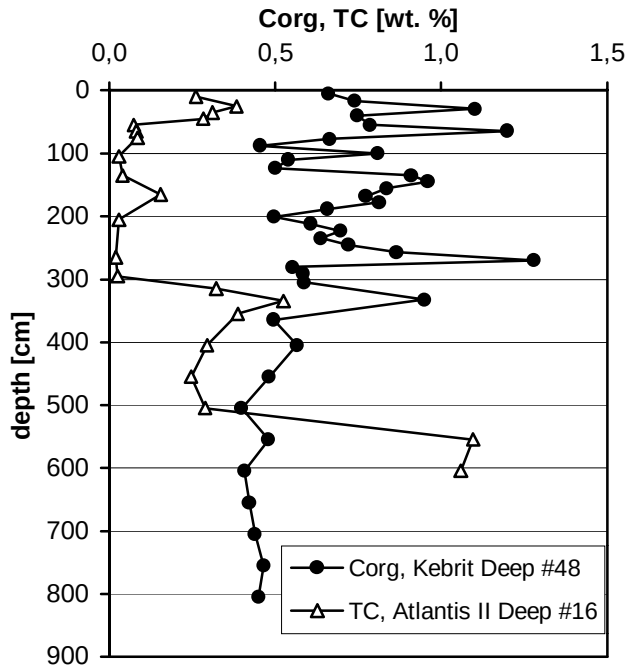

Fig. 1 Carbon content of Kebrit Deep and Atlantis II Deep sedimets.

Except for the uppermost 50 cm, very low contents of TC were found in samples recovered from the uppermost

3 m of the sediment column within the Atlantis II Deep (Table 2; Fig. 1). At 3mbsf, the values increase from < 0.05 wgt.% to >0.25 wgt.%.

Table 1 Data of Kebrit Deep sediment samples

Depth [cm]	TC [wgt.%]	C_{org} [wgt.%]	C_{carb} [wgt.%]	N [wgt.%]	C_{org}/N [mol]	TC/N [mol]	C_{org}/N [wgt.%]	DOC [µmol/l]
Kebrit Deep Stat #50: 24° 43,4'N 36° 16,7'E								
0-3	5,29	1,00	4,29					
3-6	6,51	0,80	5,71	0,10	9,5	77,6	8,1	
6-9	6,52	0,70	5,82	0,09	8,6	80,5	7,4	
9-12	6,45	0,89	5,55	0,12	8,8	63,4	7,5	
12-15	6,86	0,61	6,25	0,08	9,1	102,5	7,8	
15-18	7,10	0,32	6,79	0,04	10,1	224,8	8,6	
18-21	6,87	0,80	6,07	0,06	15,7	134,4	13,4	
21-24	7,00	1,02	5,98	0,07	17,6	121,1	15,1	
Kebrit DeepStat # 48: 24° 43,142'N 36° 16,393'E								
0-10	6,99	0,66	6,33	0,03	23,2	246,0	19,9	1000
12-22	5,77	0,74	5,03	0,06	14,1	110,5	12,1	1259
24-34	7,68	1,10	6,57	0,03	45,4	316,5	38,9	831
35-45	7,77	0,75	7,03	0,03	31,2	324,7	26,8	850
50-60	8,01	0,79	7,23	0,03	29,2	297,9	25,1	
60-70	7,94	1,20	6,75	0,04	35,3	234,2	30,3	866
72-82	7,76	0,66	7,09	0,03	23,4	273,1	20,1	
83-93	7,70	0,45	7,25	0,03	17,0	288,5	14,6	
95-105	7,89	0,81	7,08	0,04	23,8	232,5	20,4	
106-116	7,11	0,54	6,57	0,07	9,0	118,6	7,7	
118-128	7,17	0,50	6,67	0,06	9,5	136,1	8,2	812
130-140	7,47	0,91	6,56	0,07	16,0	131,1	13,7	899
140-150	7,74	0,96	6,78	0,06	19,0	152,8	16,3	
151-161	7,76	0,84	6,92	0,05	18,8	174,1	16,1	
163-173	7,02	0,77	6,25	0,05	17,2	156,3	14,8	
173-183	6,83	0,81	6,02	0,07	14,5	122,0	12,5	864
184-194	6,95	0,66	6,30	0,04	19,1	202,2	16,4	
196-206	6,93	0,50	6,43	0,04	15,1	211,3	13,0	
207-217	7,00	0,61	6,40	0,06	12,7	147,0	10,9	
218-228	6,74	0,70	6,04	0,04	19,4	187,8	16,7	
230-240	6,66	0,64	6,02	0,03	26,2	273,6	22,5	1225
241-251	6,84	0,72	6,12	0,03	31,1	294,7	26,6	
252-262	7,65	0,87	6,78	0,02	46,2	408,4	39,7	
265-275	8,27	1,28	6,99	0,03	47,0	303,8	40,3	
276-286	6,51	0,55	5,96	0,04	17,9	211,0	15,3	
287-297	6,63	0,58	6,05	0,04	16,9	192,4	14,5	
300-310	6,75	0,59	6,17	0,03	22,2	255,4	19,0	
328-338	6,98	0,95	6,03	0,03	36,9	270,6	31,6	
360-370	6,52	0,50	6,02	0,04	13,2	174,1	11,4	605
400-410	6,58	0,57	6,01	0,05	13,1	152,4	11,2	870
450-460	6,60	0,48	6,12	0,04	12,5	171,3	10,7	
500-510	6,65	0,40	6,25	0,03	13,6	226,0	11,6	789
550-560	6,70	0,48	6,22	0,04	13,1	182,8	11,2	
600-610	6,58	0,41	6,17	0,05	8,9	144,2	7,7	763
650-660	6,55	0,42	6,13	0,04	11,0	170,8	9,4	
700-710	6,52	0,44	6,08	0,04	12,4	184,4	10,7	775
750-760	6,58	0,47	6,12	0,04	12,8	180,8	11,0	
800-810	6,52	0,45	6,07	0,05	11,1	160,8	9,5	1221
Kebrit DeepStat #55 Dredge								
	7,75	0,19	7,56	0,01	17,3	701,4	14,8	

Table 2 Data of Atlantis II Deep and Umm Laaij Deep sediment samples

Depth [cm]	TC [wgt.%]	N [wgt.%]	TC/N [mol]	TC/N [wgt.%]	DOC [µmol/l]	
Atlantis II Deep Stat #15						
	0-2	0,41	0,014	33,7	28,9	
	2-5	0,28	0,017	18,9	16,2	
	5-10	0,14	0,014	11,5	9,9	
	10-15	0,17	0,008	24,7	21,2	
	15-20	0,14	0,018	9,4	8,0	
	20-25	0,17	0,010	18,9	16,2	
	25-30	0,21				
	30-35	0,23	0,020	14,0	12,0	
Atlantis II Deep Stat #16						
	ca. 5-10	0,26	0,016	18,7	16,1	80
	20-30	0,38	0,019	23,7	20,3	
	30-40	0,31	0,019	19,3	16,5	220
	40-50	0,28	0,020	16,8	14,4	
	50-60	0,07	0,019	4,5	3,9	160
	60-70	0,08	0,015	6,4	5,5	
	70-80	0,09	0,017	5,7	4,9	
	100-110	0,03	0,009	4,1	3,5	302
	130-140	0,04	0,016	3,1	2,6	
	160-170	0,16	0,014	13,4	11,5	286
	200-210	0,03	n.d.			132
	260-270	0,02	0,009	2,6	2,2	
	290-300	0,03	n.d.			
	310-320	0,32	0,011	33,2	28,4	181
	330-340	0,52	0,017	35,5	30,5	
	350-360	0,39	0,015	29,6	25,4	194
	400-410	0,29	0,017	20,2	17,4	
	450-460	0,25	0,017	16,8	14,4	313
	500-510	0,29	n.d.			
	550-560	1,10	0,019	65,8	56,5	586
	600-610	1,06	0,019	64,6	55,4	
Umm Laij Deep Stat #58//Stat #59						
		6,92	0,054	149,5	128,2	
		8,27	0,034	285,8	245,1	

A second sharp increase is observed at about 5 mbsf where below carbon contributes > 1 wgt% to the sediment. The major part of the TC appears to be Corg as determination of Ccarb for selected samples yielded extremely low values < 0.01 wgt.%, too low to be determined regarding the in most cases extremely low TC contribution and the limited sample size available. The same problem existed regarding the measurements of sedimentary nitrogen that never exceeded 0.02 wgt.% but was in some samples below the detection limit of 0.005 wgt.%. TC to N ratios varied from 2.6 to 65.8 and are increased in samples of enhanced TC content. The extraordinarily low ratios found in samples of low TC content might be reasoned by low molecular size nitrogenous compounds associated to the fine grained detrital

fraction, analogous to what is known from deep sea clays (Müller 1977). Obviously, the Atlantis II Deep sediments are severely influenced by TC prone and carbonate free hydrothermal material.

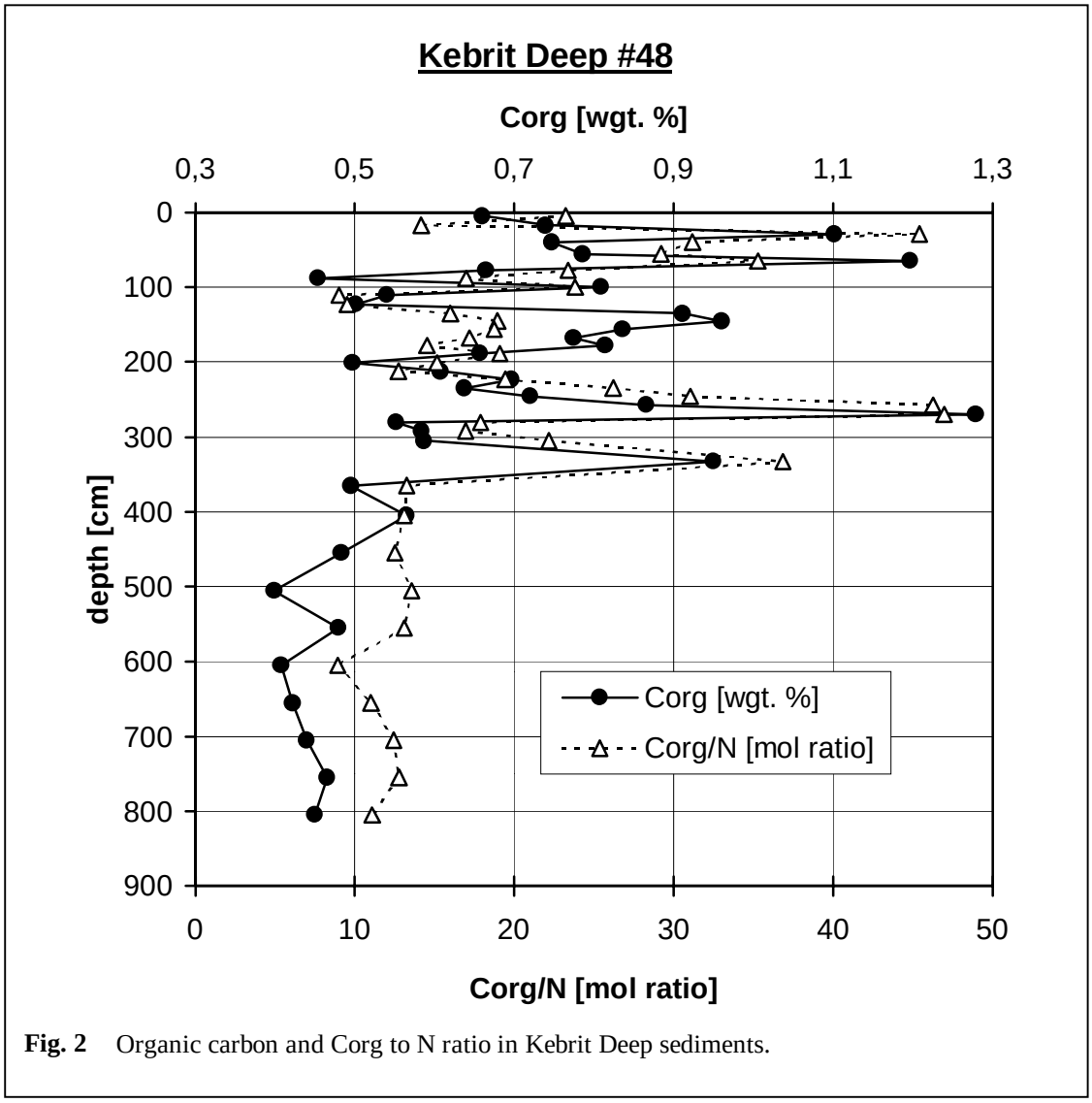

Fig. 2 Organic carbon and Corg to N ratio in Kebrit Deep sediments.

Pore waters

Pore water obtained from box core samples of the Kebrit Deep (Station 16; 21°19.8'N, 30°05.5'E) showed dissolved organic carbon (DOC) concentrations of about 800 µmol l^{-1} (605 to 1259 µmol l^{-1}) with no consistent depth related trend within the studied 0 to 8 mbsf of the sediment column (Fig. 3). In comparison, we detected much lower DOC values in pore water of Atlantis II Deep sediments (Box core, station 48; 24°43.4'N, 36°16.7'E) in the range from 80 to 586 µmol l^{-1} (average 245 µmol l^{-1}). Moreover, an increase of DOC concentrations is

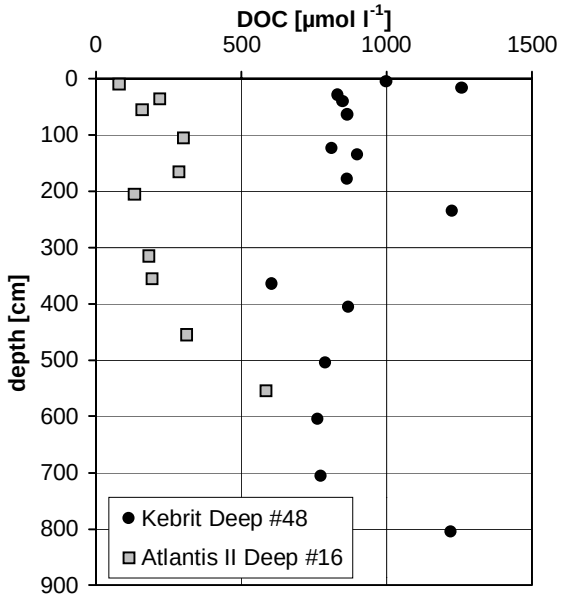

Fig. 3 DOC in pore waters.

indicated at the deepest part of the about 5.5 m long core that coincides with enhanced concentration of sedimentary carbon.

This difference between the DOC content of the pore waters from the Kebrit Deep and the Atlantis II Deep mirrors the observations made regarding the organic carbon content of the sediments and, more unexpected, the relatively enhanced DOC concentrations in the water column at the Kebrit Deep.

CTD-Rosette samples

Several water stations were covered within the Kebrit and the Atlantis II Deeps. Profiles presented in Fig. 4 are compiled from samples of different stations occupied at about 24°43,1'N, 36°16.4E (Kebrit Deep) and 21°20'N, 38°04.8'E (Atlantis II Deep). DOC concentrations at the Kebrit Deep are mostly below 500 µmol l^{1}, except for enhanced values at 1380 and 1470m water depth (Fig. 4). The latter peak reaching nearly 1400 µmol l^{1} is positioned directly above the transition zone between the high saline warm brine and the overlying Red Sea water that is illustrated by the sharp temperature shift at 1480 m. It thus might be reasoned by organic matter accumulation and enhanced microbial activity at the pycnocline. A similar phenomenon was not observed for the Atlantis II Deep. However, that might be caused by the absence of samples covering the respective depth horizon (1940 to 2000 m). The enhanced DOC concentration present between 2000 and 2050 m might be related to density gradients indicated by temperature steps within the upper brine body.

Average DOC concentration appears to be lower in the brine of Atlantis II Deep compared with that of the Kebrit Deep, especially in case of samples taken close to the sea floor. This might be attributed to the influence of sediment derived dissolved organic matter that contributes to the DOC of the overlying, high saline and stagnant water body. Another potential reason for minor DOC concentrations in the Atlantis II Deep brine is an enhanced disintegration of dissolved organic matter due to the high temperature.

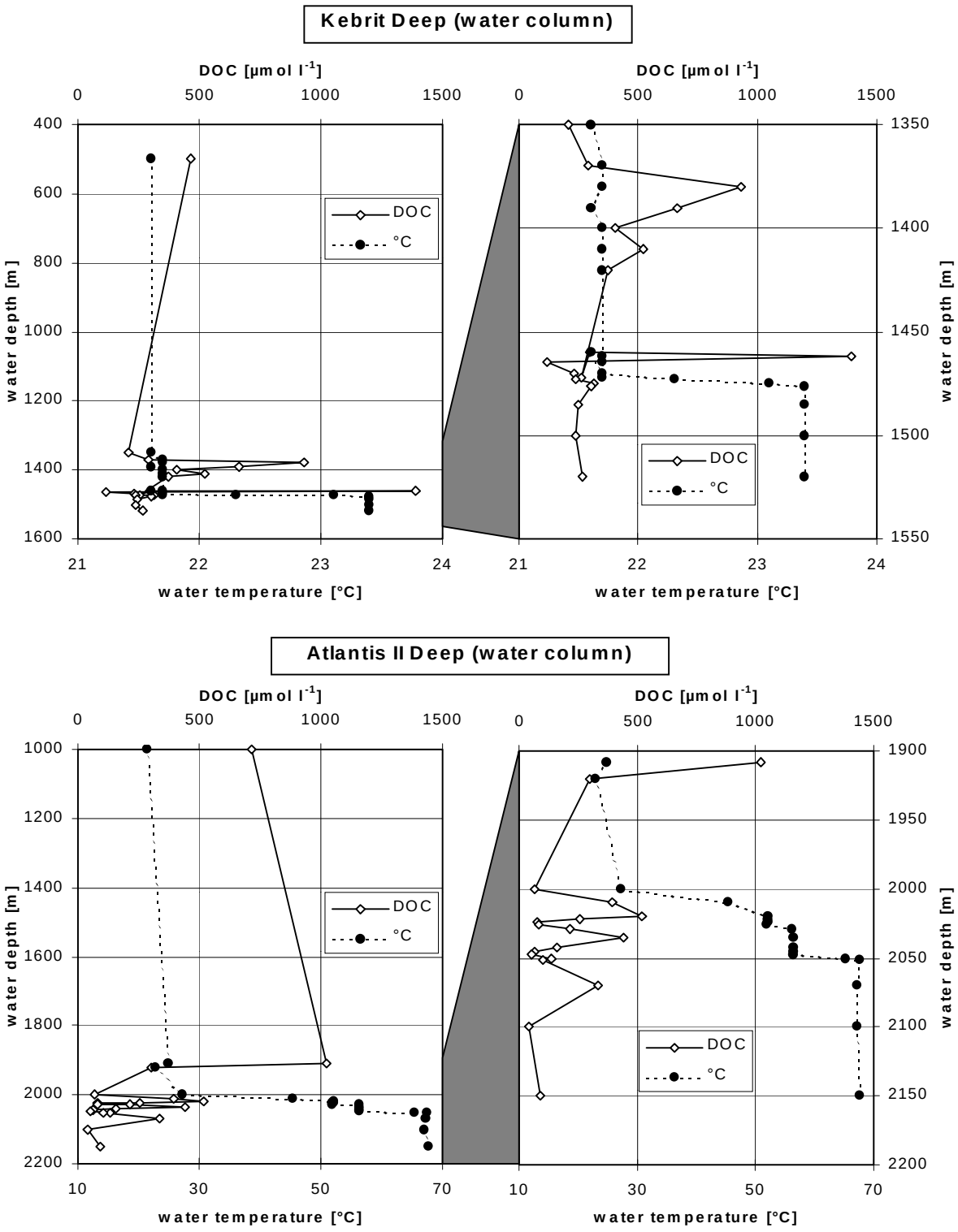

Fig. 4 Dissolved organic carbon and temperature in brines of the Kebrit Deep (above) and the Atlantis II Deep (below).

Characterisation of sedimentary organic matter

The composition of sedimentary organic matter was investigated in detail for selected sediment samples of both, the Kebrit and the Atlantis II Deep (Table 3).

Table 3 Organic fractions of selected sediments

sample / depth [cm]	Corg [wgt.%]*	extract [mg/gC]	asphaltenes [mg/gC]	polar residue [mg/gC]	fraction F1 HC [mg/gC]	fraction F2 polar comp. [mg/gC]
Kebrit Deep						
BC 0-10	0,66	122,43	33,82	30,91	n.d.	4,34
BC 12-22	0,74	51,95	14,63	17,83	0,79	1,72
MC 21-24	1,02	63,41	15,30	20,77	0,68	3,22
BC 140-150	0,96	64,25	22,93	19,65	0,51	1,05
BC 328-338	0,95	35,89	9,10	15,58	0,79	0,19
BC 800-810	0,45	46,74	24,41	n.d.	n.d.	n.d.
Atlantis II Deep						
BC 0-5	0,33	569,14	18,01	10,18	1,30	1,53
MC 160-170	0,16	165,39	35,08	2,67	4,12	1,60
MC 550-560	1,10	184,94	1,30	5,66	0,31	0,21

* Samples from the Atlantis II Deep are not decarbonized

Organic C contents and amounts of chromatographic fractions are presented in Table 3. Total Corg ranges between 0.33 and 1.1 wgt.%. These values are higher than reported for Recent open ocean and hemipelagic sediments (e.g. Romankevich, 1984; Mycke et al., 1985; Emeis et al., 1987). Highest values were observed in the deep samples of the Atlantis II Deep. However, they are lower than those reported by Simoneit et al. (1987). The data show no regular trend and indicate that the bulk of organic matter of both deeps has not undergone enhanced degrees of thermal maturation. Bitumen concentrations range from 35 to 569 mg/gC for the sediments (Table 3). The samples from the Kebrit Deep do not show increasing amounts of extractable material with depth. In the Atlantis II Deep samples bitumen ratios exceed average values for unaltered sediments, which are reported to vary between 20 and 100 mg/g Corg (Galimov and Kodina, 1983; Tissot and Welte, 1984). These high bitumen ratios of > 100 mg/g Corg may require sources other than autochthonous organic C, such as inputs from a second source. Remobilization of organic matter from deeper sediment sections by hydrothermal solutions can account for an additional organic matter input. This phenomenon has frequently been observed in hydrothermal active areas (e.g. Simoneit et al., 1984; Kawka and Simoneit, 1987). Increasing amounts of the asphaltene fraction, as often observed in hydrothermally influenced organic rich facies could not be found in the samples analysed so far.

Hydrocarbon fraction

The hydrocarbons from the sediments of the Kebrit Deep and the upper core section of the Atlantis II Deep contain n-alkanes ranging from C_{15} to C_{35} (Fig. 5 and 6).

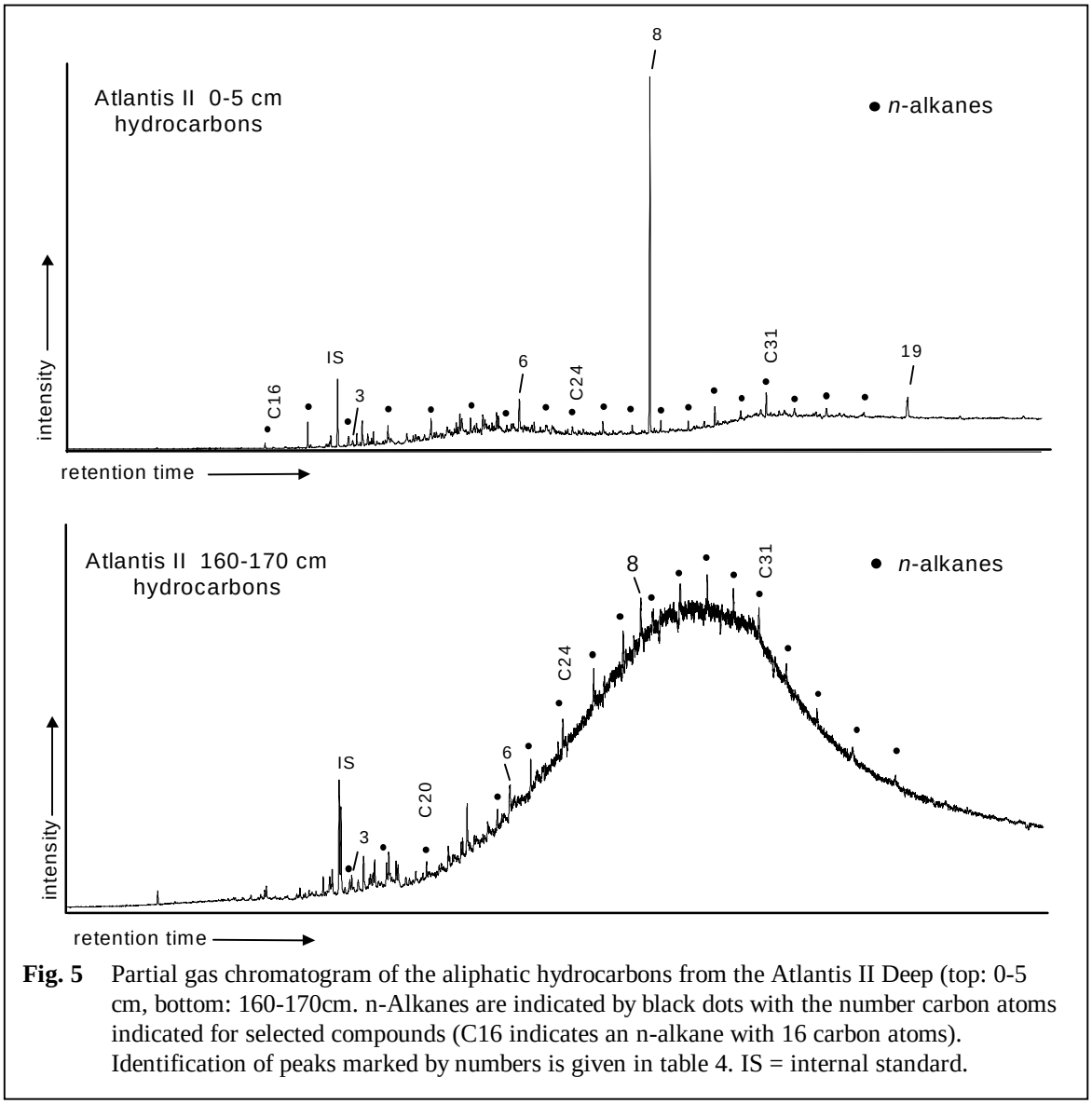

Fig. 5 Partial gas chromatogram of the aliphatic hydrocarbons from the Atlantis II Deep (top: 0-5 cm, bottom: 160-170cm. n-Alkanes are indicated by black dots with the number carbon atoms indicated for selected compounds (C16 indicates an n-alkane with 16 carbon atoms). Identification of peaks marked by numbers is given in table 4. IS = internal standard.

Table 4 Identification of Compounds of the hydrocarbon fraction (Fig. 5 and 6).

1	pristane	2	7-methylheptadecane
3	phyt-3-ene	4	C_{25}-highly branched isoprenoids (HBI)
5	C_{20}-isoprenoid thiophene	6	2,6,10,14,19-pentamethylicosane
7	2,6,10,14,19-pentamethylicosene	8	squalane
9	cholestadiene (I)	10	cholest-2-ene
11	cholestadiene (II) + 24-methylcholestadiene	12	hop-17(21)-ene
13	neohop-13(18)-ene	14	unknown hopene
15	unknown triterpenoid (friedelane type?)	16	hop-22(29)-ene (diploptene)
17	hop-21-ene	18	17β(H)-21β(H)-homohopane
19	lycopane		

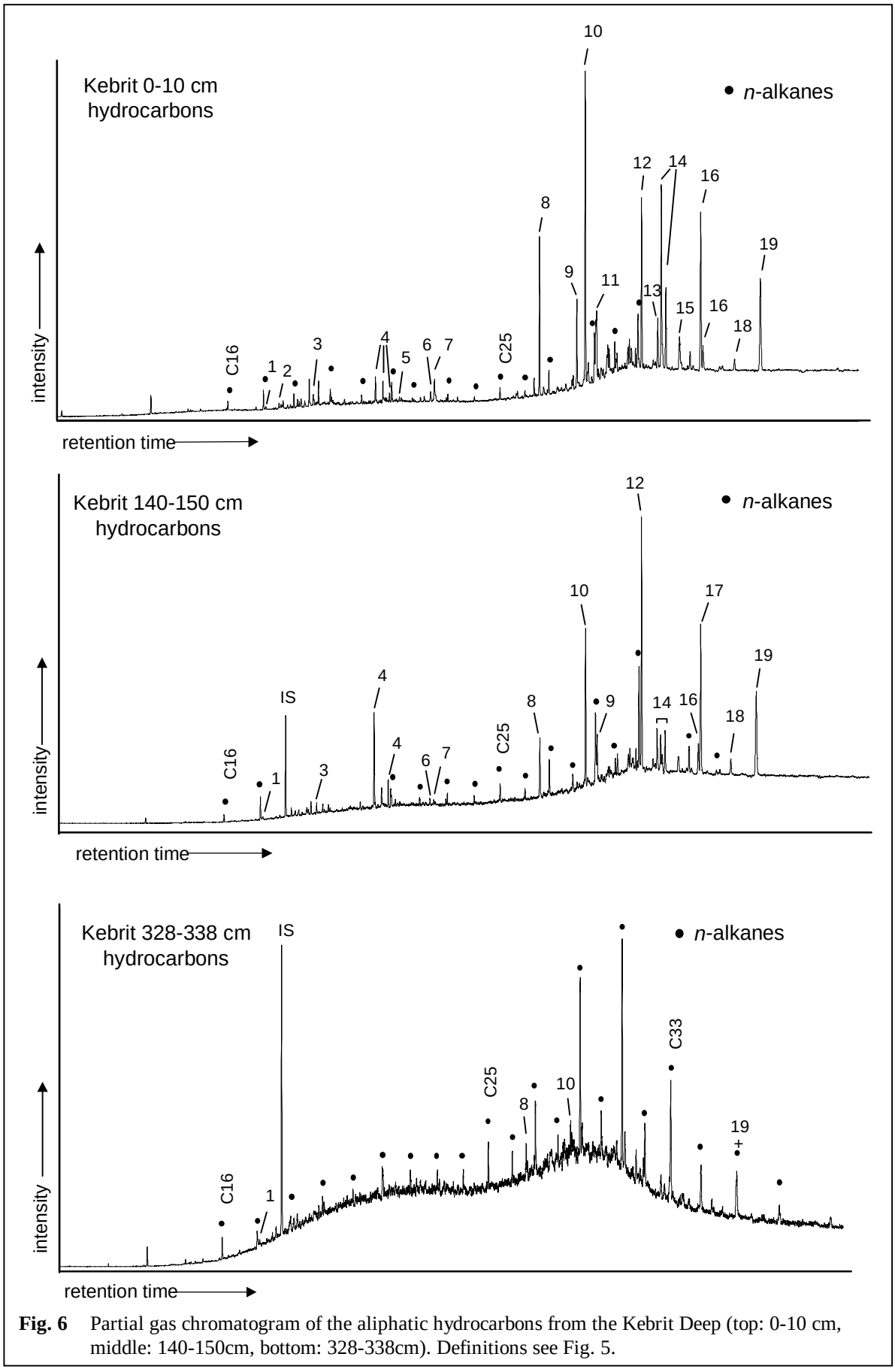

Fig. 6 Partial gas chromatogram of the aliphatic hydrocarbons from the Kebrit Deep (top: 0-10 cm, middle: 140-150cm, bottom: 328-338cm). Definitions see Fig. 5.

The high molecular weight homologues > C_{24} exhibit a small odd-to-even C-number

predominance. These hydrocarbons can derive from vascular plant waxes and may reflect a terrestrial input into the marine sediments.

Gas chromatograms of the extracted alkanes in the deepest core samples, Kebrit Deep 328-338; Atlantis II Deep 160-170cm) show significant differences with the overlying sections (Fig. 5 and 6). The hydrocarbons are dominated by a complex mixture of branched and cyclic compounds resulting in a hump of unresolvable peaks. n-Alkanes are minor components which suggests some degree of biodegradation (Connan, 1984; Kawka and Simoneit, 1987). The presence of the hump is characteristic for a petroleum of hydrothermal origin. Similar petroleums have been observed in sediments of active spreading centres (Simoneit and Londsdale, 1982; Simoneit, 1984).

Three major sources of organic matter can be distinguished from the biomarker patterns.

1.) A complex succession of mono- to tri-unsaturated steroid hydrocarbons indicates inputs from a high diversity of eukaryotic, namely algal, planktonic primary producers (most prominent compounds *9, 10, 11*; Kebrit 0-10cm, 140-150cm; Fig. 5 and 6). Further compounds which relate to inputs of sedimentary organic matter from the upper water column are 7-methylheptadecane (*2*, cyanobacteria), several isomers of highly branched C_{25}-isoprenoids (*4*, diatoms), and phytenes (*3*, chlorophyll a), and in the polar fractions, long-chain alkenones (*21*,*22*, haptophytes) (Fig. 7 and 8).

2.) A second, prominent group of biomarkers found in the Atlantis II samples and in the Kebrit sediments consists of the tail-to-tail coupled isoprenoid hydrocarbons (Fig. 5 and 6) 2,6,10,15,19-methylpentamethylicosane (PMI, compound *6*) and its unsaturated counterparts (*7*), squalane (8) and the C_{40}-isoprenoid lycopane (*19*). These hydrocarbons are indicative for contributions of organic matter from methanogenic archaebacteria and are consistent with post-depositional bacterial mineralization processes prevailing in the anaerobic sediment

3.) Abundant hopanoids reflect a significant contribution of organic matter derived from aerobic bacteria, and possibly, oxic bacterial mineralization processes of the organic matter. These compounds can be classified into two groups of different diagenetical history. Hopanoic ketones and acids present in the polar fractions (Fig. 7 and 8; compounds *8, 11, 12, 14, 15, 18, 19*) are widespread constituents of immature sediments and are likely to originate from early diagenetic transformation of hopanepolyols, bacterial cell membrane constituents. A typical feature is the preservation of the biological 17β,21β(H)-configuration which is gradually changed into the 17α, 21β(H)-configuration during thermal evolution. Likewise, hop-17(21)-ene (*12*) and neohop-13(18)-ene (*13*) have been shown to originate from the early diagenetic

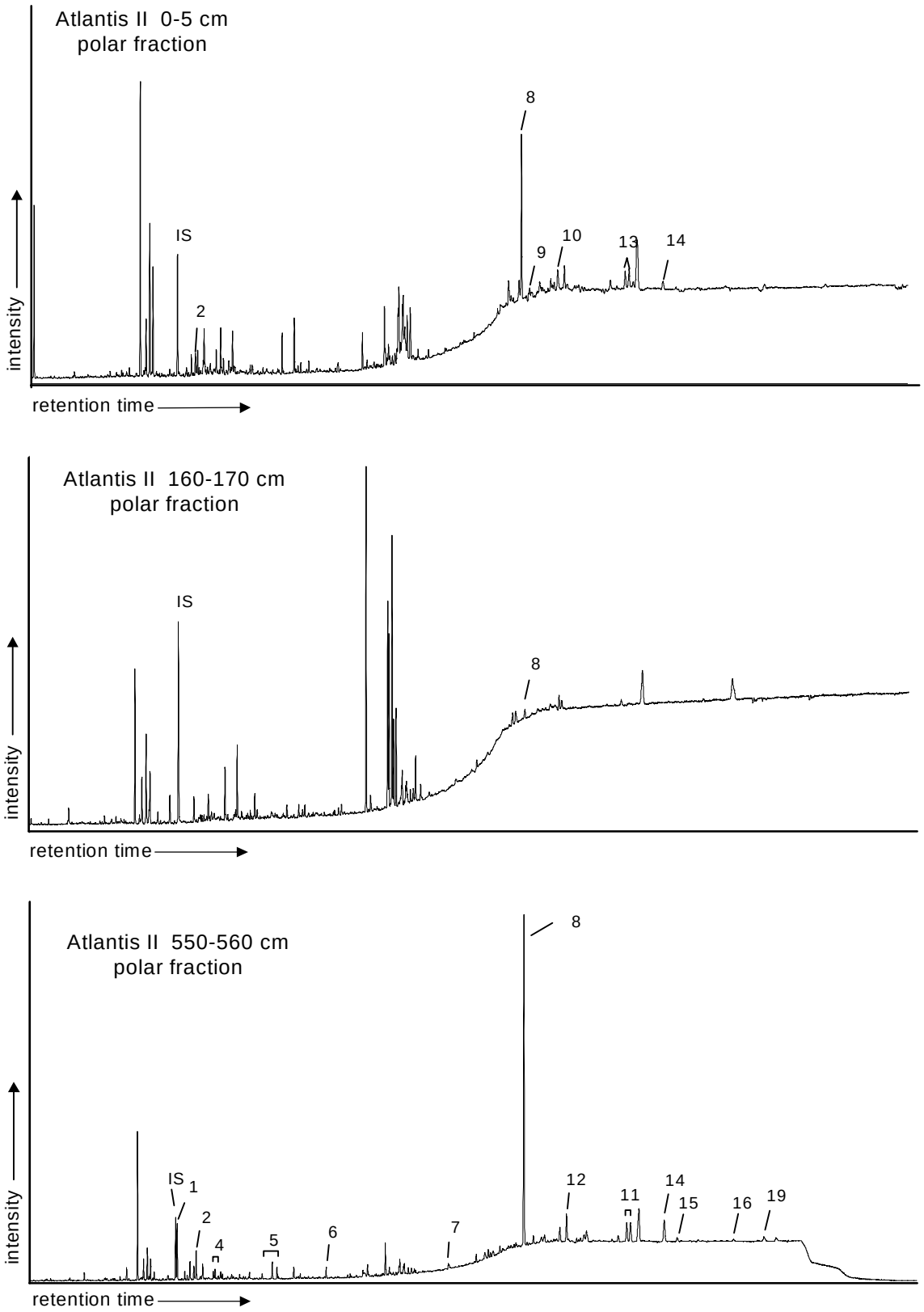

Fig. 7 Partial gas chromatogram of the polar fractions from the Atlantis II Deep (top: 0-5 cm,: middle:160-170cm, bottom 550-560cm). Identification of peaks marked by numbers is given in table 5. IS = internal standard.

rearrangement of hop-22(29)-ene (diploptene, *16*), a 'primitive' C_{30} triterpenoid which usually co-occurs with the hopanepolyols in prokaryotic lipids.

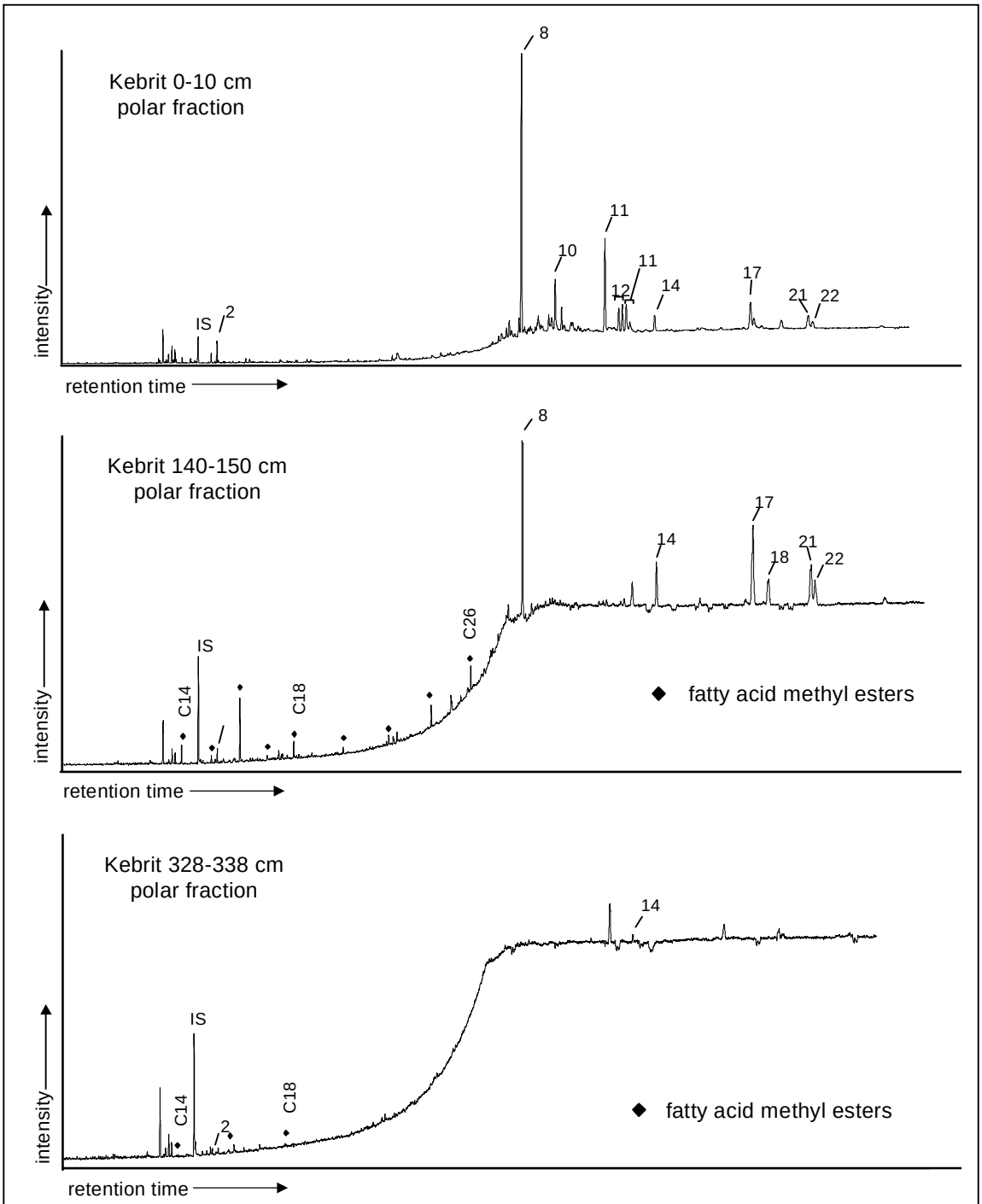

Fig. 8 Partial gas chromatogram of the aliphatic hydrocarbons from the Kebrit Deep (top: 0-10 cm, middle: 140-150cm, bottom: 328-338cm). Fatty acid methyl esters are indicated by black rhombi with the number carbon atoms indicated for selected compounds (C14 indicates an fatty acid methyl ester with 14 carbon atoms). Identification of numbers see table 5. IS = internal standard.

A second group of hopanoids comprises of hydrocarbons showing the geological, thermodynamically more stable 17α, 21β(H) configuration being characteristic for compounds of advanced thermal maturity. They may derive from fossil organic matter (e.g. crude oil seepage) but also from thermal overprinting of freshly deposited hopanoids. However, since

these compounds occur as trace compounds in Atlantis II 0-5cm and Kebrit 328-338 only, it is suggested that most of the hopanoids present in the samples studied derive from newly produced precursors which received only slight, early diagenetic alteration.

Hydrothermally generated petroleum very often contains polynuclear aromatic hydrocarbons (PAH) (Simoneit et al., 1984). The Red Sea samples did not contain these compounds in concentrations as high as reported from the Guaymas Basin or the Gorda Ridge (Kvenvolden et al., 1986); however, some members of these compound class are present (Fig. 7 and 8). In samples from the Atlantis II Deep the PAH fraction comprises phenanthrene and anthracene.

Table 5 Identification of Compounds of the polar fraction (Fig. 7 and 8).

1	phenanthrene/ anthracene	2	octadecane-2-one
3	methyldibenzothiophene	4	methylanthracene / methylphenantrene
5	fluoranthene/pyrene	6	henicosan-2-one
7	squalene	8	C_{27}-22,29,30-trisnorhopanone
9	cholesta-3,5-diene-7-one	10	4α,23,24-trimethylcholest-22-ene-3β-ol
11	C_{30}-hopanol	12	C_{30}-hopanone
13	17α(H)-21β(H)-hopanoid	14	C_{30}-hopanoic acid methyl ester
15	C_{31}-homohopanone	16	C_{32}-bishomohopanone
17	heptatriacontadien-2-one	18	17β(H)-21β(H)-bishomohopanoic acid methyl ester
19	C_{33}-trishomohopanone	20	C_{32}-bishomohopanol
21	octatriacontadien-3-one	22	octatriacontadien-2-one

Summary

Considerable differences exist between the Kebrit Deep and the Atlantis II Deep.

- While carbonates contribute about 50% to the Kebrit Deep sediments, only traces are present in Atlantis II Deep sediments.

- The content of organic carbon in the sediments and in the pore waters of the upper 5 m of the sediment column is much higher in the Kebrit Deep. Below 5 mbsf, concentrations of sedimentary carbon and pore water DOC increase strongly in the Atlantis II Deep, but not in the Kebrit Deep.

- DOC concentrations in Kebrit Deep brine waters exceed those found in the Atlantis II Deep.

High concentrations of dissolved organic carbon appear close to pycnolclines at the upper brine – sea water boundary.

Sediments of enhanced organic carbon content reveal high Corg to N ratios. This might indicate impregnation with hydrothermally altered and mobilised organic matter. The appearance of those indications within distinct horizons in the upper part of the sediment column argues for lateral inputs, at least in case of the Kebrit Deep.

Extracts from samples of the Kebrit Deep contained normal, branched and cyclic alkanes typical for an autochthonous sedimentation of organic substances. An increase of maturation with depth is observed (increase of α,β-hopanes and of the unresolved complex mixture). The in situ thermal alteration of the sediments should be minimal because unusually high concentrations of immature polar compounds are present.

The sources of the sedimentary organic matter could be characterised by biomarkers. Identified are contributions from marine algae (diatoms, haptophytes), cyanobacteria, archaebacteria, and aerobic bacteria.

For Atlantis II Deep samples, the different thermal maturities give evidence for an impregnation of the Recent, immature autochthonous material by hydrothermally derived organic compounds from deeper sections. The migrating organic phase increasingly dominates the recent organic material with greater depth.

References

Connan J. (1984) Biodegradation of crude oils in reservoirs. In *Advances of Petroleum Geochemistry* (eds. J. Brooks and D. H. Welte), Vol 1, pp. 299-335. Academic Press.

Emeis K. C., Mycke B., Richnow H.-H., Spitzy A., and Degens E. T. (1987) Organic carbon and nitrogen, sediment composition, and clay mineralogy of deep sea drilling project site 603; western Atlantic ocean. In *Initial Reports of the Deep Sea Drilling Project* (eds. J. E. van Hinte, J. P. S. W. Wise Jr., et al.), Vol XCIII, pp. 1245-1256. U. S. Government Printing Office.

Galimov E. M. and Kodina L. A. (1983) Organic matter in sediments of high thermogradient (DSDP Leg 64, Gulf of California). In *Advances in Organic Geochemistry 1981* (eds. M Bjoroy, P. Albrecht, et al.), pp 431-437. Pergamon Press.

Kawka O. E. and Simoneit B. R. T. (1987) Surves of hydrothermally-generated petroleums from the Guaymas Basin spreading centre. *Org. Geochem*. **11**, 311-328.

Kvenvolden K. A., Rapp J. B., Hostettler F. D., Morton J. L., King J. D., and Claypool G. E. (1986) Petroleum associated with polymetallic sufide in sediments from Gorda Ridge, *Science* **234**, 1231-1234.

Michaelis W., Jenisch A., and Richnow H. H. (1990) Hydrothermal petroleum generation in Red Sea sediments from the Kebrit and Shaban Deeps. *Applied Geochem*. **5**, 103-114.

Müller P. (1977) C/N ratios in Pacific deep sea sediments: Effect of inorganic ammonium and organic nitrogen compounds sorbed by clays. *Geochim. Cosmochim. Acta* **41**, 765-776.

Mycke B., Emeis K. C., and Degens E. T. (1985) Diagenesis of organic compounds in hole 593, Leg 90 (Tasman Sea). In *Initial Reports of the Deep Sea Drilling Project* (eds. P. Kennet, J. P. von der Borch et al.), Vol XC, Chap. 35, pp. 1265-1269. U. S. Government Printing Office.

Romankevich E. A. (1984) *Geochemistry of organic matter in the ocean*. Springer Verlag.

Simoneit B. R. T. (1984) Hydrothermal effects on organic matter – high vs low temperature components. *Org. Geochem.* **6**, 857-864.

Simoneit B. R. T. and Londsdale P. F. (1982) Hydrothermal petroleum in mineralised mounds at the seabed of Guaymas Basin. *Nature* **29**, 198-202.

Simoneit B. R. T., Grimalt J. O., Hayes J. M., and Hartmann H. (1987) Low temperature hydrothermal maturation in sediments of the Atlantis II Deep, Red Sea. *Geochim. Cosmochim. Acta* **51**, 879-894.

Simoneit B. R. T., Philp R. P., Jenden P. D., and Galimov E. M. (1984) Organic geochemistry of deep sea drilling project sediments from the Gulf of California-Hydrothermal effects on unconsolidated diatom ooze. *Org. Geochem.* **7**, 173-205.

Tissot B. P. and Welte D. H. (1984) *Petroleum Formation and Occurrence.* Springer Verlag.

13. List of Publications resulting from SO121 cruise (Papers, Abstracts)

W. Eder, W. Ludwig, R. Huber (1999) Novel 16S rRNA gene sequences retrieved from highly saline brine sediments of Kebrit Deep, Red Sea Arch Microbiol **172**, 213 - 218

Eder W. and Huber R. (1999) Recovery of novel procaryotic rRNA sequences from low-temperature, saline brine sediments of Kebrit Deep, Red Sea. *BMBF-Statusseminar, Meeresforschung mit FS Sonne,* Freiberg.

Faber E., Botz R., Poggenburg J., Schmidt M., Stoffers P., and Hartmann M. (1998) Methane in Red Sea brine waters. *Org. Geochemistry* **29**(1-3), 363-379.

Garbe-Schönberg CD, Scholten JC, Moammar MO, Stoffers P (1998) Trace element chemistry of brines and brine-interfaces in the Atlantis-II, Chain, and Discovery Deep in the Red Sea: First results. - EOS Transactions, AGU Vol. **79**, S. F947.

Garbe-Schönberg, C-D, Arpe, T, Krause P, Grote-Bartscher B (1998) Direct determination of trace elements in seawater by sector-field HR-ICPMS using a micro-nebulizer and membrane desolvation. - ICP Inform. Newsl., **23**, 330.

Hartmann M., Scholten J. C., and Stoffers P. (1998) Hydrographic structure of brine-filled deeps in the Red Sea: correction of Atlantis II Deep temperatures. *Mar. Geol.* **144**, 331-332.

Huber R. (1999) Die Laserpinzette als Basis für Einzelzellenkultivierung. *Biospektrum* **4**, 289-291.

Schmidt M., Faber E., Botz R., Poggenburg J., Schmitt M., and Stoffers P. (1998) Origin of hydrocarbon trace gases in brine-filled Red Sea deeps. *Mineralogical Magazine* **62A**, 1347-1348.

Schmidt, M. Faber, E. Botz, R. Poggenburg, J.,Schmitt, M., Stoffers, P. (1999) Hydrocarbon gases in brine - filled Red Sea deeps. *BMBF-Statusseminar, Meeresforschung mit FS Sonne,* Freiberg.

Schmidt M., Faber E., Botz R., Poggenburg J., Schmitt M., Stoffers P., and Moammar M. (1999) Hydrocarbon gases in brine-filled Red Sea deeps. *Second Symposium on Red Sea Marine Environment,* Jeddah.

Schöps, D.,Plüger, W. L.,Stoffers, P.: Charakterisierung von Massivsulfiden aus dem Kebrit - Tief (Rotes Meer) (Abstr.). Berichte der Deutschen Mineralogischen Gesellschaft. Beih. z. Eur. J. Mineral., Vol.10, No. 1, S. 261

Schöps, D.(1999). SO 121: Geochemie der Massivsulfide aus dem Kebrit - Tief (Rotes Meer). Statusseminar des BMBF: „Meeresforschung mit der FS SONNE“. Tagungsband, 387 - 390

Scholten J., Stoffers P., Garbe-Schönberg D., and Moammar M. (2000) Hydrothermal Mineralization in the Red Sea. In *Marine Mineral Deposits* (ed. D. S. Cronan), pp. 369 - 395.

Stoffers, P; Moammar, M.; Abu-Ouf, M.; Ackermandt, D.; Alassif, O.; Al-Hazim, Y.; Boldt, S.; Botz, R.; Eder, W.; El-Garafi, A.; El-Mamoney, M.; Fleitmann, D.; Garbe-Schönberg, D.;

Geiselhard, Goedecke, D.; Hartmann, M.; Klauke, S.;Moussa, K.; Mühlhan, N.; Mühlstrasser, T.; Poggenburg, J.;Rehder, W.; Schmidt, M.; Schmitt, M.; Schoeps, D.; Scholten, J.; Shbalaby, M.; Wismann, A.; Yohannes, E. (1998) Hydrography, hydrothermalism and paleoceanography in the Red Sea –Cruise Report Sonne 121-. *Berichte-Reports Geol.Paläont. Inst. Univ. Kiel* **88**, pp. 107.

Winckler, G., Aeschbach - Hertig, W., Kipfer, R., Botz, R., Bayer, R., Schmidt, M., Stoffers, P.(to be submitted to EPSL) Constraints on the origin and evolution of the Red Sea brines from helium and argon isotopes.

Winckler G., Kipfer R., Aeschbach-Hertig W., Botz R., Schmidt M., Schuler S., Bayer R. (in press).Sub sea floor boiling of Red Sea Brines - New indication from noble gas data. *Geochim. Cosmochim. Acta.*